UNIVERSITY OF THE
FREE STATE
UNIVERSITEIT VAN DIE
VRYSTAAT
YUNIVESITHI YA
FREISTATA

UFS
UV

GEOPHYSICAL INVESTIGATIONS IN THE KHAKHEA-BRAY TRANSBOUNDARY AQUIFER

Thandeka Fortunate Ngobe

Submitted in fulfilment of the requirements for the degree

Magister Scientiae in Geohydrology

in the

Faculty of Natural and Agricultural Sciences

(Institute for Groundwater Studies)

at the

University of the Free State

Supervisor: Professor Modreck Gomo

11 November 2022

DECLARATION

I, Thandeka F. Ngobe, hereby declare that the dissertation hereby submitted by me to the Institute for Groundwater Studies in the Faculty of Natural and Agricultural Sciences at the University of the Free State, in fulfilment of the degree of Magister Scientiae, is my own independent work. It has not previously been submitted by me to any other institution of higher education. In addition, I declare that all sources cited have been acknowledged by means of a list of references.

I furthermore cede the copyright of the dissertation and its contents in favour of the University of the Free State.

Thandeka F. Ngobe

November 2022

ACKNOWLEDGMENTS

The success of this research study was made possible by a number of people, and I would like to specifically thank the following individuals:

- My academic supervisor, Professor Modreck Gomo, for his advice and extensive discussions which all culminated in the success of this research project. It was a great privilege to do this research under his guidance.
- My parents, siblings, and friends, thank you for being my biggest cheerleaders, your prayers and words of encouragement made it possible for me to complete this research.
- I would like to express my gratitude to the JRS Biodiversity Foundation and the Southern African Development Community-Groundwater Management Institute (SADC-GMI) for funding this project and covering all of my educational expenses.
- Rachel Mpe, from the Department of Water and Sanitation, and Brighton Munyai for their assistance in data collection.

ABSTRACT

A limited number of transboundary aquifers (TBAs) in the Southern African Development Community (SADC) region have been subjected to investigations that will improve the hydrogeological understanding of the shared groundwater resource. The Khakhea-Bray transboundary aquifer, shared between Botswana and South Africa, is one of the TBAs that lacks a conceptual understanding of the groundwater systems. Therefore, this study aims to contribute to filling this research gap by conducting a geophysical investigation in the Khakhea-Bray TBA. The study applied the magnetotelluric approach to understanding the factors influencing groundwater occurrence in the dolomite of the Khakhea-Bray TBA.

An ADMT-300S groundwater detectors of the ADMT series products was used to conduct the geophysical survey. This equipment measures the electric potential difference of the subsurface geology for 300 m below the surface measured at a 5 m depth interval. The magnetotelluric geophysical survey was carried out by targeting existing boreholes with accessible drilling data within the TBA. The survey stations were spaced at 3 to 5 Km intervals in areas with no boreholes. The integrated analysis approach used lithology data and water strike information from seven boreholes. The lithology data provided insight into the subsurface geology of the study area. The water strikes information of boreholes was used to calibrate the geophysical data of the dolomite aquifer system. This was done to identify the electrical properties of the water strike zones within the aquifer system, establishing the factors influencing groundwater occurrence. The geophysical data from survey stations on the same transverse line was processed into electric potential difference cross section models using RockWorks 2021 software. The distance weighting anisotropic method was applied to interpolate the data between the survey stations.

The results show that the weathered-fractured zone is the main factor influencing the groundwater occurrence in the dolomite rock. The weathered-fractured zone was characterized by electric potential difference values varying between 0.02 mV to 0.065 mV. The weathered fractured zones in the dolomite were observed at shallow depths ranging between 7.5 m and 90 m. These dolomite aquifers were confirmed by the water strikes of the existing boreholes that were drilled targeting the dolomite aquifer zones. Another zone exhibiting the electric potential difference values ranging between 0.02 mV and 0.065 mV was observed at depths between 165 m and 300 m. The zone below 165 m showing the electric potential difference values between 0.02 mV and 0.065 mV was regarded as an unconfirmed potential weathered-fractured zone that needs to be validated with lithology and water strike data. Since the weathered-fractured zone was identified as the factor for groundwater occurrence in the dolomite of the study area, this suggests that during groundwater exploration for

borehole drilling in the study area, the zones showing electric properties of a weathered-fractured aquifer zone must be targeted to increase the success rate of the borehole.

The developed models showed the subsurface stratigraphy and the potential zones for groundwater occurrence within the transboundary dolomitic aquifer system of Khakhea-Bray TBA. This implies that the MT has the ability to map the aquifers and delineate the subsurface stratigraphic layers in dolomite settings. The models also revealed that the dolomite aquifers are confined, suggesting that these aquifers are less vulnerable to pollution from surface sources. The confined aquifer also suggests that the aquifer is not recharged directly from the top but through preferential flow paths on the dolomite rock surface.

Key Words

Conceptual models; Dolomite aquifer; Electric potential difference; Magnetotelluric geophysics; Transboundary Aquifer

TABLE OF CONTENTS

LIST OF FIGURES

LIST OF TABLES

ABBREVIATIONS

ADMT	Audiomagnetotellurics
MT	Magnetotelluric
LMT	Longer period magnetic
CSAMT	Controlled Source Audio Magnetotelluric
CGS	Council of Geoscience
S	Station number
TBA	Transboundary Aquifer
ORASECOM	Orange Senqu River Commission
NGA	National Groundwater Archive
BH	Boreholes
ANOVA	Analysis of Variance
MS	Mean square
SDGs	Sustainable Development Goals
LVWMA	Lower Vaal Water Management
IDW	Inverse Distance Weighting
DWS	Department of Water and Sanitation

UNITS

Electrical Potential difference	Millivolts (mV)
Frequency	hertz (Hz)
Temperature	Degrees Celsius (ºC)
Current	Ampere (A)
Resistivity	Ohms (Ω.m)
Magnetic flux density	Weber per square meter (Wb/m^2)
Voltage	Volt (V)

SYMBOLS

Ω	Ohms
Ω	Angular frequency
Σ	Conductivity
μ	Magnetic permeability
F	Frequency
Z	Cagniard impendance
B_y B_x	Magnetic field
E_x E_y	Electric field

CHAPTER 1 INTRODUCTION

1.1 BACKGROUND

One of the key international challenges to groundwater sustainable development and management is limited knowledge of the aquifer systems. The conceptual hydrogeological understanding of the groundwater systems has not yet been fully developed at the transboundary aquifers (TBAs) level. This has impeded the cooperative and long-term aquifer development of the TBAs. According to Nijsten et al. (2018), seventy-two TBAs have been mapped throughout Africa. However, only fifteen percent of the TBAs have been subjected to some form of scientific investigations, despite groundwater being essentially needed to achieve the Sustainable Development Goals (SDGs). The Stampriet TBA (UNESCO-IHP, 2016), Tuli Karoo TBA (Gomo & Vermeulen, 2017), and Ramotswa TBA (Altchenko, et al., 2017) in South Africa have all been the research focus that aims to advance our understanding of the hydrogeology of the shared aquifers.

The Khakhea-Bray dolomite transboundary aquifer shared between Botswana and South Africa Figure 1.1 is one of the TBA's that has not been subjected to investigations to try to understand the groundwater systems of the TBA. The groundwater resource in the dolomite aquifers of the TBA plays a significant role in livestock farming, domestic uses, and agricultural activities in areas within the TBA. Therefore, this necessitates hydrogeological investigation of the TBA, which will contribute to the effective management of the groundwater resource. However, this current study is not focused on the whole TBA, but the outcome of the study will contribute to the bigger picture of the TBA. The study focused on the South Africa side of the TBA, which had existing boreholes with readily available data.

The complex nature of groundwater systems calls for scientific tools that can enhance understanding of the subsurface geology hosting groundwater. Geophysics is one of these tools that has been increasingly used to investigate subsurface geology. During geophysical investigations, the subsurface material's geophysical properties, such as electric, magnetic or gravitational properties, are directly or indirectly measured (Rix, et al., 2019). When such

subsurface geophysical data is collected, processed, and analysed, it gives factual information about the physical properties of the rocks hosting groundwater.

The current study employs the magnetotelluric (MT) geophysical approach to obtain the properties of the subsurface. This method has been applied by researchers in several studies and in different geological settings: for deep aquifer exploration in limestone and sand environment (Abderahman & Kotb, 2019), for geophysical investigation of groundwater potential in sedimentary terrain (Kashouty, et al., 2010), to delineate groundwater potential zones in basement terrain (Agyemang, 2020), groundwater exploration in alluvial deposits (Abound, et al., 2014) amongst other examples. This makes the MT a potential approach that can be used in the scientific investigations of the groundwater resource aiding in effective hydrogeological understanding of the aquifers. Therefore, this study also seeks to demonstrate the application of the method in dolomite settings and in a groundwater investigation at TBA level.

1.2 PROBLEM STATEMENT

The Khakhea-Bray dolomite transboundary aquifer is one of the TBAs that has not been subjected to detailed studies to enhance the understanding of the groundwater systems within the TBA (Nijsten, et al., 2018). This has led to the issue of over-abstraction in some areas of the TBA such as Pomfret, Tosca, and Vergelegen areas (Godfrey & van Dyk, 2002). If the groundwater occurrences and the factors that influence the aquifer occurrence are unknown in the TBA, the resource cannot be managed and protected accordingly. Conflicts between the countries that share the aquifers may arise. It is envisaged that the poor groundwater management is due to the lack of conceptual understanding of the groundwater resource system within the TBA.

1.3 AIM AND OBJECTIVES

The study aims to investigate groundwater occurrence within the Khakhea-Bray dolomite transboundary aquifer through the audio magnetotelluricgeophysical investigation. This research contributes to a larger project funded by JRS biodiversity Foundation through the Southern Africa Development Community-Groundwater Management Institute (SADC-GMI). The bigger project aims to improve the hydrogeological conceptual understanding of the Khakhea-Bray Transboundary aquifer. This research study has the following objectives:

- Understanding the principles and application of the magnetotelluric geophysical method.
- Investigate the relationship between the electric conductivity as measured by the audiomagnetotellurics and the groundwater occurrence in dolomite
- Develop groundwater occurrence models of the study area.

1.4 RESEARCH CONTRIBUTION

The conceptualized understanding of the groundwater resource is critical, particularly at the transboundary level, where managing the resource shared between states is challenging. A better understanding of the groundwater dynamics assists decision-makers in making more informed decisions on managing and protecting groundwater resources. The outcome of this study will provide key insight into understanding groundwater occurrence and the factors that influence the occurrence in the TBA. This knowledge provides a framework for scientifically grounded agreements on the management and governance of the TBA. Groundwater specialists can use the data from this research as baseline data during borehole siting. It provides critical information on the areas that can be targeted for shallow groundwater or deep groundwater aquifers. It also contributes toward addressing the prevalent problem of groundwater scarcity within the study area, as the output of the study is modelled subsurface data showing potential aquifer zones. The study uses an audio magnetotelluric geophysical method which according to literature is not widely used in groundwater investigations. Therefore, the study contributes towards bringing more understanding of the application of this geophysical approach in groundwater studies particularly in dolomite settings.

1.5 SITE DESCRIPTION

1.5.1 Study area

The Khakhea-Bray Dolomite Transboundary Aquifer is situated at the lower Vaal water management area (LVWMA) in the Northwest Province of South Africa. This aquifer is shared between Botswana and South Africa. The transboundary aquifer covers an area of about 25 000 km^2 with a low population density of 1- 10 persons/km^2 (Nijsten, et al., 2018). South Africa has a significant share of the aquifer coverage. The boundary of the Khakhea-Bray dolomite transboundary aquifer presented in Figure 1.1 has been delineated by ORASECOM (2018).

The focus of this study is on the South African side of the dolomite transboundary aquifer. This section of the TBA was chosen as the study area for this research thesis due to the availability of existing boreholes data to calibrate the MT data and the accessibility of some of these boreholes in order to conduct the survey at a very close range to the borehole. The study area is located in the North-West Province in South Africa as shown in Figure 1.1.

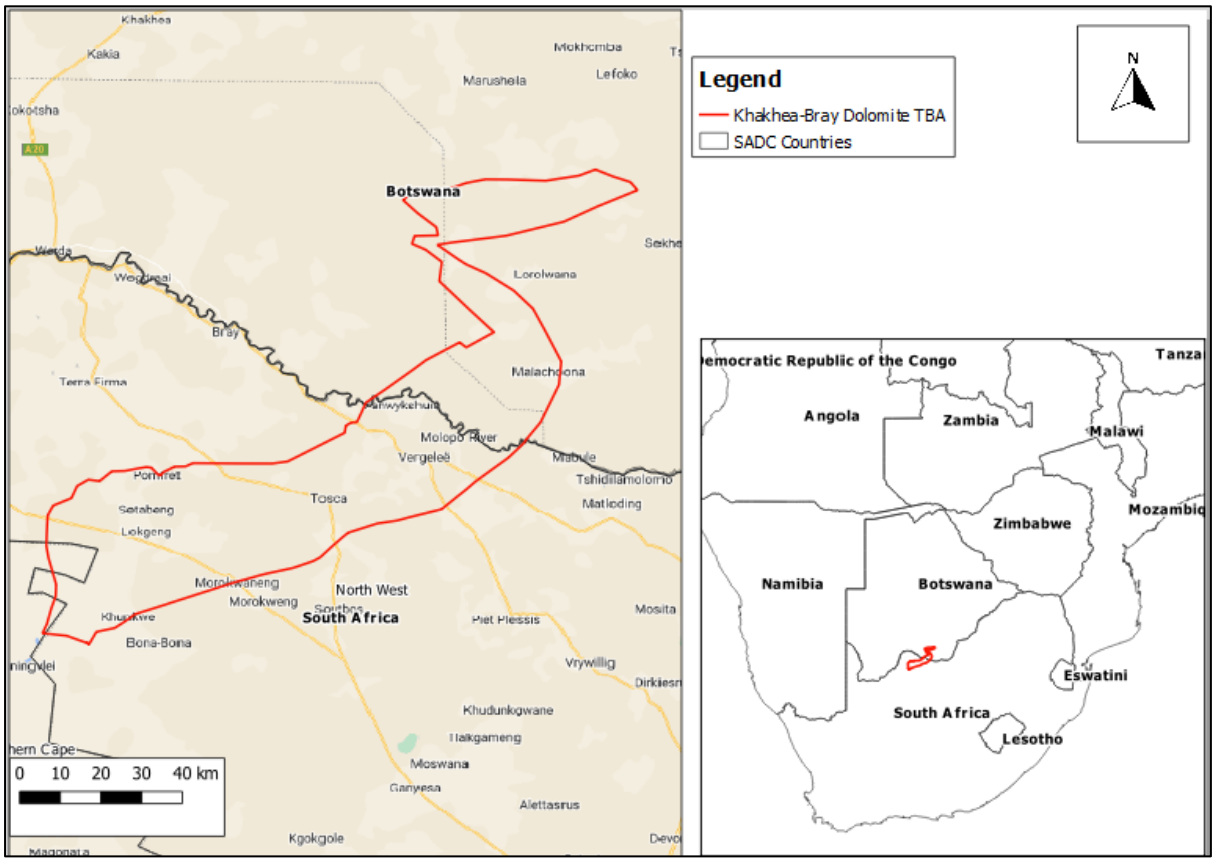

Figure 1.1 Location of the Khakhea-Bray Dolomite Transboundary Aquifer (ORASECOM, 2018)

1.5.2 Climate

The climate of the Lower Vaal water management area is characterized by arid to semi-arid to arid conditions with mean annual precipitation of an average of 350 mm. The rainfall season of the area is unevenly distributed between the months of November to March. The summer months of area occurs from August to March with temperatures ranging between 22 and 34 ˚C. The winter season on the other hand starts from May to July with average minimum temperatures of 2 degrees and average maximum of 20 degrees Celsius (DWAF, 2004).

1.5.3 Vegetation

The vegetation of the study area is characterized by sparsely spread majestic camel thorn trees with clumped grass cover on relatively flat terrain, as shown in Figure 1.2 (a). This vegetation cover is particularly prevalent in areas where the surface is covered with aeolian sand. In areas where dolomites or calcrete outcrops on the surface, there is little grass cover but a predominance of sparsely spaced, thorny camel trees Figure 1.2 (b). This results from the shallow soil cover, which hinders the growth of dense vegetation. Dense vegetation with large trees along river channels are particularly noticeable (Bootsman, 1998).

The study area is mostly privately owned farmland used primarily for livestock farming and wildlife grazing. Subsistence crop farming is occasional in the villages within the study area. This could be attributed to the poor fertility of the Kalahari sandy soil.

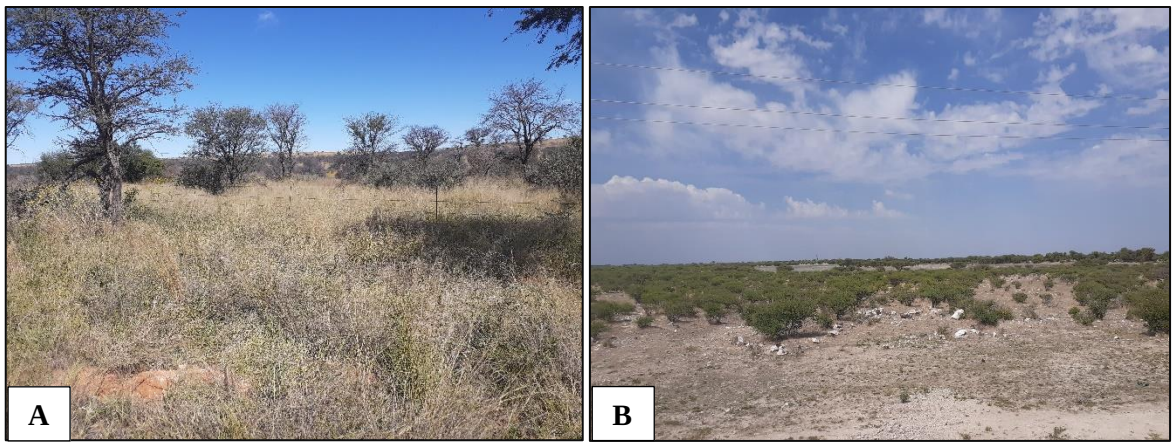

Figure 1.2 Vegetation cover (a) areas where the dolomite is covered by aeolian sand (b) areas where dolomite and calcrete on surface

1.5.4 Topography

The dolomite unit's topography is characterized by relatively flat terrain and gradually elevated areas varying from approximately 1027 to 1231 meters above mean sea level, as shown in Figure 1.3. The elevated areas in the South of the dolomite unit are the escarpments from the highly resistive iron stone formation. The Botswana side of the dolomite is mainly flat at about 1078 mamsl with no visible highland areas. The visibly low-lying areas of about 1027 mamsl are mostly river channels buried by sand deposits.

The study area section within the dolomite unit shows elevated areas in the South-West, where the dolomite outcrops to the surface. The topography appears to be relatively flat towards the

Molopo River with some low-lying areas pointing to river channels. The study area is situated within the Molopo drainage basin. The Molopo River draining on the western highland of South Africa to the East of the sediment-filled Kalahari Basin is the primary active river within the study area with some tributaries (Bootsman, 1998).

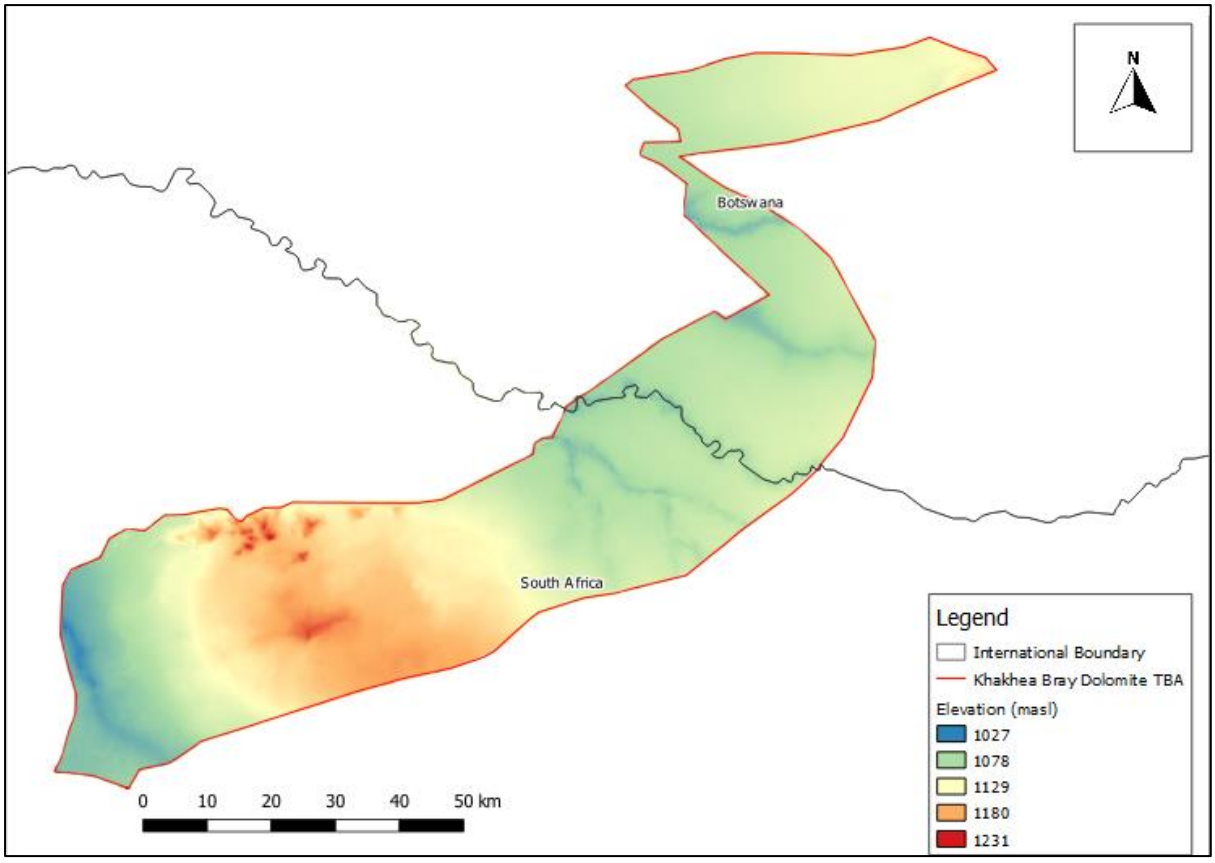

Figure 1.3 Elevation map of the Khakhea-Bray Transboundary Aquifer.

1.5.5 Geology

The geology of the Khakhea Bray Transboundary aquifer is found in the 1:50 000 geology maps of Botswana and South Africa (Figure 7.1 and Figure 7.2, respectively). The study area is part of the Molopo-Nossob basin. A simplified geological map of the basin proposed by Carlsson, et al. (2009) gives the surficial geology cover of the TBA at a regional scale. The map in Figure 1.4 shows that the dolomite unit of the Transvaal Super group is bounded by Archean rocks, and the Kalahari group dominates the Southern part of the dolomite unit.

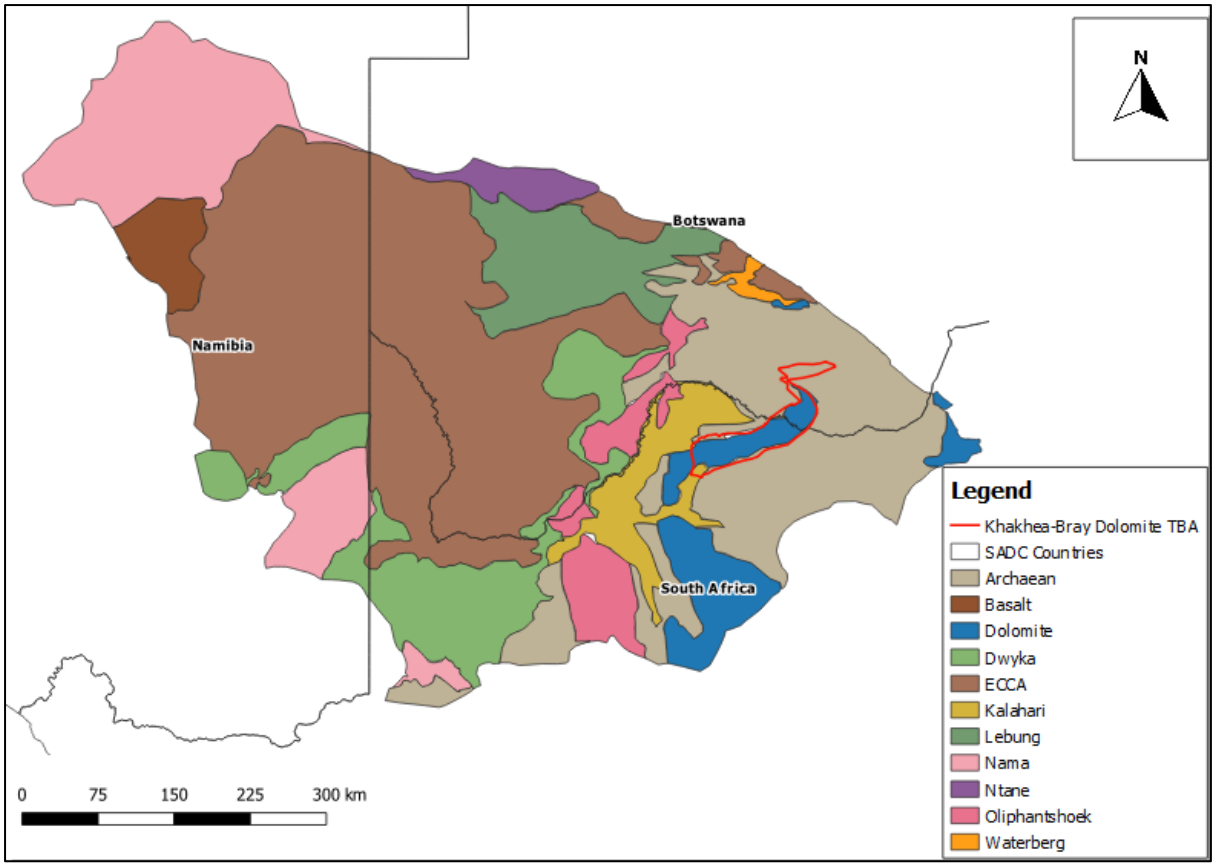

Figure 1.4 The simplified geology map of Molopo-Nossob

The stratigraphy of the study area on the South African side is sourced from the 1: 250 000 maps of the Quaternary map sheets that cover the area; 2522Bray, 2524Mafikeng, and 2622Morokweng. These stratigraphy maps combined give a detailed localized stratigraphy map of the South African side of the study area.

The surficial geology of the study area can be divided into two central stratigraphic units; the Kalahari group and the Ghaap group of the Transvaal super group. The Ghaap group comprises mainly four dolomite formations under the Campbell rand subgroup (Fairfield, Reivilo, Klippan, and Gamohaan) and the Kuruman formation under the Asbestos Hills subgroup. The four dolomite formations are differentiated based on the colour, grain sizes of the dolomite, chert, stromatolite content, and shale interbedding. The stromatolitic dolomites forms outcrops in the region of the study area. These dolomites are intruded by prominent Cretaceous post-Karoo dolerite dykes.

The dolomites formation of the Campbell rand subgroup is overlain in the South-West (Perth / Heingvlei) of the dolomite unit by the bended iron-formation of Asbestos Hill formation

forming prominent high relief features (Godfrey & van Dyk, 2002). This formation is also visible in the North part (Pomfret).

The dolomite formations are overlain by the young deposits of the Kalahari group consisting mainly of four formations (Mokalaneni, Gordonia, Eden, and Lonely). The red-brown Aeolian sand covers most of the study area but most significantly between Tosca and Molopo River. The thickness of the sand becomes bigger (about 120 m), towards the Molopo River, and shallower (12 m) in areas where the dolomite is in shallow depth (Godfrey & van Dyk, 2002). Table 1.1 summerizes the lithostratigraphic units of the study area of the South African side of the TBA.

Table 1.2 The lithostratigraphic units of the study area

Era	Supergroup	Group	Subgroup	Formation	Description
Cretaceous to recent	Kalahari			Mokalaneni	Calcrete, Calcareous gravel and grit, siltstone, and indurated pan sediments.
				Gordonia	Aeolian sand (cover sands and sand dunes)
				Eden	Tuffaceous calcrete, hardpan calcrete, calcrete conglomerate and gravel
				Lonely	Conglomerate, sandstone, siltstone, limestone, calcrete, dolocrete.
Precambrian	Transvaal	Ghaap	Campbell Rand	Fairfield	Brown/stromatolic dolomite, chert; light grey, chert-grey, chert rich dolomite in top part
				Reivilo	Grey, medium-grained/ stromatolitic dolomite, chert; brown chert rich dolomite in the top part.
				Klippan	Dolomite and shale
				Gamohaan	Dolomite with interbedded chert and shale towards the top.

				Kuruman Asbestos Hills	Banded iron formation, riebeckite-amphibolite, chert, minor minnesotaite and crocidolite.
				Dani lskuil	Jaspilite, iron formation, chert, mudrock, quartzite
			Koegas	Ponnetjie	Quartzite, jaspilite
Cretaceous					Dolerite Intrusion and dykes

1.5.6 Hydrogeology

The groundwater occurrence is associated with the karstic aquifers of the dolomite formations of the Campbell rand subgroup. Carlsson, et al., (2009) defined the aquifer type of this dolomite unit to be fractured, karstified, and fissured with medium (1.8-7.2 cubic meters/hour) to high (>7.2 cubic meters/hour) borehole yield. The highest potential yield of the dolomite unit has been identified to be on the South Africa side of the dolomite transboundary. Godfrey & van Dyk (2002) reveals that this high-yielding zone of the dolomite unit is influenced by brecciated and leached zones along faults, fracture zones linked to the dolerite dykes and sills intrusions on the dolomite, and contact zones between dolomite, shale, and the banded iron stone.

CHAPTER 2
LITERATURE REVIEW

This chapter discusses the theoretical background of the magnetotelluric (MT) geophysical method on which the succeeding chapters are based. The governing equations on the principles of how the Earth's apparent resistivity is measured are presented in section 2.1. This chapter also covers data processing (2.2), data presentation (2.3), data interpretation (2.4) strengths and weaknesses (2.5) of the magnetotelluric method, and examples where the magnetolluric approach has been successfully applied (2.6).

2.1 THE PRINCIPLES OF THE MAGNETOTELLURIC METHOD

The magnetotelluric (MT) method is an electromagnetic geophysical technique. This method uses naturally occurring, time-varying electromagnetic waves to study the electrical properties of the subsurface at depths ranging from tens of meters to tens of kilometers. The method commonly utilizes electromagnetic fields in the frequency range lying between 10^{-4} Hz and in the frequency spectrum (Vozoff, 1990).

The low frequency range of less than 1 Hz originate from interaction between the solar wind in the ionosphere with the earth's magnetic field. This frequency range allows the investigation of the electrical properties of the Earth in the deep crustal zones. The high frequency range (>1Hz) natural magnetic waves on the other hand, originates from electrical storms. These waves enable the investigation of the subsurface electrical properties at shallow depths (the upper crust). The MT method's depth of investigation is predominantly determined by the depth of penetration of these waves (Simpson, 2005).

However, artificial fields in the range of 10 to 100 Hz are used in areas where these naturally occurring electromagnetic waves are weak. This type of MT method that utilizes artificial magnetic fields is known as the controlled source audio magnetotellurics (CSAMT) (Vozoff, 1990). .

MT method indirectly measures the electric properties of the Earth through direct measurements of the electric (E) and the Earth's magnetic field (H) to estimate the subsurface' s resistivity or apparent resistivity. The H_x, H_y, and H_z are obtained by measuring the Earth's surface magnetic field in orthogonal directions. E_x and E_y are obtained by measuring the electrical field component in the two horizontal directions. The E_z is zero, hence it is not

measured (Simpson, 2005). The electric field component is generally measured by the electric field sensor in the form of electrodes and the magnetic field is measured the magnetic field in a field setup that illustrated in Figure 2.1. In other magnetotelluric equipment, the magnetic field is measured using induction coils which are normally buried in the ground during the data collection. Burring the coils in the ground reduces noise from the sun or wind which negatively affect the true readings of the MT method.

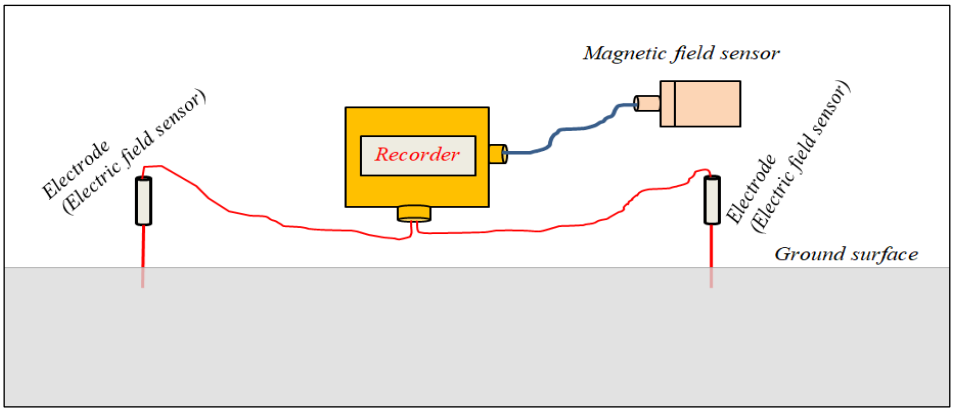

Figure 2.1 A typical field setup of the Magnetotelluric components (Gomo, 2021)

The behaviour of the electric field (E) and magnetic field (H) with respect to change in time is defined by Maxwell's equations. Maxwell's equations, given in Equations 2.1 to 2.4 in the differential form, are imperative in understanding the basics of electromagnetism (Telford, et al., 1990) (Tikhonov, 1973).

$$\nabla \mathrm{x}\, \mathrm{E} = -\frac{\partial \mathrm{B}}{\partial \mathrm{t}} \tag{2.1}$$

$$\nabla\, x\, B = \mu_0 \left(J + \frac{\partial D}{\partial t}\right) \tag{2.2}$$

$$\nabla \cdot E = \frac{\rho}{\varepsilon_0} \tag{2.3}$$

$$\nabla \cdot \mathrm{B} = 0 \tag{2.4}$$

Where E is the electrical field strength (V/m), B denotes the magnetic flux density (T (teslas)), μ_0 is the magnetic permeability of free space = 4π x 10^{-7} H/m (Tm/A), J is the conduction current density, ρ is known as the charge density, D is the displacement current density, and ε_0 is the permittivity of free space = 8.85 x 10^{-12} (F/m).

Equation 2.1 is Faraday's law which describes the phenomenon of induction, Equation 2.2 is Ampere's law, and Equation 2.3 is Gauss's law.

Another set of equations known as the constitutive equations are given in Equations 2.5-2.7 in their simplest form. These equations define the relationship between auxiliary and electromagnetic fields in relation to the electrical response of materials.

$$D = \varepsilon_0 E \tag{2.5}$$

$$J = \sigma E \tag{2.6}$$

$$B = \mu_0 H \tag{2.7}$$

Where σ is specific conductivity, J is conduction current density, B is magnetic flux density, D is the displacement current density, and H is the magnetic field strength.

Maxwell's equations (Equations 2.1 to 2.2) can be combined with the constitutive relations and simplified further to give rise to Equations 2.8 and 2.9. These equations describe the behaviour of electric and magnetic fields in the time domain.

$$V^2 E - \mu\varepsilon \frac{\partial^2 E}{\partial t^2} - \mu\sigma \frac{\partial E}{\partial} = 0 \tag{2.8}$$

$$V^2 H - \mu\varepsilon \frac{\partial^2 H}{\partial t^2} - \mu\sigma \frac{\partial H}{\partial t} = 0 \tag{2.9}$$

The above Equations 2.8 and 2.9 can further be simplified to Equations 2.10 and 2.11 by applying the assumption that displacement currents are less than conduction currents so that $\varepsilon << \sigma$,therefore, ε is equated to 0, resulting in pure wave equations for real earth materials. Equations 2.10 and 2.11 are also diffusion equations defining the diffusive behaviour of the

electromagnetic waves in real earth materials. These equations uniquely define the MT method compared to the other geophysical techniques.

$$V^2E - \mu\sigma\frac{\partial E}{\partial} = 0 \tag{2.10}$$

$$V^2H - \mu\sigma\frac{\partial H}{\partial t} = 0 \tag{2.11}$$

The MT technique records varying frequencies and periods for both the electrical and magnetic fields: 400Hz (0.0025s) to 0.0001Hz (10 000s). However, another type of MT technique known as Audio magnetotelluric (ADMT) is used to record much higher frequencies up to 10 kHz. For more extended periods of up to 100 000s are recorded with longer period's magnetotelluric (LMT) (Vozoff, 1990) (Babarinde & Nwankwo, 2020**)**.

Resistivity is generally derived from the resistance and potential difference or resultant voltage. This parameter governs the amount of current that passes when a potential difference is created. The resistivity (ρ) relates to the resistance (R) through equation 2.12 (Al-Amri, 2018), where the resistance is dependent on the length (L), area (A) and resistivity of the material.

$$R = \rho\frac{L}{A}, where\ \rho = \frac{VA}{IL} \tag{2.12}$$

The apparent resistivity is defined as the average of the true resistivity of the Earth's subsurface under the premise that Earth is homogeneous (Hersir, 2015). The apparent resistivity value can be calculated from the voltage (V) and current (I) given by:

$$\rho_a = K\frac{V}{I} = KR \tag{2.13}$$

Where K is the geometric factor, V and I are the voltage and current respectively.

The apparent resistivity is explicitly defined by Reynolds (1997), who connected it to frequency and the impendence. The apparent resistivity equation is given by Equation 2.14.

$$\rho_a = \frac{0.2}{f}\left|\frac{E_x}{B_y}\right|^2 = \frac{0.2}{f}\left|\frac{E_x}{H_y}\right|^2 = \frac{0.2}{f}|Z|^2 \tag{2.14}$$

Where E_x is an electric component (nV/ Km), B_y is the magnetic components (nT), f is frequency, and Z is the Cagniard impedance given by Equation 2.15. The electric and magnetic field ratio is an impendence used to derive the Earth's subsurface resistivity. This ratio can be expressed:

$$Z = \frac{E_x}{H_y} \tag{2.15}$$

Where E_x and H_y are the orthogonal components of the electric field and magnetic field, respectively.

The skin depth (Equation 2.16) for the MT approach relates to the apparent resistivity and the frequency. Therefore, the depth of investigation is derived from

$$\delta(\omega) = \sqrt{\frac{2}{|k^2|}} = \sqrt{\frac{2}{\omega \mu \sigma}} \approx 500\sqrt{\frac{\rho}{f}} \text{ (meters)} \tag{2.16}$$

Where ω is angular frequency, σ is conductivity, μ is magnetic (Abderahman & Kotb, 2019).

Resistivity is a common parameter in most magnetotelluric studies. This can be attributed to the fact that the resistivity was a common parameter in the years of development of the approach. Hence, most studies conducted using the MT method reports the electric properties of the Earth using the resistivity.

Some magnetotelluric equipment only measures the electric component of the electromagnetic field. This equipment then characterizes the subsurface electric properties using the electric potential difference parameter. The electric potential difference (ΔV), also known as voltage, is generally defined as the work or energy required to move a charge from the point of higher potential to the point of lower potential in the electric field. In the field during data collection the energy required to move a charge from one electrode to the other is measured.

This intrinsic electric property of the Earth's material is not so common in the magnetotelluric studies mainly because the resistivity has been perceived as the traditional way of estimating the electric property of the subsurface.

A study conducted by Abderahman & Kotb (2019) demonstrate that the electrical potential difference can be equally used to estimate the subsurface electrical properties of the subsurface when the MT approach is applied during groundwater studies. This is because from the Ohms law it can be deduced that the electrical potential difference is directly related to the

subsurface's electric resistivity, making it another significant electric property. According to a recent study by Gomo (2023), the electric potential difference parameter is sufficient to examine groundwater potential zones and further define vertical geological changes.

The electric potential difference (V) can be derived from Ohm's law Equation 2.17, which states that the current through a conductive material is directly proportional to the voltage.

$$V=IR \tag{2.17}$$

Where V is the voltage (Volts), I is the current (Amp), and R is the resistance (ohm).

The electric potential difference can further be expressed as the work done to move charges between two points divided by the charge (Sakindi, 2012).

2.2 DATA PROCESSING

The recorded data from each of the magnetotelluric stations consist of two electric field components and three magnetic field components which are used to estimate the subsurface electric properties and related measured frequency domain functions. As shown in Figure 2.2, the raw data must be subjected to step-by-step processing stages such as power spectrum analysis and data filtering before such information may be retrieved. Because of the increase in computer capacity, MT's data collecting, and processing stages have greatly improved. This has resulted in MT tools being equipped with processing software such as SSMT 200 software and ACQ24 package subsequently eliminates the need for manual step-by-step processing (Abound, et al., 2014) (Handush, 2018). This also allows real-time data processing in the field; hence the data quality can be assessed during the data collection.

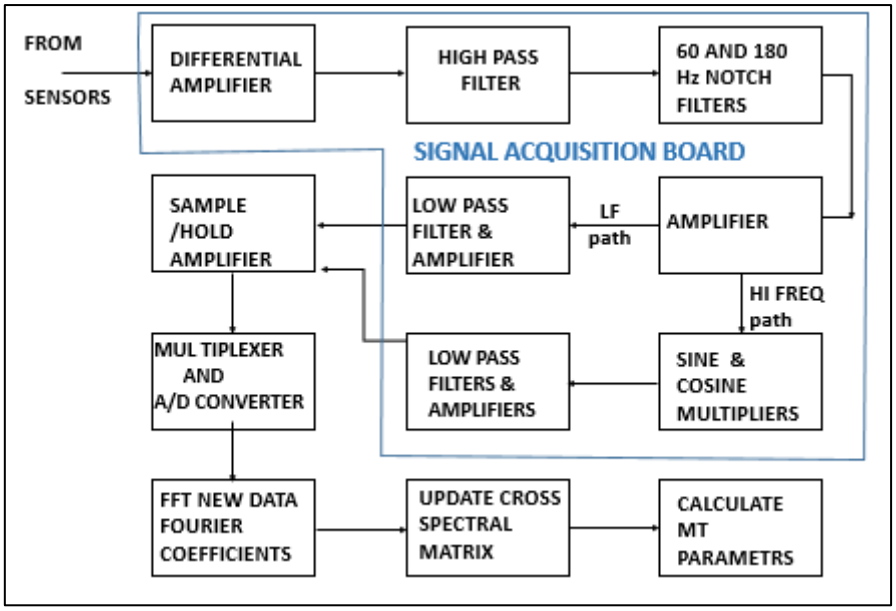

Figure 2.2 A flow diagram showing the wide band MT with computerized data processing (Carlsson, et al., 2009)

During the data processing stage, the recorded time series data is transformed to the frequency domain by applying Fourier transformation, where the electric and magnetic fields data is converted from the time domain to the frequency domain. This transformation primarily makes it easier to analyse the MT impedance data. Several mathematical steps are involved during the data transformation (Hersir, 2015). Equations 2.8 and 2.9, which define the electromagnetic field in the time domain, can be transformed to Equations 2.18 and 2.19 using Fourier transformation. These equations then describe the electric and magnetic field in frequency domain.

$$\nabla^2 E^* + (\mu\varepsilon\omega^2 - i\mu\sigma\omega)E^* = 0 \qquad (2.18)$$

$$\nabla^2 H^* + (\mu\varepsilon\omega^2 - i\mu\sigma\omega)H^* = 0 \qquad (2.19)$$

Where i the imaginary and the star is a distinguishing feature between the frequency and time domains. The Equations 2.18 and 2.19 can also be expressed in terms of the wave number (k) which is equal to the term in brackets.

The MT data processing includes static shift correction, commonly known as MT data static distortion. The unevenness of the Earth's surface where the MT data is recorded is frequently the cause of distortion. The static shift on the MT data can be visually inspected on phase shift

curves, where the electrical properties data is plotted against frequency data sets. The curves with a static shift are usually shifted from their correct positions (Orange, 1989). Several ways have been proposed and successfully implemented to correct the shift in MT data. This includes using data processing algorithms, and data obtained by other geophysical methods such as electrical resistivity tomography (ERT) (Singarimbun, et al., 2017) (Delhaye, et al., 2016). Topography information can be considered within the inversion process to eliminate the need for static shift correction (Fuentes-Arreazola, et al., 2021).

Dimensionality analysis is another MT data processing stage performed prior to MT modeling. This is mostly done to ascertain the subsurface resistive structure's dimension (1D, 2D, and 3D) and the orientation of the underlying substructures. Swift skew, Bhar's skew, normalized weights, phase tensor (PT) analysis, and Wall's rotational invariant approach have all been used to estimate subsurface dimensionality from MT data. A detailed discussion of these techniques is documented by Kumar, et al. (2021).

The inversion and modeling process is a critical step for data processing that yields the true distribution of the Earth's electrical properties as a function of depth from the frequency domain data. This can be achieved through forward data modelling and inversion processes. Several data inversion and modeling techniques have been successfully used in MT data. One-dimensional forward models, one-dimensional continuous inverse, one-dimensional analytic inverse, two-dimensional forward and inverse, and three-dimensional forward models are examples of these techniques (Orange, 1989). In 1D modelling, it is assumed that the Earth's subsurface is horizontally layered, and the resistivity of the Earth's material only changes vertically with depth. In 2D modelling, electric properties varies with depth, and in one lateral direction, with the other directions remaining constant and this is regarded as the standard for data interpretation. In 3D modelling, the electric properties of the earth materials is allowed to vary in all the orthogonal directions (Hersir, 2015).

To improve the data quality, some studies conducted by Unsworth, et al. (2005), Amatyakul, et al. (2021), and Fuentes-Arreazola, et al. (2021) employed the remote reference technique suggested by (Goubau, et al., 1978). This technique necessitates the cross-correlation of MT data obtained simultaneously at the study site, which is most likely to be located near noise sources, and data recorded at stations free of EM noise, which is typically located hundreds of meters to kilometers away from noise sources. The apparent resistivity curves of unprocessed MT data are often inconsistent. This is caused by reduced resistivity, particularly in the

frequency regions between 10 and 0.1 HZ, which are typically regarded as shallow conductors. In order to achieve smoother curves and remove the reduced resistivity in the process, the remote reference technique helps remove the inconsistent patterns in the apparent resistivity curves (Unsworth, et al., 2005).

2.3 DATA PRESENTATION

Processed MT data in the form apparent resistivity or electric potential difference is often plotted in graphs on excel as individual stations showing the variation of the electric parameter with depth. This enables better visualization of the MT data. This is a straightforward and practical way of presenting the resistivity or electric potential difference profile of each station. This data display strategy, however, becomes difficult when data is collected over a greater distance. Pseudo-section data plots can be created using a variety of applications, including Zonde MT and Rockworks, to display large volumes of MT data. These applications produce an ultimate contoured image of subsurface resistivity distribution. When the data is well presented, data outliers due to noise or faulty equipment can easily be identified by unusually low or high apparent resistivity (Orange, 1989).

2.4 DATA INTERPRETATION

In general, the low resistivity means that electrons can easily flow through the material. Likewise, the low electric potential difference suggest that low amount of work is required to move a charge from one position to another. Therefore, the electric potential difference is directly proportional to resistivity hence both can be used independently to characterize the electric properties of the subsurface. The relationship between geological materials and their resistivity properties was discussed by Loke (1999) and is presented in Figure 2.3. This prior knowledge is crucial for modelling and data interpretation. The resistivity values of the subsurface vary depending on the geology type, the degree of fracturing or weathering state of the rocks, and saturation of the subsurface. Sedimentary rocks, clay soils, and water have noticeably lower resistivity values than igneous and metamorphic rocks, which appear to have higher resistance values. Fractures and groundwater in rocks cause the bulk resistivity of the rock to decrease, resulting in low resistivity zones, which are commonly linked with aquifer zones (Loke, 1999).

Table 2.1 Electrical resistivity of geological material (Loke, 1999)

Material	Resistivity (Ω.m)	Conductivity (Siemen/m)
Igneous and metamorphic rocks		
Granite	5×10^3 - 10^6	10^{-6} – 2×10^{-4}
Basalt	10^3 - 10^6	10^{-6} – 10^{-3}
Slate	6×10^2- 4×10^7	2.5×10^{-8} – 1.7×10^{-3}
Marble	10^2 -2.5×10^8	4×10^{-9} – 10^{-2}
Quartzite	10^2 – 2×10^8	5×10^{-9} – 10^{-2}
Sedimentary Rocks		
Sandstone	8 - 4×10^3	2.5×10^{-4} – 0.125
Shale	20 – 2×10^3	5×10^{-4} – 0.05
Limestone	50 – 4×10^2	2.5×10^{-3} – 0.02
Soils and waters		
Clay	1 - 100	0.01 – 1
Alluvium	10 - 800	1.25 – 10^{-3} – 0.1
Groundwater (fresh)	10 – 100	0.01 – 0.1
Sea water	0.2	5
Chemicals		
Iron	9.07×10^{-8}	1.102×10^7
0.01 M Potassium chloride	0.708	1.413
0.01 M Sodium chloride	0.843	1.185
0.01 M acetic acid	6.13	0.163
Xylene	6.998×10^{16}	1.429×10^{-17}

When analysing MT data, detailed borehole logs data are crucial. The log information can be correlated with the MT data to image the subsurface material and reveal remarkable information about the subsurface.

In most MT applications, low resistivity or low electric potential difference values are associated with possible groundwater occurrence zones in groundwater studies and prospective geothermal reservoirs in geothermal studies. Experience in MT data interpretation and a clear understanding of the MT concept are prerequisites for effectual analysis and interpretation of MT data.

2.5 STRENGTHS AND WEAKNESSES OF THE MT METHOD

Like other geophysical methods, the MT method has its strengths and limitations. The wide application of this method in varying geological complexities and industries has made it easier to identify the MT strengths and drawbacks. This is crucial information about the method because it helps with the technique's future improve and ensures efficient application of this geophysical approach (Orange, 1989) (Babarinde & Nwankwo, 2020). Historically, the MT tools had limitations such as constrained field access because the devices were installed in vehicles and powered by generators. The newly developed magnetotelluric tools are portable and automated with advanced data processing technologies. Orange (1989) has documented a list of strengths and weaknesses of this technique.

2.5.1 Strengths

The magnetotelluric method can be applied in complex environments where other geophysical techniques, such as the seismic method, gravity, and other electromagnetic methods, have failed to image the subsurface effectively. Such complex environments include ice-covered regions, basalt-covered areas, and high-velocity areas. As a result, in such circumstances, the MT approach has been considered as a complementary geophysical method (Orange, 1989) or a lead method for selecting the appropriate placement of seismic survey lines.

The MT method's sensitivity to conductive anomalies like groundwater-bearing zones and geothermal energy sources has resulted in this method being the most preferred geophysical technique for resource exploration. Because the MT methods employ natural signal sources, they are considered less expensive to operate than other geophysical methods, such as controlled source EM methods.

The MT method can uniquely probe tens of meters to kilometres through the crust and upper mantle with limited effort in terms of costs and labour. This has resulted in an enormous increase in the application of the method in different industries, such as minerals exploration (hydrocarbons, water resources), mining, and geotechnical industries.

The MT data may be easily matched with drill log data to provide subsurface information. When the MT data are correctly analysed and interpreted, they can provide essential and unique information on the geological features beneath the surface.

2.5.2 Weaknesses

Despite being widely applied and having undergone advancements over time, the magnetotelluric approach still has several shortcomings. One of these downsides is the low resolution of the data in comparison to ERT data. Some MT devices only record data at intervals of 5 or 10 meters in depth, which leaves out some crucial information between intervals. Larger station spacing in most MT systems also contributes to low lateral resolution.

The magnetotelluric approach is based on electromagnetic principles, hence an electrical properties contrast is required to obtain representative data. This becomes a limitation where the electrical characteristics of the formation are comparable.

Secondary data, such as data from other geophysical techniques, drill logs, or geological knowledge, are necessary for a better interpretation of the MT data. The apparent resistivity of subsurface materials is assessed using an electromagnetic field; thus, it is vulnerable to EM sources.

2.6 MAGNETOTELLURIC EXPLORATION APPLICATIONS

This section provides an overview of case studies from the literature that shows where the magnetotelluric technique has been in applied in different studies. These studies give insightful discoveries on the strength and weaknesses of the MT technique, which are covered in section 2.5 of this chapter.

The magnetotelluric method's applicability has significantly evolved over the years. Between the years 1960 and 1970s, the MT method was widely applied in gas and oil industries for exploration purposes (Zhdanov, 2010). Due to advancements in processing power, the applicability of this technology was eventually broadened to encompass aquifer exploration, geothermal studies, and mineral minerals exploration.

2.6.1 Geothermal exploration

The magnetotelluric method is one of the leading geophysical methods that can effectively delineate geothermal prospects, outline a production field, and locate suitable drilling targets. This method can examine the resistivity properties of rocks hosting geothermal systems. These rocks are often susceptible to faulting and fracturing activities, which are used as pathways for geothermal fluid circulation in the rock matrix. The resistivity of these rocks is largely

influenced by the temperature and salinity of the geothermal fluid, which relates to geothermal activities. Therefore, the presence of high temperature geothermal zones in the subsurface creates a resistivity contrast with surrounding rocks. In several studies, the high temperature geothermal zones are identified by a high resistivity zone surrounded by a low resistivity zone (Georgson, 2013).

During geothermal investigations, the MT method is often used in conjunction with other geophysical techniques such as the ERT and TEM (Transient Electro-Magnetic) approach. These methods are primarily applied to explore shallow depths of the subsurface at high resolution yielding detailed information which can be used as a preliminary findings to improve the interpretation of the MT data at deeper depths (Singarimbun, et al., 2017) (Georgson, 2013). ERT data can further be used to correct static distortion of the MT data, hence improving data quality (Amatyakul, et al., 2021)

Several geothermal studies have been conducted with the application of the MT method to investigate geothermal zones in various parts of the world, for example, in China (Zhang, et al., 2014); (Wu, 2018); (Bai, et al., 2001); (Pham, et al., 1995); (Han, et al., 2019)); in Thailand (Amatyakul, et al., 2021)(Handush, 2018).

A resistivity cross section from the Rehai geothermal field near Tengchong, southern China, is shown in Figure 2.3. It shows high resistivity (200 – >1000 ohm.m) in the upper most kilometres and a dome –like structure of low resistivity (<10 ohm.m) zone between 6 and 13 Kilometres. This low resistivity zone is surrounded by geological material with a significantly higher resistance (Bai, et al., 2001) .

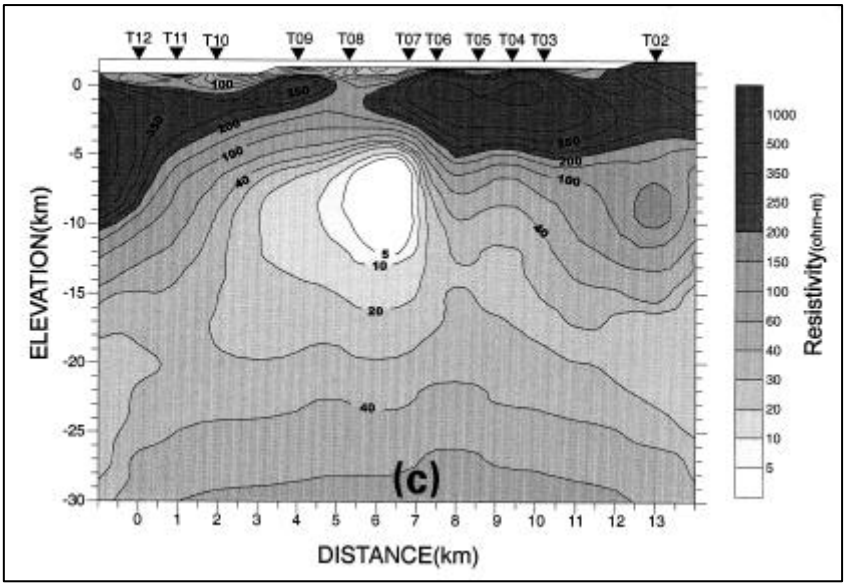

Figure 2.3 MT cross section from Rehai geothermal field (Bai, et al., 2001)

2.6.2 Hydrocarbon Investigations

In the search for hydrocarbons, particularly natural gases and petroleum, the MT method plays an incomparable role. This method is often employed during the field discovery and evaluation stages of hydrocarbon explorations to improve the characterization of the hydrocarbon's reservoirs, especially in complex geological environments. The MT method does not only help with imaging greater depths of the subsurface but also in the estimation of bulk fluid properties, such as the porosity of rocks in the subsurface. Porosity is an important parameter that contributes to estimating the occurrence of hydrocarbons. The porosity parameter can be connected with depth to assess the porosity/depth trends, which give profound information about the age and timing of petroleum emplacement (Ganat, 2020). In complex geological environments where the seismic method fails to give interpretable results, the MT method is applied to complement the seismic method which has always been the preferred method (Unsworth, et al., 2005). Such environments include areas where the high resistivity overlies low resistivity layers (Patro, 2017).

There are several hydrocarbon explorations studies where the MT method has been successfully applied. This include, an example in Japan by Mitsuhata, et al. (1999); in Iraq (Mansoori, et al., 2015) in Guinea (Christopherson, 1991); (Zhang, et al., 2014).

2.6.3 Minerals Exploration

The electromagnetic methods in particular the MT method is generally applied to investigate the subsurface variability in resistivity properties caused by variation in lithology, alteration processes, temperature, and fluid properties. The MT method has been widely applied in the explorations of minerals to delineate deeply buried ore bodies of minerals such as silicate minerals, copper, gold, lead, silver, uranium, and iron deposits (Kalscheuer, et al., 2017; Tuncer, et al., 2006; Zhang & Chouteau, 1991; Zeng, et al., 2020; Heinson, et al., 2006; Hubert, 2016). The deposition of ore bodies is often associated with intrusive activities such as rock alteration resulting in rock fracturing, and shear zones. This result to a resistivity contrast between the ore body, mineralization rock, and the wall rock areas. This then enables the effective application of this method to delineate zones of ore deposits. The resistivity values of the ore deposits are often characterized by relatively low resistivity than that of the wall rock area.

Figure 2.4 shows a resistivity profile from a study conducted in Tuokuzibayi gold deposit located in the Altay Fold Zone of Xinjiang in north western China. The processed MT results shows two low resistivity (<150 ohm.m) anomalies denoted as B and C on the 2D resistivity profile. These zones are representation of a gold ore body extending up to 400 m at zone B.

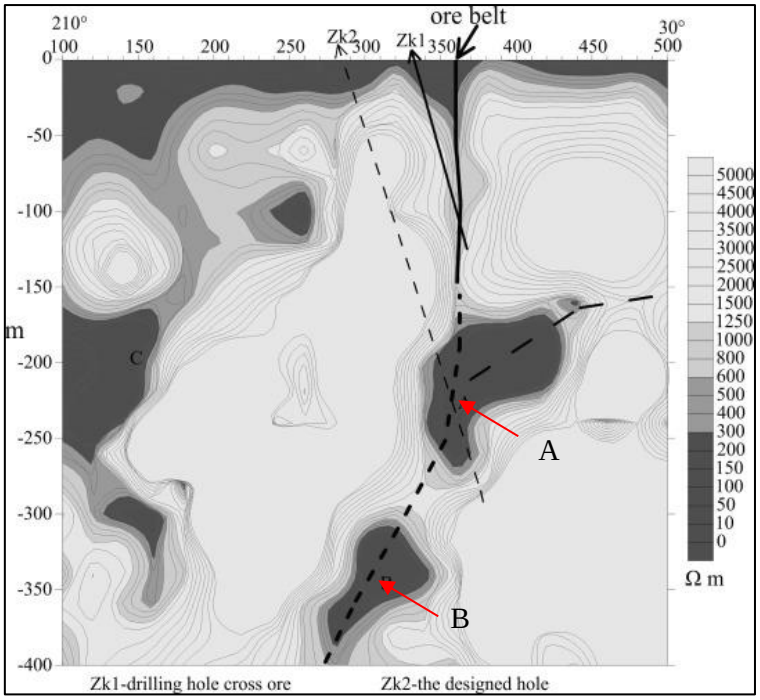

Figure 2.4 2D resistivity model of the 95th exploration line of the Tuokuzibayi gold deposit located in the Altay Fold Zone of Xinjiang in north-western China (Zeng, et al., 2020)

2.6.4 Groundwater studies

The magnetotelluric method has been effectively used for aquifer exploration and assessment in Ghana, Mexico, and Saudi Arabia and other countries due to its unique capacity to probe hundreds of meters in the subsurface, hence enabling the exploration of deep aquifers. This method has a significant role in groundwater studies such as borehole siting activities (Agyemang, 2020), estimation of effective porosity (Giroux, et al., 1997) and aquifer characterization (Ailes & Rodriguez, 2015; Sumanovac, 2012; Abderahman & Kotb, 2019 Abound, et al., 2014). All these publications reported the electrical properties of the subsurface in apparent resistivity. The use of the electric potential difference in groundwater studies is rare in international publications. Abderahman & Kotb, (2019) and Gomo (2023) are the two recent groundwater studies where the electric potential difference was used to characterize the electric properties of the subsurface during groundwater investigation. The MT method is generally effective for deep aquifers, especially in locations where groundwater is a challenge. Zaher, et al. (2021) suggests that the MT method can sometimes be used in conjunction with other geophysical techniques to investigate shallow aquifers at high resolution. In MT methods, the groundwater preferential zones (fracture zones, faults) are often characterized by low resistivity values embedded in relatively high resistivity materials. Remarkable information such as the

aquifer thickness and depth can be derived from MT processed data. When it comes to drilling planning, this information is crucial because the prospective borehole location and projected depth are the key takeaways from the MT approach when used in aquifer exploration and assessment. The aquifer thickness and depth are also vital information for aquifer modelling.

In another study by Giroux, et al. (1997) the MT data was further used to estimate the effective porosity of the various geological mediums. This was done on the bases that the resistivity of the Earth's material is a function of effective porosity. Archie's formula, which relates resistivity to effective porosity and pore fluid resistivity was used to achieve this initiative as shown in Equation 2.20.

$$\rho_s = a\rho_w \emptyset_e{}^{-m} S_s{}^{-2} \tag{2.20}$$

Where ρ_s is the effective porosity, a and m are empirical factors, S_s is saturation, ρ_w pore fluid resistivity, and $\emptyset_e$ effective porosity.

CHAPTER 3
MATERIALS AND METHODS

This chapter gives an overview of the research strategies applied to achieve the study's aim and objectives. The investigation in the Khakhea-Bray dolomite transboundary aquifer used existing boreholes data, previous studies, and fieldwork specific to this research study. This chapter is subdivided into three sections: description of the study area, field data collection, and data processing and evaluation. Each section includes an extensive discussion of the activities that were carried out.

3.1 DATA COLLECTION

3.1.1 Desktop study

The first implementation phase of the research project involved a desktop study. The purpose of the desktop study was to outline the boundary of the study area and to explore databases with historical drilling data for boreholes located within the study area. The boundary of the Khakhea-Bray transboundary dolomite aquifer was sourced from the ORASECOM (2018).

The Council of Geoscience (CGS) and the Department of Water and Sanitation (DWS) were consulted to gather information on existing boreholes within the study area. The DWS, through the National Groundwater Archive (NGA), provides data on existing monitoring boreholes. The data extracted from NGA included boreholes coordinates, water level data, water strike data, and lithology logs for the existing boreholes within the study area. The CGS was consulted for logging cores from exploration boreholes near the study area.

During the desktop study, reports from previous studies conducted in areas that are part of the study area were also collected. These publications provided background knowledge on the hydrogeology and geology of the region. The following reports made a significant contribution to a better understanding of the study area:

- The evolution of the Molopo drainage by Bootsman (1998),
- The review of the Molopo-Nossob basin by ORASOCOM (2009),
- The reserve determination of the Pomfret-Vergelegen dolomite aquifer by Godfrey & van Dyk (2002).

3.1.2 Geological data

The regional geology of the Khakhea-Bray dolomite transboundary aquifer was sourced from the South Africa (Figure 7.2- Appendix) and Botswana geological maps (Figure 7.1-Appendix) at a scale of 1:50 000 and the simplified Molopo-Nossob geological map. The 1:25 000 geological maps of the 2522 Bray area (Figure 7.3- Appendix), 2524 Mafikeng area (Figure 7.4- Appendix), and 2622 Morokweng area (Figure 7.5- Appendix) served as a source for more detailed lithostratigraphy of the TBA on the South African side. These maps were obtained as shape files from the Council of Geoscience website. The lithological data from the boreholes discovered during the desktop study was valuable for comprehending the site-specific lithology.

3.2 GEOPHYSICAL INVESTIGATION

3.2.1 Instrumentation

The magnetotelluric method was used to carry out the geophysical survey. For this investigation, an ADMT Electrical Groundwater Detector (Figure 3.1) that is part of the ADMT Series products was used (Aidu Energy Technology, 2020). This tool directly measures the electric field component of the naturally occurring electromagnetic fields following the principles of the MT surface geophysics method presented in the literature review in Chapter Two. The components of the ADMT electric groundwater detector include electrodes, a data recorder, and a cable to connect the electrodes to the data recorder system (Table 3.1). The ADMT equipment specifications are presented in Table 3.1 (product brochure, single channel device).

Figure 3.1 The ADMT 300s Electrical Groundwater Detector tool.

Table 3.1 Specifications of the ADMT-300S electrical water detector device used during the study

Parameter	**Specification**
Detection depth	300 m
Frequency	1 to 8 KHz
Resolution	0.5 µV
Battery	600 mA
Sampling time (s)	4-280

3.2.2 Field testing of the Magnetotelluric Equipment

Since the Audio magnetotelluric geophysical technique is not widely applied in groundwater studies, the tool had to be tested to assess its performance prior to fieldwork for this project. The testing was done at the campus test site at the University of Free State, in South Africa. The campus site was selected as the most suitable location to test the equipment since it has been thoroughly characterized, providing enough knowledge to serve as the foundation for testing.

The Campus test site mainly comprises of a bedding plane fracture that is situated at about 21 m below the surface within the sandstone (Botha, et al., 1998). When designing the geophysical survey for this test, the campus test site map showing the geometry of the fracture (Figure 3.2) was used to identify the survey positions where the fracture is located and positions without fracture. Therefore the survey was conducted at survey stations on the fracture and outside the fracture. This aimed to determine if the tool can effectively detect the fracture by exhibiting different electric properties from the stations conducted outside the fracture.

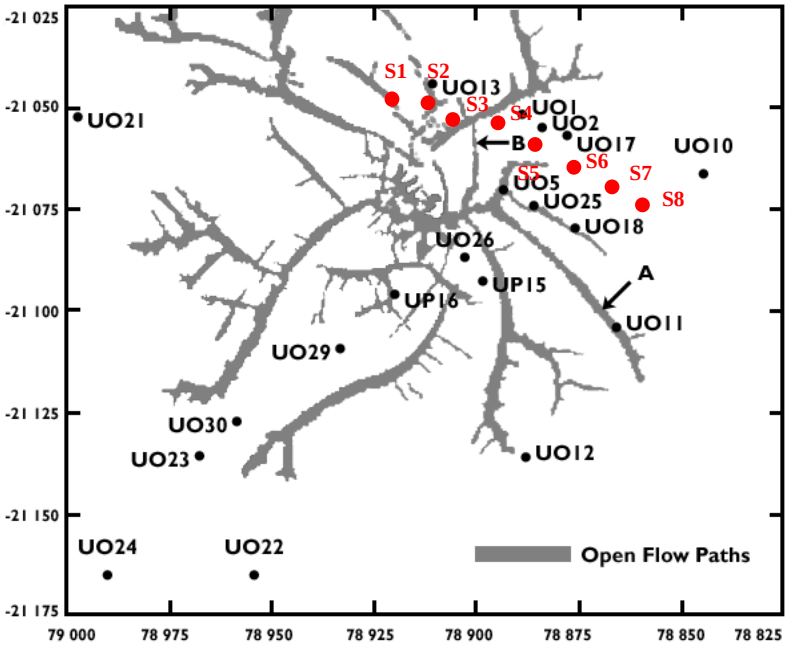

Figure 3.2 The geometry of the fracture on Campus Test site (Van der Voort and Van Tonder, 2000). The red dots show the survey stations used during the equipment testing.

3.2.3 Data quality control

A total of 10 survey stations were identified in the field for data quality control. During the field data collection, the electric potential difference readings were routinely taken six times in each of these survey stations. The repetition of the measurements in each station enabled the application of the Analysis Of Variance (ANOVA) test. The ANOVA test was mainly used to assess if there was a statistically significant difference in the electric potential difference values measured six times in each station. This was to determine the repeatability of the electric potential difference at the same station.

An analysis of variance (ANOVA) test was carried out on Microsoft Excel. This test uses variance parameters to quantify the equality of the electric potential difference means. In this study, the single factor ANOVA with replications is used to determine if statistically significant differences exist in the mean of the electric potential difference values measured on the same MT stations at different time periods. This method tests the statistical differences in the data when one factor is varied (Moore, et al., 2013). Time of data collection is the only factor that was varied during the MT survey.

The variance of parameters estimated by the Single factor ANOVA method include the F-statistic (F), the mean square (MS), the probability value, and the critical statistic value. The

mean square (MS) determines the significance of the factor. The F-statistic, also known as the F-ratio, measures how significantly the means of the data sets differ. This variance is given by the ratio between the measure of effect and error. The probability (p-value) is employed to check the hypothesis validity against the observed data (Sawyer, 2017).

The ANOVA analysis generally checks the null hypothesis (the overall null), which presumes no difference in means. This hypothesis can either be accepted or rejected based on the analysis of variance parameters (Sawyer, 2017).

3.2.3.1 Survey procedure at the Khakhea–Bray

Before the commencement of data collection at the study site, the coordinates of the monitoring boreholes identified in section 3.1.1 were projected on a Google Earth map. This was to assess the accessibility of the monitoring boreholes and comprehend their location in relation to the Khakhea-Bray dolomite TBA. The geophysical surveys were conducted closer to the accessible monitoring boreholes and other existing boreholes identified during the survey. Where possible, groundwater levels were measured during the survey on the existing boreholes.

The survey stations were placed 3 to 5 kilometres apart in locations without boreholes to form a traverse. This space between survey stations enabled the coverage of a wider portion of the study area within the stipulated data collection period. The inaccessibility of some areas of the study area due to privately owned farms constrained the wider coverage of the geophysical survey; hence, the geophysical surveys were conducted along public roads. The geophysical survey was completed with 52 stations across the study area (Figure 3.3).

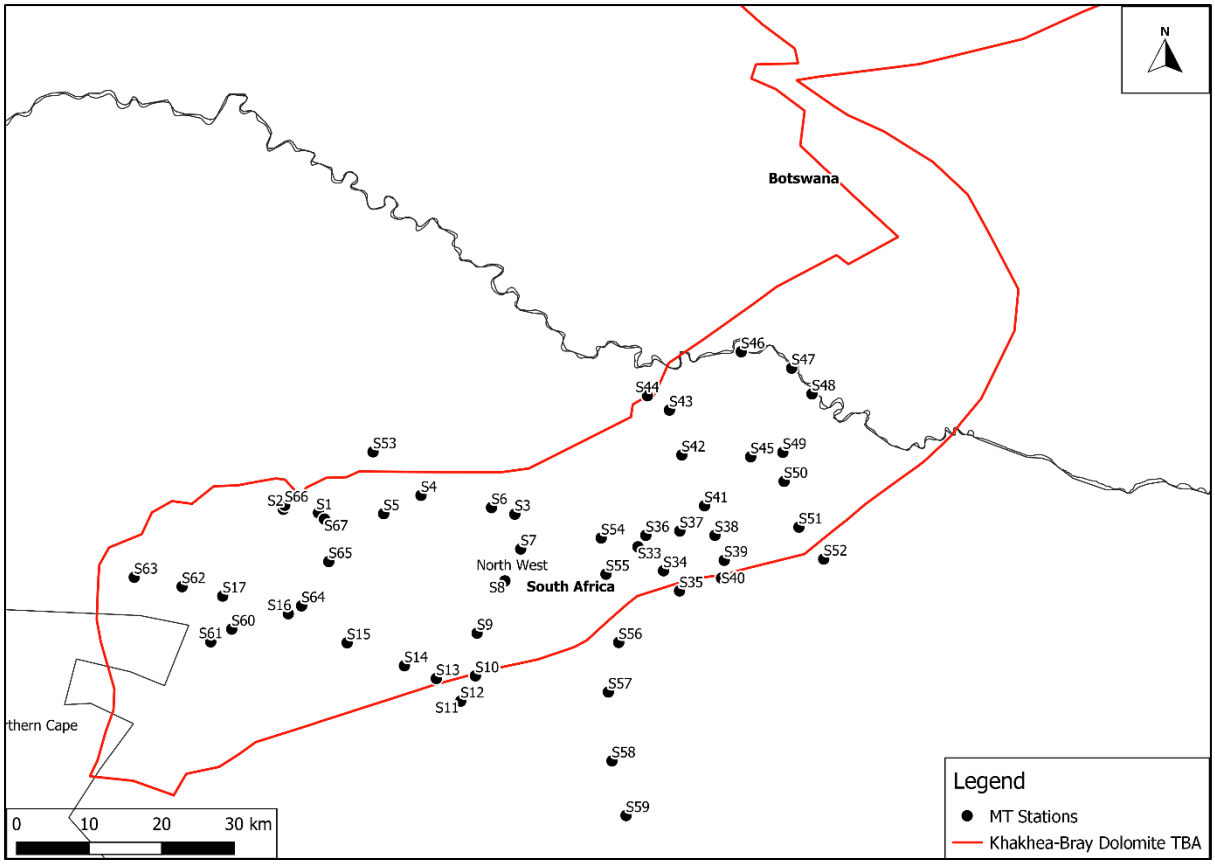

Figure 3.3 A map showing the location of MT survey stations at the study area

A distance was kept between the boreholes and the geophysical survey station during the survey to reduce the impact of noise from metal objects (Figure 3.4b). Like all other geophysical approaches, power lines, pipelines, and fences were avoided during data collecting because of their noise influence on the data.

The electric potential difference measurements were repeated three times per station to check for data consistency. The typical field configuration for the ADMT water detector series, with electrodes spaced 10 m apart, is shown in Figure 3.4a and Figure 3.5.

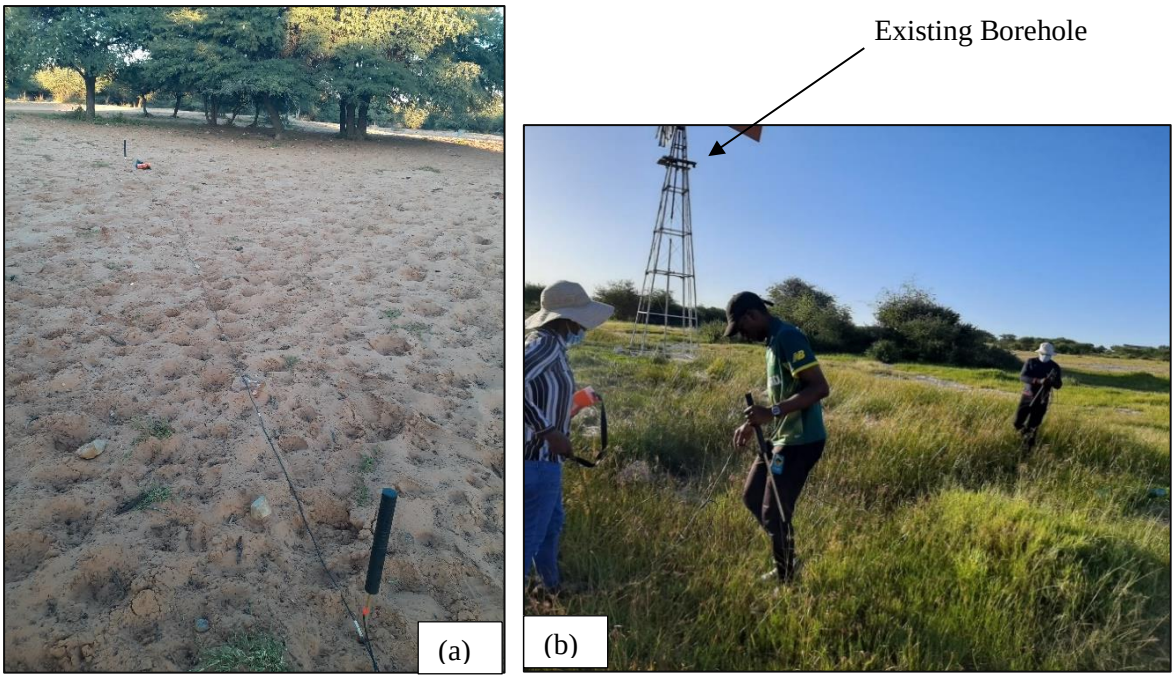

Figure 3.4 Pictures showing geophysical data collection (a) a station S62 on the Aeolian sand and (b) a survey for station S15 conducted closer to a community windmill in Lokgeng village

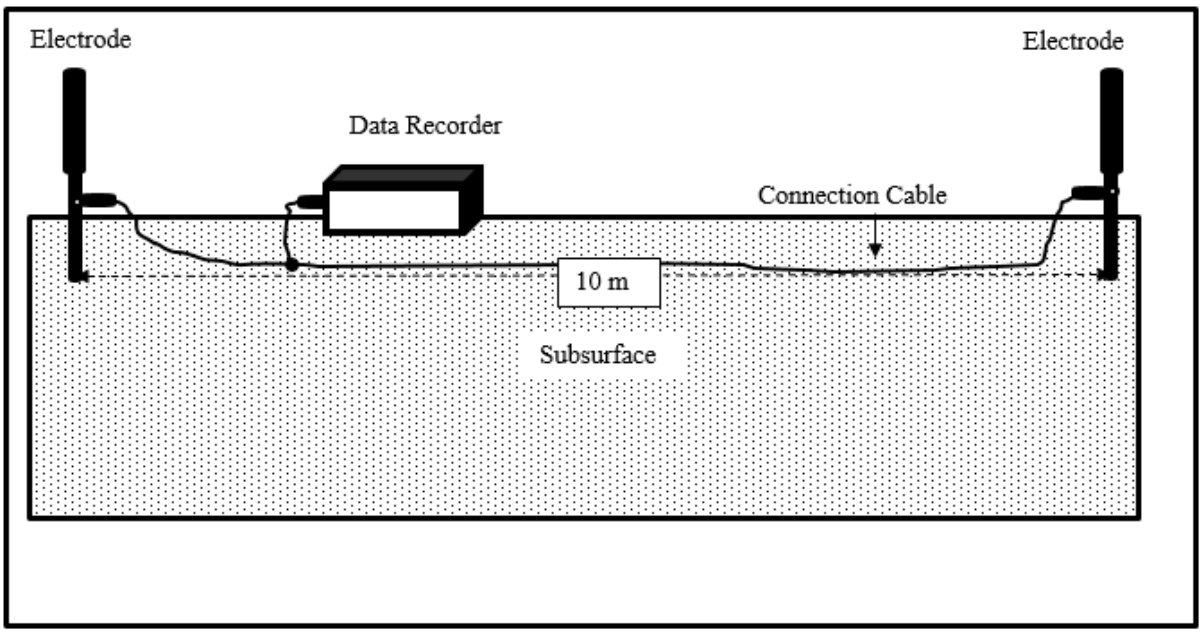

Figure 3.5 A schematic of the Audio magnetotelluric field layout.

3.2.3.2 Core Logging

The core logging was carried out at Pretoria's Council of Geoscience (CGS) core shed. Firstly, the CGS website was used to access the core library to explore boreholes with core logs. Following the identification of the boreholes that were closer to the study area, an email request was sent to the institution requesting access to the logs. The core logging activity aimed at a detailed understanding of the study area's lithostratigraphy. The boreholes identified in section 3.1.1 provided the lithology for not deeper than 160 m. However, the MT geophysical method provides the electric potential difference data for up to 300 m below the ground surface. Therefore, the core logs from deeper boreholes complemented the lithology data from the drilling logs.

During the data collection period from 3 June to 7 June 2022, the Council of Geoscience did not have boreholes within the study area. Nonetheless, the boreholes with available cores closer to the study area were considered with the notion that the lithostratigraphy might not be significantly different from the study area, particularly at deeper depths.

Core logs from three boreholes situated closer to the study area were logged (Figure 3.6). The closest borehole BHW. 2859 is situated 40 km from the study area. The other two boreholes (BH) are situated 160 km SE of the study area. The details of the logged boreholes are summarized in Table 3.2.

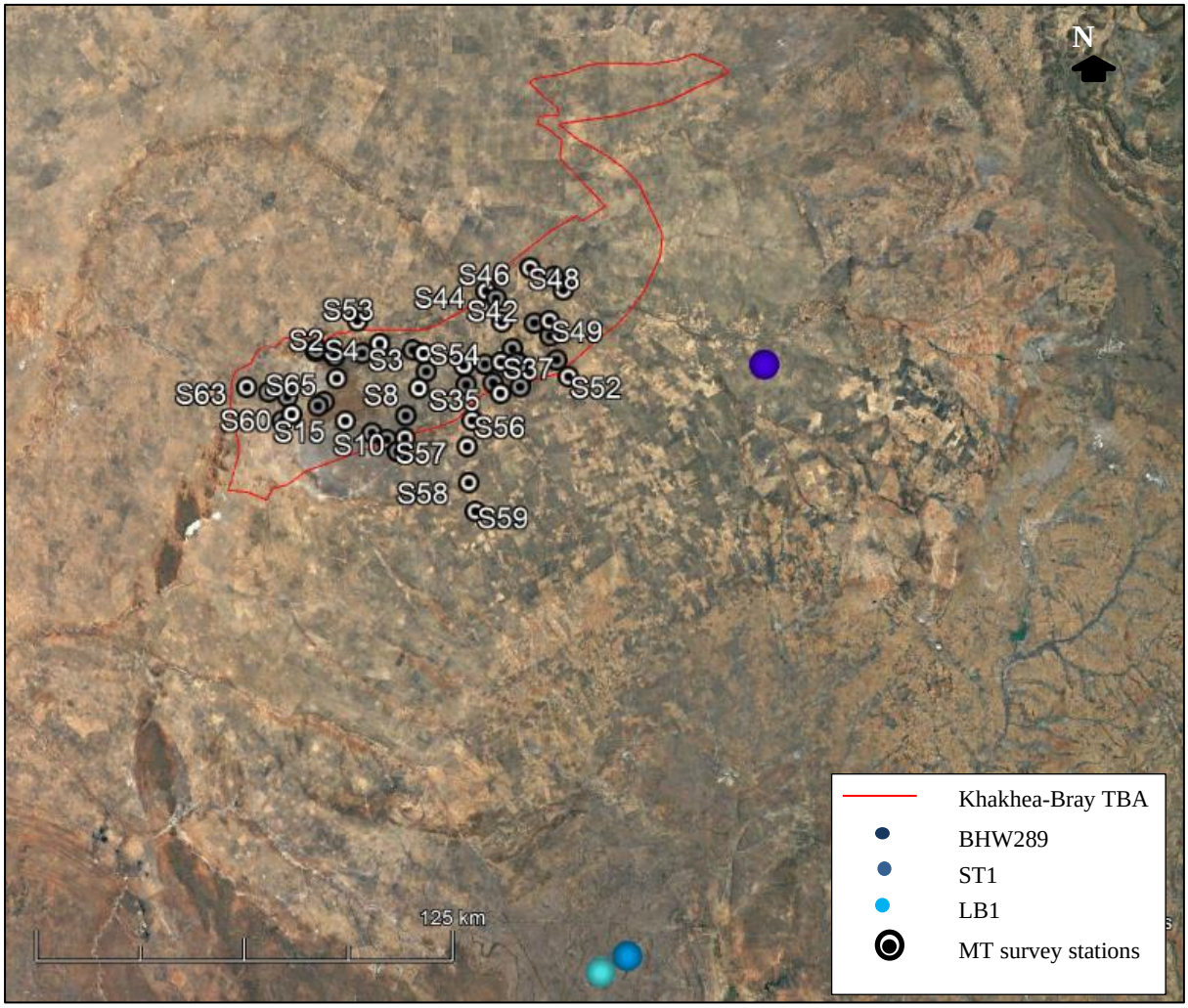

Figure 3.6 Google Earth map showing the location of the CGS boreholes in relation to the Khakhea-Bray dolomite TBA

Table 3.2 CGS boreholes closer to the study area with core logs

CGS borehole ID	Coordinates	Borehole depth	Distance from the boundary of the study area
BHW.289	- 25.8837, 24.8360	538.87 m	40 Km, W
ST1	- 27.4810, 24.3597	299.11 m	162 Km, SE
LB1	- 27.4380, 24.4395	182.88 m	165 Km, SE

The data gathered from the core samples during logging include:

- The rock description,

- Weathered/ fractured zones depth,
- Geological contacts, and
- Any other structures of hydrogeological significance, such as veins and intrusions.

3.3 DATA PROCESSING AND EVALUATION

The equipment's field data was initially downloaded to Microsoft Excel on a computer. The data was plotted on Excel for better visualization. Before the analysis of the electric potential difference data, the data was first subjected to a screening process. The purpose of the data screening was to locate survey points that showed inconsistency in the recorded data when compared to the data from the other stations. The electric potential difference data from survey points that showed noise were manually removed from the dataset. The noise impact in the electric potential difference data precludes comparison to other survey sites. As an illustration, Figure 3.7 illustrates the electric potential difference profile (a) that depicts the impact of noise which might be emanating from a buried metal substance and (b) that of the same station but away from the noise source. The three data sets from each station were averaged following the evaluation of the data to produce a single data set that was calibrated with lithology in section 4.3.

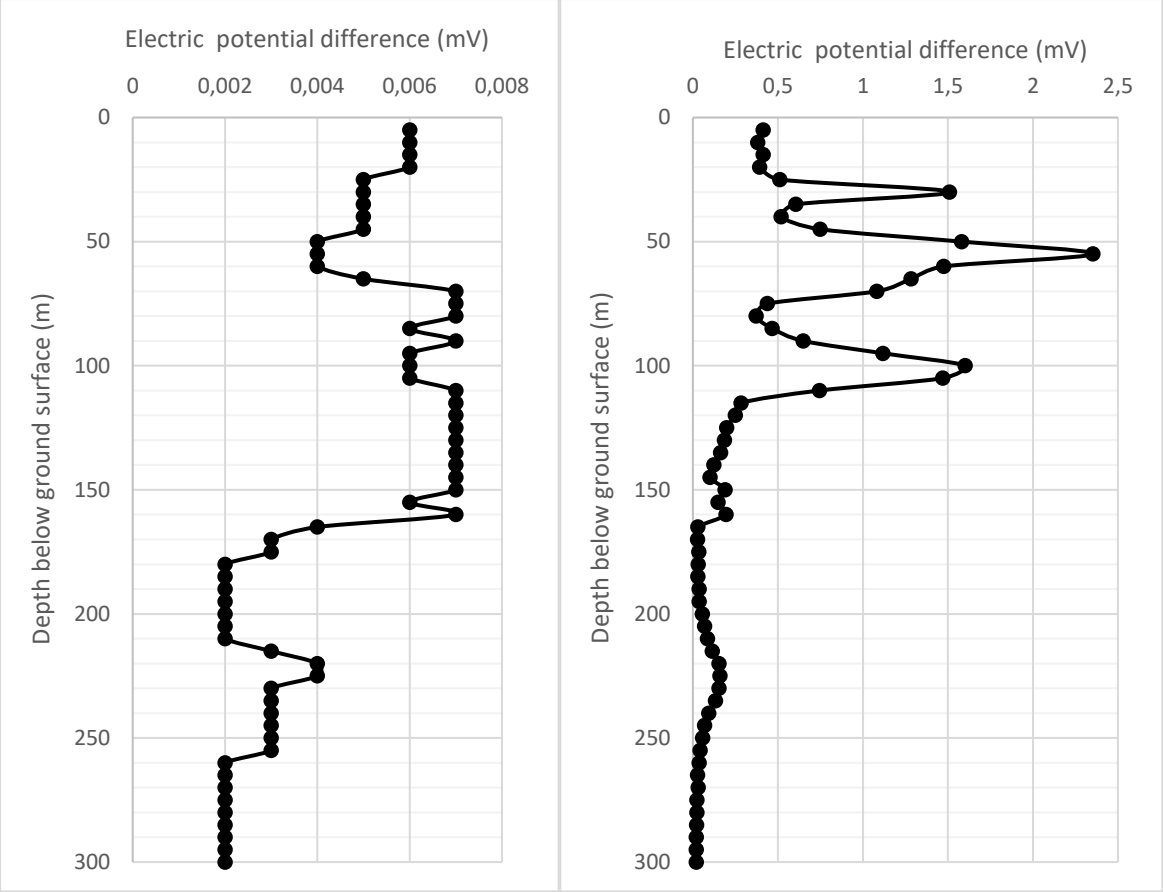

Figure 3.7 (a) The electric potential difference profile that shows the effect of noise and (b) is the electric potential difference profile in the same station but away from the noise source.

3.4 DATA ANALYSIS AND INTERPRETATION

After the data has been evaluated, the three data sets from each station were averaged to get a single data set that was calibrated with lithology. The electric potential difference was calibrated using borehole drilling data gathered from the NGA. The calibration procedure aimed at giving the electric potential difference hydrogeological meaning and establishing the factors that influence groundwater occurrence in the dolomite of the study area. The drilling data (lithology, water strike and water level) of each borehole was plotted against the electric potential difference profile of the corresponding survey station. This was to assess the relationship between electric potential, water strikes, and geological variation. The linkage between the boreholes data and the electric potential difference is fundamental to see the electric potential difference values corresponding to the recorded water strikes, hence establishing the factors that influence groundwater occurrence in the dolomites.

For this study, the electric potential difference of the subsurface was modelled using the Rockworks tool. This application is covered in full in Section 3.4.1. The hydrogeological conceptual model is discussed in Section 3.4.2.

3.4.1 Modelling subsurface electric potential difference

Resistivity models are usually presented in the form of a 2D and 3D resistivity maps or as cross-sections along transverse lines. Several geophysical software are commercially available for producing 2D and 3D resistivity models. For electric potential difference data from the MT method, the ZondMT2D software, designed specifically for producing 2D models from MT soundings, has been applied in studies by Agyemang (2020).

For this study, the Rockware Company's commercial product Rockworks was used to model the electric potential difference data in 2D cross-sections. A 2021 version 2021.11.17 standard licensed Rockworks software was used. Rockworks is a 2D and 3D data visualizing, analysing, and modelling tool (Rockwares, 2022).

Following the instructions in the Rockworks manual, the field data set containing the coordinates, elevation and the electric potential difference data for each station was imported into the Rockworks excel file format (Rockwares, 2022). In Rockworks, the survey stations were imported as boreholes. Google Earth was used to derive the elevation data for the survey stations. The borehole depth was specified to be 300 m for all the stations because the electric potential difference data was for up to 300 m below the surface. Geophysical data are classified as P data in Rockworks.

The Rockworks software provides two approaches for modelling 2D P data: a hole-to-hole P data section and a model-based P data section. The hole-to-hole data section generates an electric potential difference cross-section model without specifying the applied interpolation method. The model-based interpolation method gives the allowance to choose the interpolation method to be used when generating the electric potential difference models. Therefore, for this study, the model- based P data section was used. The interpolation of spatial data is crucial because it estimates values at unknown points from initially discrete sampling points (Agerberg, 2020). The model-based P data section offers nine interpolation methods that can be used to generate the electric potential difference model cross-section. Data from survey stations along cross-section A-A' was used to generate the electric potential difference models using the different interpolation methods. The created models were visually evaluated to

identify an interpolation method that shows a better representation of the subsurface data. The method that was identified to show better presentation of the interpreted and modelled data was further cross validated. During the cross validation, the electric potential difference profile from three stations along the cross section were plotted on top of the generated model. This was done to ensure that the modelled data is coherent to the field data.

The Inverse Distance Weighting methods are generally based on the assumption that the influence of the sampled parameter decreases with distance from the sampled location. The general mathematical expression of the IDW method is presented in Eq. 3.3. Eq. 3.4 shows how the distances between estimation location and sample point is calculated (Babak & Deutsch, 2008).

$$Z^*(u) = \sum_{i=1}^{n} \lambda_i Z(u_i) \tag{3.3}$$

Where $Z^*(u)$ is the inverse distance estimate at the estimated location, u is the estimation location, u_i where i = 1,…n are the location of the sample points within the search neighbourhood, λ_i i= 1,...n weights assigned to each sample point and $Z(u_i)$ i= 1,...n are the conditioning data at sampled points.

$$\boldsymbol{\lambda_i} = \frac{\left(\frac{1}{d_i^p}\right)}{\sum_{i=1}^{n}\left(\frac{1}{d_i^p}\right)}, \text{ i=1,….n} \tag{3.4}$$

Where d_i are the Euclidian distances between estimation location and sample points, and exponent p is the power or distance exponent value.

The anisotropic IDW interpolation method improves precision by factoring in the spatial anisotropic effect, which distinguishes it from other IDW interpolation methods (Jinbiao, et al., 2021). According to Rockware (2022), the disadvantage of this method is that it is slower than the IDW isotropic method because it filters neighboring points while assigning node values during the interpolation process. The method's benefit has been cited as being an improvement in the interpolation of voxel values between data point clusters (Rockwares, 2022). Tomczak (1998) utilized and cross-validated the IDW anisotropic approach for interpolating rainfall data.

3.4.2 Groundwater Occurrence Models

The groundwater occurrence models in this study sought to elucidate the pictorial visualization of the groundwater in the dolomites, mainly by means of harmonizing the resistivity properties of the subsurface and the general geology of the area. The pseudo-2D electric potential difference cross-section models generated in Rockworks served as the basis for the groundwater occurrence models. The electric potential difference models showing the potential aquifer zones to be characterized by electrical potential difference values of fractures and weathered zones were transformed into groundwater occurrence models. The geology between surface and 165 m was generalized to dolomite and uncharacterized between 165 m and 300 m. Microsoft Word was used to hand build the groundwater occurrence models (Figure 4.27,4.31, 4.34 and 4.37) of the cross-sections across the study area.

CHAPTER 4
RESULTS AND DISCUSSION

This chapter presents and discusses the results of a geophysical field survey conducted on the Khakhea-Bray dolomite transboundary aquifer in the North West Province of South Africa. The study focuses on the data collected from the South Africa part of the TBA.

The first section (4.1) of the chapter is devoted to discussing the limitations that could affect the study's findings and conclusion. The section 4.2 presents the results from the Bloemfontein Campus test site, where the geophysical survey equipment was tested before using it at the Khakhea-Bray Transboundary Aquifer. The third section (4.3) of this chapter discusses in detail the data quality controls from ten stations within the study area that were used to perform quality test. Section 4.5 presents the electric potential data from stations that were conducted closer to a borehole with drilling data and discusses the correlation between the data set. Section 4.5 is mainly on evaluating the modelling algorithms of RocksWorks to identify the ideal algorithm used in this study. The chapter ends with section 4.6 which gives a detailed discussions on the modelled cross sections using the identified method in 4.4.

Through a geophysical assessment of the subsurface, this field survey aims to learn where potential groundwater aquifers occur within the dolomite and the factors that influence the groundwater occurrence. To establish this understanding of the aquifer systems of the study area, the electric potential difference data obtained using the magnetotelluric geophysical technique is coupled with drilling data from existing boreholes within the area. The electrical potential difference results for all the stations used in the discussion is found in Table 7.4 to Table 7.7 in the appendices.

4.1 STUDY LIMITATIONS

In geophysical methods the qualitative characterization of the subsurface is usually achieved through the calibration of the geophysical data with the subsurface geological information. The geophysical data is enhanced by geological knowledge, hence improving subsurface characterization. The primary impediment to the subsurface characterization utilizing the geophysical data in this investigation was the subsurface geological knowledge of the study area. The National Groundwater Archive provided the study with drilling data from existing boreholes. The location of these existing boreholes varied throughout the investigation. This

led to the generalization of subsurface geological information in areas lacking geological information from existing boreholes.

The drilling data of available boreholes covered up to 165 m below surface while the geophysical data extend to 300 m below the surface. As a result, the subsurface between 165 and 300 m remained uncharacterized due to the limitations of the current drilling data. As an alternative to the existing drilling boreholes in NGA, geological data for the deeper depths was gathered from exploration boreholes. This data could not be used to calibrate the MT geophysical data because it was discovered that the exploration boreholes were outside the study area.

The weathering state of the geology in NGA was not known, therefore only the geophysical data was utilized to infer the weathered or fractured zones in the surface. As a result, the qualitative interpretation of the geophysical data is as accurate as the information currently accessible. Another limiting aspect in the study area was accessibility to some sites within the study area, so the surveys were done on routes that were easily accessible. If all the locations can be accessed, this suggests that there is space for improvement in the characterization of the subsurface within the study area.

4.2 TESTING OF EQUIPMENT

The electric potential difference profiles obtained from the survey show that the audio magnetotelluric tool was able to detect the fractured aquifer zone, which, according to Botha, et al. (1998), is located at about 21 m. On the geophysical data, this aquifer zone was characterized by relatively low electrical potential difference at depths between 22.5 and 27 m which are closer to the reported fracture position. Figure 4.1 shows the electric potential difference profile obtained in relation to the positions on the fracture according to the fracture geometry of the study area. These survey stations show the lowest electrical potential difference values between 0.049 to 0.068 mV at 25 m suggesting a groundwater potential zone at this depth.

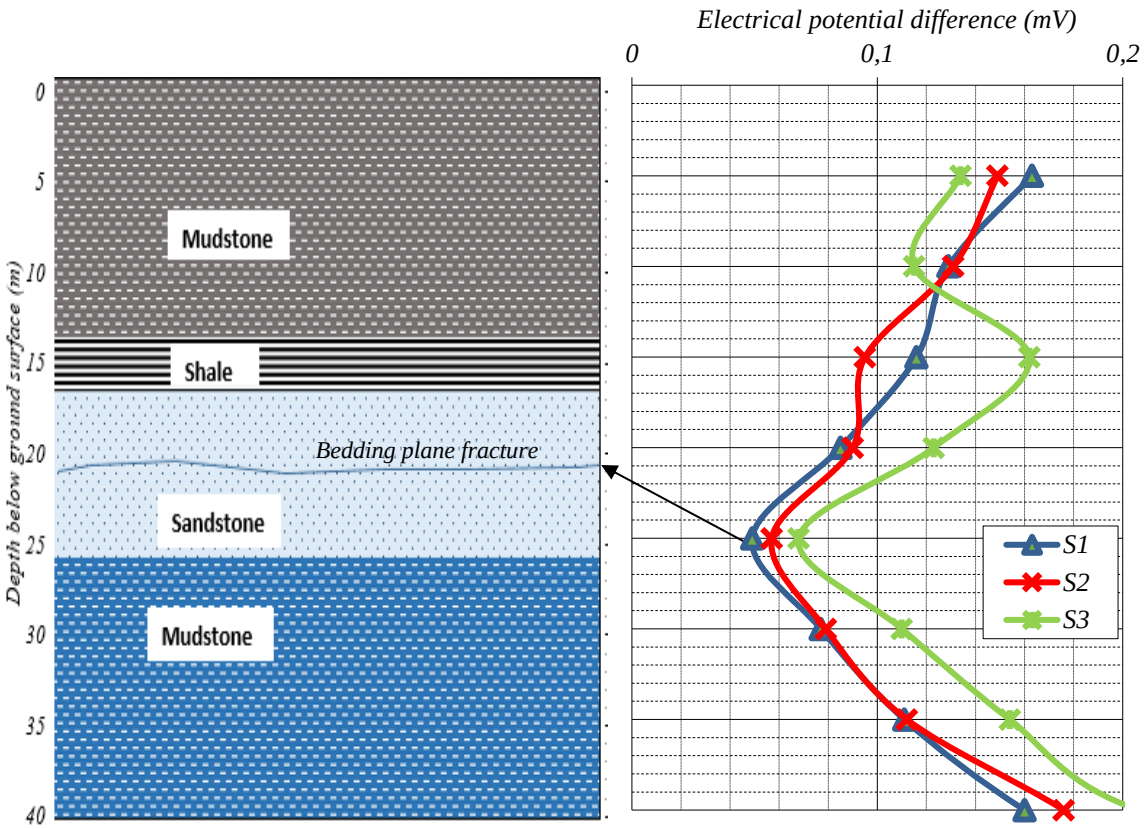

Figure 4.1 Campus test site subsurface profile (Botha, et al., 1998) and the electrical potential difference profile for stations conducted on the bedding plan fracture positions. The black arrow shows the bedding plane fracture

Figure 4.2 shows the electric potential difference profile from the stations which are located outside the fracture position. It shows that at these positions, the fracture is absent because the electrical potential difference appears to be increasing at 25 m, suggesting different electric properties of the subsurface at positions at this which marked the absence of the fracture. Therefore, this assured that the Audio Magnetotelluric equipment could effectively map the depth of the groundwater aquifer zones.

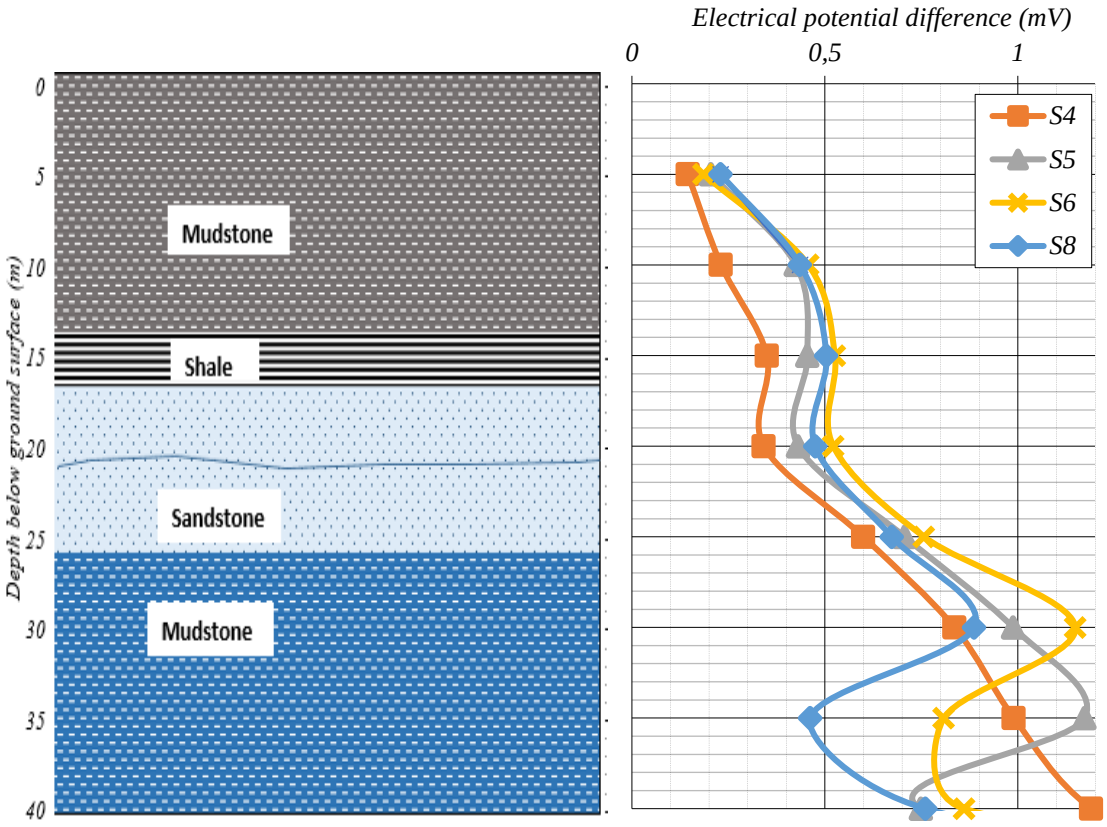

Figure 4.2 campus test site subsurface profile (Botha, et al., 1998) and the electrical potential difference profile for stations conducted outside the bedding plan fracture position.

4.3 DATA QUALITY EVALUATION

Table 4.1 presents the single factor ANOVA of the electric potential difference data analyzed from the 6 readings per survey station.

Table 4.1 Electric potential difference data from the MT survey were analyzed using the single factor ANOVA

station no	MS	F	p Value	F critic	
S5	0,000790439	0,037918285	0,962799431	3,047012139	
S7	0,008003072	0,020013412	0,980187744	3,047012139	
S13	0,003436572	0,056707211	0,944887836	3,047012139	
S18	0,00818405	0,068453307	0,933861772	3,047012139	
S41	0,000229539	0,005922318	0,994095381	3,047012139	
S44	0,002010288	0,073006087	0,990269929	2,40224849	
S46	0,000103072	0,005001485	0,995011142	3,047012139	
S49	0,003502956	0,041613764	0,959249584	3,047012139	
S51	0,002907772	0,009722194	0,990325442	3,047012139	
S53	0,083006067	0,032517287	0,968011497	3,047012139	

MS—Mean squares, F—test statistic, p-value—is the probability of calculating a given test statistic assuming that the means of your groups are identical and Fcrit critical statistic

For the 10 MT stations that were used to perform the data quality control, it can be observed that when comparing the test statistic (F) and the critical value (Fcritic), the test statistic values are smaller than the critical value (F < Fcritic). This implies that with a 95 % confidence level, it can be concluded that there are no statistical differences between the repeated measurements across all station. The p-value was used to assess the probability to which the observed difference (even if not significant) among groups is attributable to influence of random factors or the sampling methods (test factor) (Gomo, et al., 2017).The p-values of at least 0.93 at all the stations shows that probability that the observed difference among the electric potential difference measurements is due to random chance is 93%. This gives confidence that the geophysical data collected was consistency and largely not affected by the nature of the equipment used.

4.4 CORRELATION OF BOREHOLE LITHOLOGY AND THE ELECTRIC POTENTIAL DIFFERENCE

In this section, the geophysical surveys conducted closer to existing boreholes with drilling data are presented as an electric potential difference profile plotted against the borehole data. This is to calibrate the electric potential difference data of the research area using the existing borehole information. Because the borehole data does not provide information on the weathering/fracturing state of the rocks, the contrast in electric potential difference is analysed to suggest the state of the rock. However, this is a limitation on the calibration of the ADMT data as it has to be assumed that the contrast in electric potential difference properties within the same lithology might be an indication that the rock is in different states that influence the change in the electric potential difference.

The depth of the existing boreholes used to calibrate the electric potential difference data ranges between 56 m and 166 m. Therefore, an electric potential difference profile of up to 200 m was used. Table 4.2 summarizes the borehole information for calibrating the electric potential difference data and their corresponding magnetotelluric station numbers.

Table 4.2 Boreholes with drilling data

ADMT Station ID	NGA Borehole ID	Coordinates	Borehole depth (mbgs)	Water strike (mbgs)	First Water level (mbgs)	
S3	2523DD00099	-25.85303 23.838	118	-	16	Measured after 2 months
S8	2523DD00097	-25.94798 23.82902	166	11, 34	4.8	Measured 16 days after drilling
S33	2524CC00093	-25.89804 24.00652	130	31, 78	13.21	Measured next day after drilling (affected by pumping)
S34	2524CC00091	-25.92888 24.04374	166	21, 147	21.57	Measured next day after drilling (affected by pumping)
S38	2523DD00095	-25.79398 23.9755	166	55, 112, 120	45.65	Measured next day after drilling
S41	2523DD00096	-25.88714 23.85707	150	81, 107, 116	25.86	Measured 16 days after drilling
S50	2524CC00236	-25.80825 24.2109	150	-	52.50	Measured 4 months after drilling

mbgs – meters below ground surface

4.4.1 Survey Station S3- BH 2523DD00099

Figure 4.3 presents the electric potential difference profile from the ADMT station S3 plotted against the borehole information for borehole 2523DD00099. The lithology profile of the borehole shows a 1 m thin layer of sand on the surface, underlain by a 43 m thick calcrete layer and dolomite rock occurring from 46 m to 118 m below the surface.

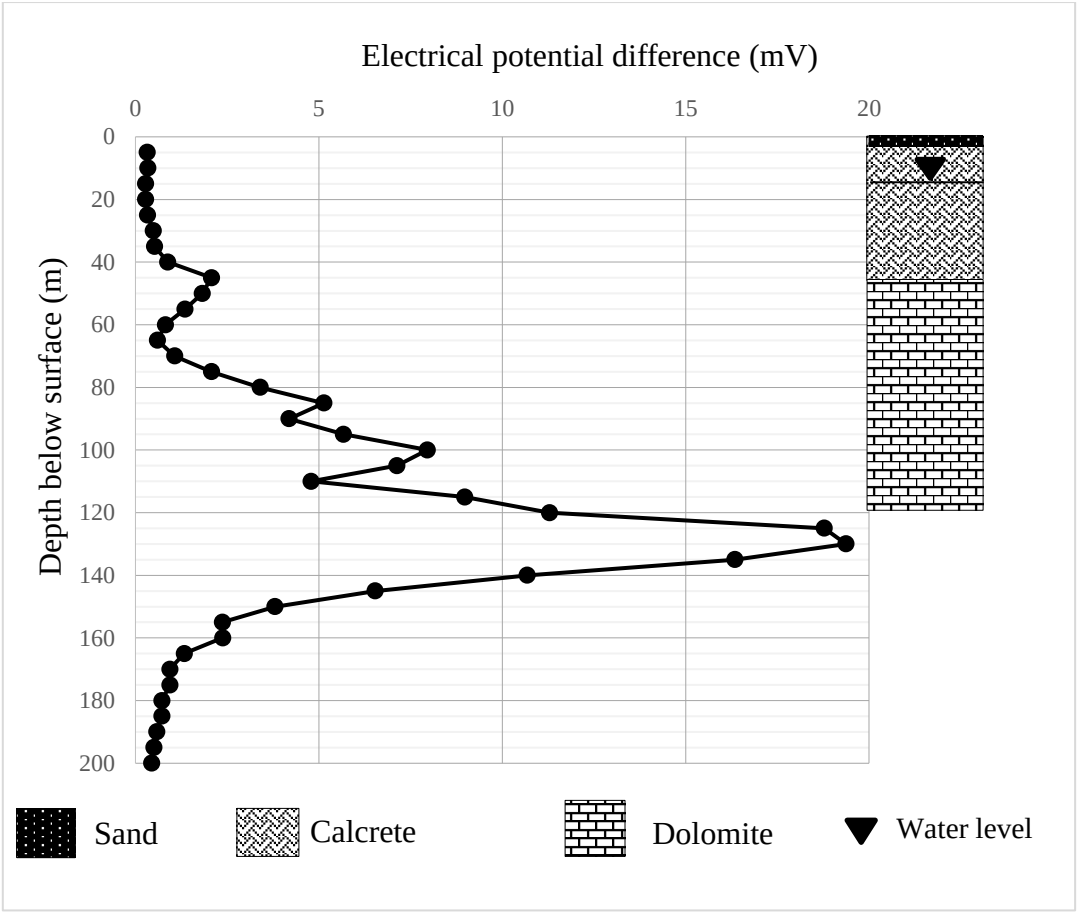

Figure 4.3 Electric potential difference profile for ADMT station S3 and borehole data from borehole 2523DD00099

The profile shows an electric potential difference of 0.317 mV and 0.338 mV at 5 m and 10 m respectively, coinciding with the lithology log's top part of the calcrete. The electric potential difference on the calcrete then decreases to 0.278 mV at 15 m and 20 m below the surface. The electric potential difference on the calcrete after 20 m gradually increases towards the contact with dolomite at 45 m. This suggests that the calcrete is harder at 5 m and 10 m compared to the calcrete at 15 m and 20 m. The general profile of calcrete has been reported to have two zones; the upper zone, which is characterized by a hard layer, referred to as a hard pan, and a lower zone where the calcrete occurs as nodular/columnar or tubular forms (Eren, et al., 2008). Therefore, the higher electric potential difference between 5 m and 10 m, suggests that the calcrete occurs as a hard pan in this zone. The decrease in electric potential difference at 15 and 20 m suggest that the calcrete might be occurring as a nodular/columnar/tabular form. The gradual increase of electric potential difference towards the contact at 45 m attaining an electric potential difference of 2.07 mV could imply that the contact zone might be hard with low chances of being a preferential flow zone for groundwater.

The dolomite zone starting from 45 m below the surface shows varying electric potential difference properties. The wide range of the dolomite's electric potential difference values may be explained by a number of factors, including (1) the possibility that the dolomite rock might not be homogenous in terms of formation, which could lead to variations in its chemical composition and texture (Gomaa, et al., 2014), (2) there might be zones within the dolomite that are weathered or fractured, which are characterized by the lower electric potential difference values, between fresh zones, which are characterized by higher electric potential difference values, and (3) there might be chert beds which are not prone to dissolution; therefore, they remain as hard layers when the dolomite undergo dissolution processes (Dippenaar, et al., 2019). All these inferences are made because the borehole data does not provide a detailed description of the recorded lithology.

The dolomite's electric potential difference gradually decreases from 45 m (2.07 mV) to 65 m (0.60 mV), increasing again after 65 m. This imply that at 65 m, there might be contact between dolomites formations of different properties, causing the variation in electric properties.

There are no records of water strikes for the borehole. This suggests that the borehole might have been dry during drilling. According to the data on the NGA, the first water level of this borehole was measured two months after drilling, and the level was recorded at 16 m. This shallow groundwater level suggests there might have been water seepages from the contacts zones between the different geological formations. A zone between 15 m and 20 m appears to be the only zone with a realistic chance of getting groundwater. This is due to the lowest electric potential difference in this zone.

4.4.2 Survey Station S8 – BH 2523DD00097

Figure 4.4 presents the borehole data from borehole 2523DD00097 plotted against the subsurface electric potential difference data from the ADMT station S8. The borehole data shows a 1 m thick sand on the surface, underlain by a 10 m thick layer of calcrete extending to 11 m below the surface. Below the calcrete, a dolomite rock was recorded from 11 m to the end of the borehole at 56 m.

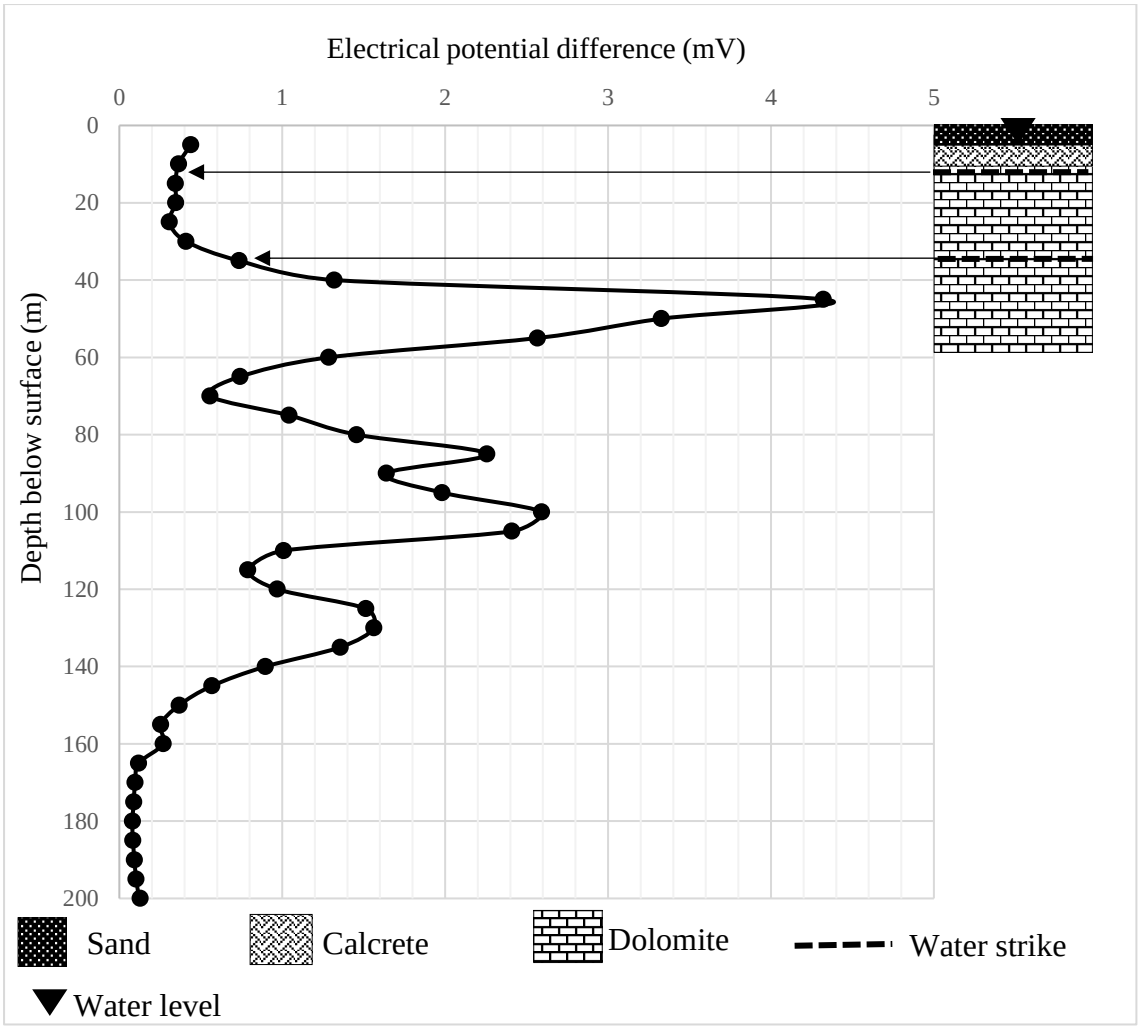

Figure 4.4 Electric potential difference profile for ADMT station S8 and borehole data from borehole 2523DD00097

The electric potential difference profile of the borehole reveals that the calcrete layer has an electric potential difference value of 0.439 mV on top and decrease towards the contact with dolomite at 11 m. The highest electric potential difference of calcrete on top and lower electric potential difference on the bottom may again suggest that the calcrete occurs as a hardpan layer on top hence the higher electric potential difference and as a nodular or the columnar or tabular form at the lower zone suggesting the lower electric potential difference.

The dolomite's electric potential difference appears to gradually increase from 0.344 mV at 15 m to 1.32 mV at 40 m. A sudden increase in electric potential difference from 1.32 mV at 40 m to 4.32 mV at 45 m is also noticeable. The lithology log of the borehole does not show any changes in lithology at this zone.

The water strikes for borehole 2523DD00097 were at 11 m and 34 m. The first water strike at 11 m occurs at the contact zone between calcrete and dolomite. The potential difference at this zone is measured to be 0.360 mV which is lower than the potential difference at the top of the calcrete (0.439 mV), suggesting that the calcrete is less hard at the lower part due to the water in this zone. The second water strike at 34 m is associated with the contact zone between dolomite of different electric properties. The potential difference at the water strike is 0.72 mV.

According to the NGA data for borehole 2523DD00097, the first water level was recorded at 4.8 m after 16 days the borehole was drilled. The shallow water level suggests that the aquifer is confined possibly by the calcrete layer showing electric potential difference value of 0.439 mV; hence the water was able to rise above the first water strike.

4.4.3 Survey Station S33- BH 2524CC00093

Figure 4.5 presents the electric potential difference profile for survey station S33 along with the 2524CC00093 borehole data. The lithology log of the borehole generally shows a layer of sand from ground surface to 2 m deep. The sand is underlain by a 16 m thick calcrete layer extending to 18 m depth. The dolomite rock occurs from 18 m to 155 m with 1 m shale lenses at 32 m below the surface.

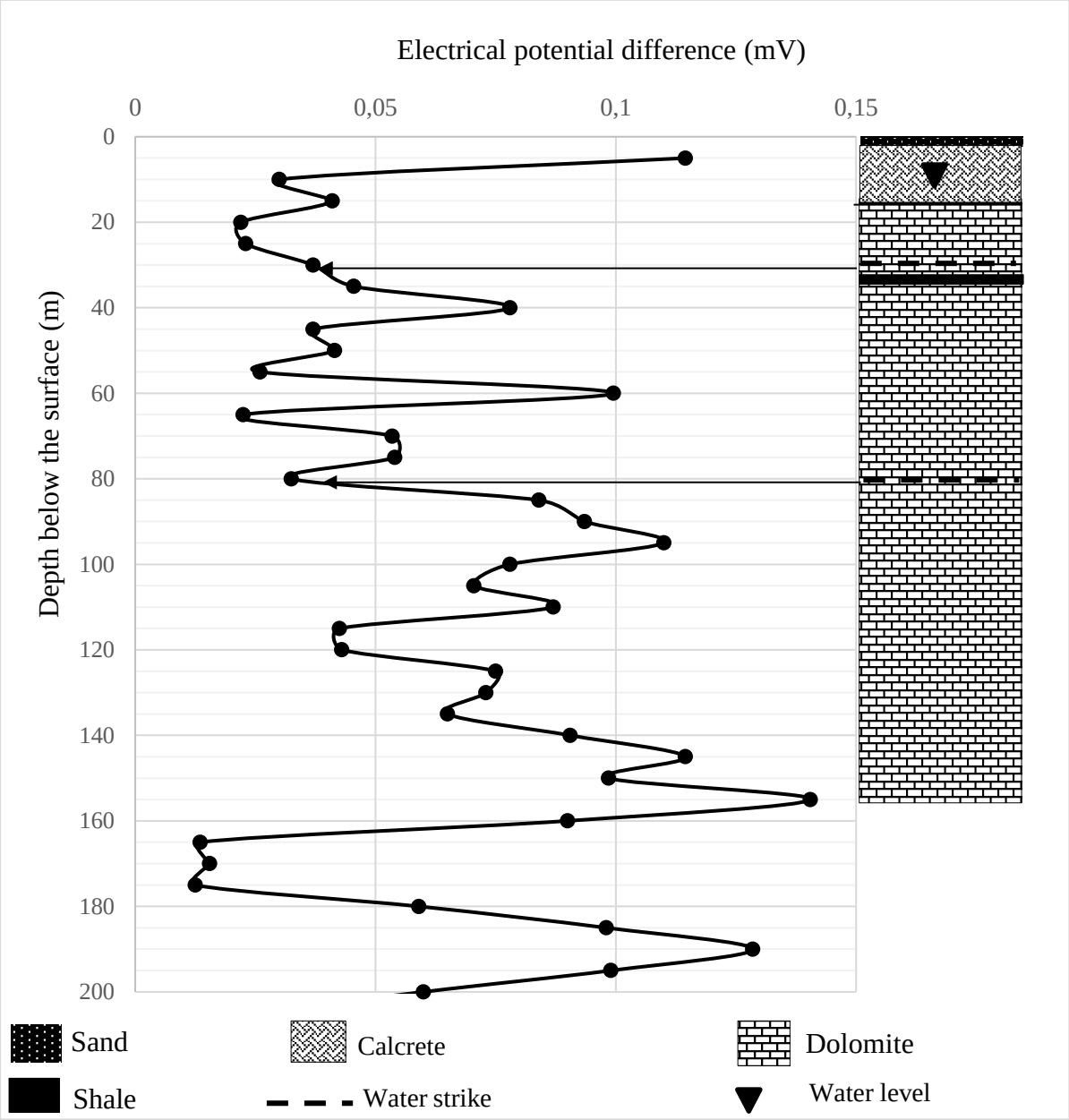

Figure 4.5 Electric potential difference profile for ADMT station S33 and borehole data from borehole 2524CC00093

The electric potential difference profile for this borehole shows an electric potential difference ranging between 0.1405 mV to 0.022 mV. The highest potential difference of 0.1405 mV appears to be at the bottom of the borehole, which suggests that the drilling ended where the dolomite was the hardest at 155 m which might suggest a relatively fresh dolomite. The calcrete layer also shows an elevated potential difference value of 0.1145 mV at 5 m but decreases towards the contact at 20 m (0.022 mV). The decrease in electric potential difference values to less than 0.1 mV on the calcrete towards the contact with dolomite at 20 m suggests that the

contact zone is softer than the upper section of the calcrete and the contact may have some water. The dolomite section appears to have electric potential difference values varying between 0.022 mV and 0.14 mV. The possible attributes of the variation of the electric potential difference in dolomite have been discussed in 4.4.1. The electric potential difference of the dolomite between the 20 m and 80 m deep appears to be constantly between 0.02 mV and 0.06 mV except for the isolated elevated electric potential difference anomalies at 40 m and 60 m. This elevated potential difference anomalies in dolomite exhibiting relatively high electric potential difference could be chert beds, quartz veins, or any other formation that may be prone to dissolution. The potential electric difference ranging from 0.02 mV to 0.06 mV observed between 20 m and 80 m suggests that the dolomite is weathered-fractured as compared to the dolomite between 80 m and 152 m which appears to be of higher electric potential difference (0.0425 mV– 0.1405 mV) with some variations. The water strikes at 31 m and 79 m confirms the weathered or fractured zones between 20 m and 80 m below the ground surface.

The first water strike at 31 m occurs at the contact between shale and dolomite. According to the electric potential difference profile, the contact has an electric potential difference of 0.037 mV. The second water strike at 81 m occurs at the dolomite with electric potential difference 0.032 mV. This is where the dolomite electric potential difference appears to be increasing, suggesting a different dolomite formation or a relatively fresh zone below. The electric potential difference profile reveals that both groundwater strikes occur where the electric potential difference starts to increase after being low. This implies that the groundwater is collected by the fresh zones (aquiclude), which can dam the water draining from the weathered-fractured zones characterized by lower electric potential difference.

The static water level of the borehole was measured to be at 13.21 m on the next day after drilling. According to the NGA records for this borehole, the measured water level was affected by pumping from a nearby borehole. This suggests that without pumping, the water level might have been shallower. The shallow water level indicates that the aquifers could be confined by the calcrete formation exhibiting higher electric potential difference, which means that the water must have been under pressure; hence it can rise above the water strikes. The shallow water level also implies that there might have been some zones within the dolomite that had water seepages but were not recorded as water strikes as they were not visible during drilling.

4.4.4 Survey Station S34- BH 2524CC00091

Figure 4.6 presents a 200 m electric potential difference profile from survey station S34 plotted against the borehole information of the 167 m deep borehole 2524CC00091. The lithological log from the borehole shows a 2 m thin layer of sand on the surface, underlain by a 6 m thick layer of calcrete and dolomite. The dolomite occurs from 11 m below the surface to 162 m with 1 m and 2 m thick shale lenses situated at 31 m and 92 m, respectively, below ground surface. The drilling records show that groundwater strikes were at 21.57 m and 147 m below the surface.

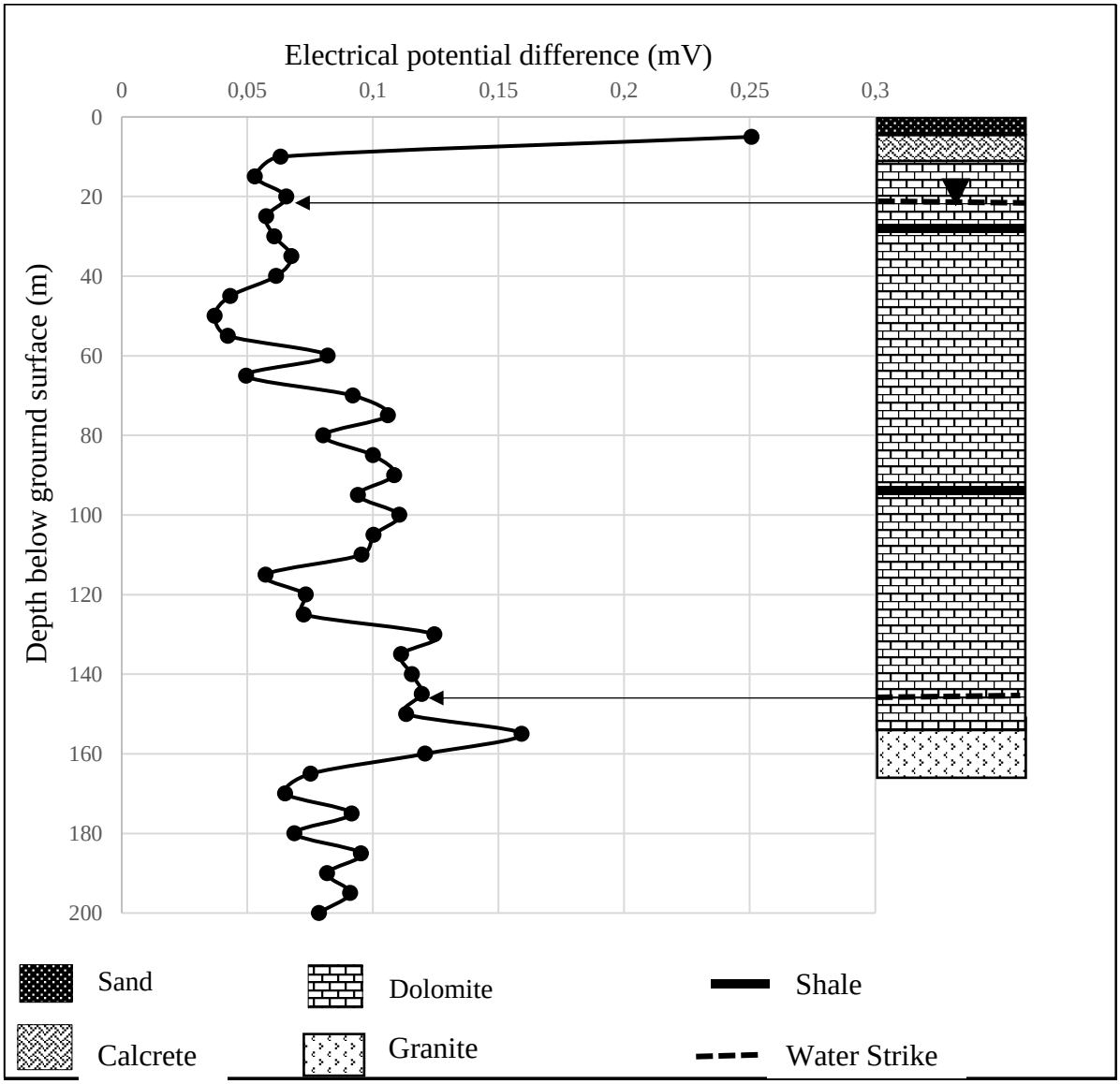

Figure 4.6 Electric potential difference profile for ADMT station S34 and 2524CC00091 borehole data

The electric potential difference profile for this station shows an electric potential difference range between 0.037 mV and 0.25 mV. The highest electric potential difference of 0.25 mV on the profile occurs at 5m deep, coinciding with the calcrete layer's top part. This elevated electric potential difference suggests that the calcrete is occurring as a hardpan, as discussed in section 4.4.1. The decrease in electric potential difference towards the contact with dolomite at 10 m suggests that the calcrete at the contact might be softer. The dolomite appears to have varying electric potential difference values ranging from 0.037 mV to 0.159 mV suggesting varying dolomite formations.

The lithological log shows that actual lithology changes occur at 2 m, 11 m, 30 m, 96 m, and 162 m. On the other hand, the electric potential difference profile shows a significant change in electric properties at 40 m, 60 m, 110 m, and 150 m. The contrast in the electric potential difference at these depths might be associated with contact between two different geological materials. According to the lithology log, the contact between dolomite and granite occurs at 162 m, which may be related to the electric potential difference contrast at 150 m. The water strike that was recorded at 147 m might also be linked to the contact between granite and dolomite at 150 m.

The water strike at 21.57 m below the ground surface corresponds to the dolomite's electric potential difference values between 0.0655 and 0.0575 mV. The second water strike at 150 m corresponds to an electric potential difference value of 0.113 mV at the contact between the dolomite and granite. This suggests that the first water strike occurs in a zone that is weathered or fractured, characterized by lower electric potential difference values within the dolomite compared to the second water strike, where the electric potential difference is slightly higher than the zone of the first water strike.

The water level in borehole 2524CC00091 was measured at 21.57 m. According to the records on NGA, this water level was measured the next day after drilling, and it was recorded that the water level was affected by pumping from a nearby borehole. This suggests that the water level might have been shallower without the effect of nearby pumping. This implies that there might have been seepages from other zones within the dolomite contributing to the rise in water level.

The shallow water level could further suggest that the aquifer was confined, possibly by the calcrete layer showing electric potential difference value of 0.25 mV at 5 m below the surface.

4.4.5 Survey Station S38 – BH 2523DD00095

Figure 4.7 presents the borehole data from borehole 2523DD00095 and the electric potential difference of station S38. The lithology data of the borehole shows a 2 m thick layer of sand from the surface. Beneath the sand, there is a 2 m thick dolomite layer underlain by an 11 m thick sandstone. The calcrete layer occurs from 15 m below surface to 56 m. A clay layer of 32 m thick was recorded from 56 m to 88 m below the surface. Below the clay, the dolomite rock was recorded up to 163 m.

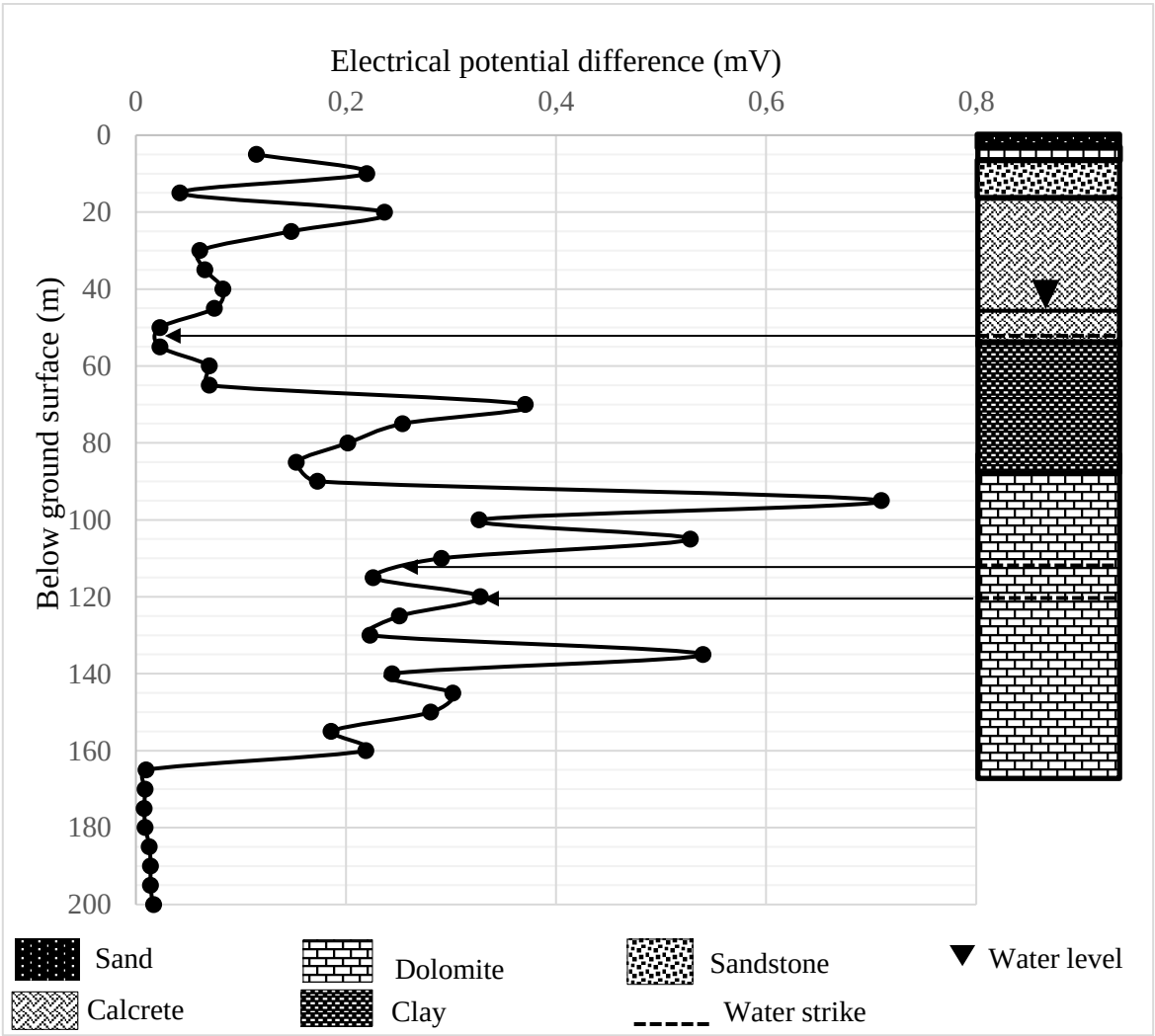

Figure 4.7 Electric potential difference profile for ADMT station S38 and borehole data from borehole 2523DD00095

The electric potential difference profile shows that the sandstone layer has an electric potential difference of about 0.22 mV at 10 m, then decreases to 0.042 mV at contact with calcrete at 15 m below the surface. The electric potential difference of 0.22 mV at 10 m indicates that the sandstone might be fresh in the upper part. However, the decrease in electric potential difference of the sandstone towards the contact with calcrete at 15 m suggests that the contact zone might be softer with some chances of being a preferential flow zone for groundwater.

The electric potential difference of the calcrete is 0.23 mV at 20 m below the surface, then decreases towards contact with the clay. The higher electric potential difference on the upper part of the calcrete indicates that the calcrete occurs as a hard pan on top and then occurs as a different form in the lower zones where the electric potential difference decreases. The lowest electric potential difference of 0.023 mV occurs at 50 m and 55 m below the surface, corresponding to the contact between the calcrete and clay. The first water strike at 55 m was recorded at the zone with the electric potential difference of 0.023 mV, suggesting that this is a potential aquifer zone, and the lowest electric potential difference might have been caused by groundwater saturation.

The clay zone shows varying electric potential difference properties. The upper 10 m of the clay electric potential difference 0.023 mV at 55 m, and 0.07 mV at 60 m and 65 m, which could possibly be influenced by the contact zone with calcrete, recorded as the first water strike. Therefore, the upper 10 m zone of the clay might be weathered or soft. The zone between 65 m and 70 m shows an increase in electric potential difference, which could characterize an unweathered clay zone. The electric potential difference of the clay after 70 m appears to decrease again towards the contact with dolomite at 90 m. This suggests a weaker contact zone between the two formations, which could be a preferential flow path for groundwater.

The dolomite zone also shows a variation in electric potential difference. The possible attribute to this variation has been discussed in section 4.4.1. The last two water strikes at 112 m and 120 m below the surface occurs on the dolomite, where the electric potential differences 0.25 mV and 0.328 mV, respectively. The electric potential at these zones points to a contact between dolomites of different formations or a vein or chert bed that occurs at 120 m causing electric properties contrast and preferential groundwater flow path.

According to the NGA records, the water level for borehole 2523DD00095 was recorded to be 45.65 m below the surface a day after drilling. This water level occurs above the water strikes suggesting confined conditions.

4.4.6 Survey Station S41 - BH 2523DD00096

Figure 4.8 Presents the electric potential difference profile of ADMT station S41 along with the borehole data of the borehole 2523DD00096. The lithological data shows a 28 m thick layer of calcrete overlain by a thin layer of sand. The dolomite occurs at about 32 m below the surface, extending to the bottom of the borehole at 152 m. Lenses of 2 m thick mudstone at 43 m and 1m thick shale at 102 m and 140 m are observed in the logs.

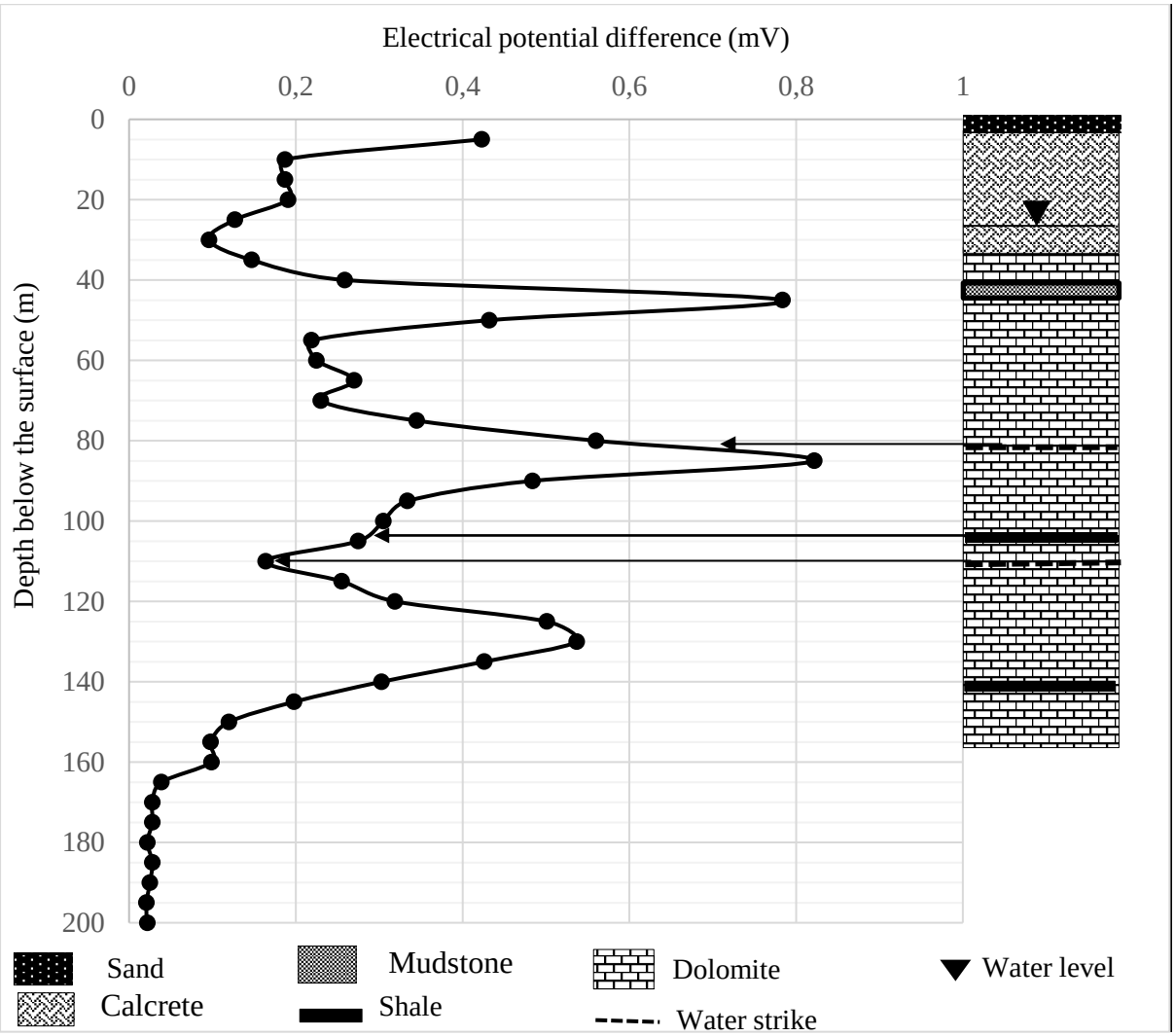

Figure 4.8 Electric potential difference profile for ADMT station S41 and 2523DD00096 borehole data

The profile shows that the upper section of the calcrete layer exhibits an electric potential difference of 0.423 mV, followed by a decline in electric potential difference to 0.18 mV at 10 m and an even greater reduction at the contact with the dolomite. The elevated electric potential difference on the calcrete might be suggesting a hard pan calcrete. The decrease in the electric

potential difference of the calcrete towards the contact with dolomite suggests a weaker zone which can possibly be a groundwater preferential flow zone because the electric potential difference increases again after the contact in the dolomite section. Elevated electric potential difference anomalies of 0.78 mV and 0.822 mV are observed at 45 m and 85 m, respectively. The lithology at 45 m has been recorded as a 2 m thick mudstone.

The first water strike at 81 m is linked to a contact between the dolomite of different electric properties. The second and third water strikes at 107 m and 116 could be linked to the contact between dolomite and shale. The NGA data shows that the water level for the borehole 2523DD00096 was measured at 25 m after 16 days the borehole has been drilled. This may imply that the borehole was left for a while to allow more water to accumulate from the water strikes.

4.4.7 Survey Station S50-BH 2524CC00236

Figure 4.9 presents the borehole data from borehole 2524CC00236 along with the electric potential difference profile for station S50. The borehole data reveals a 5 m thick sand layer from the surface, underlain by 10 m calcrete from 5 m to 15 m below the surface. The dolomite rock was recorded from 15 m to the end of the borehole at 150 m.

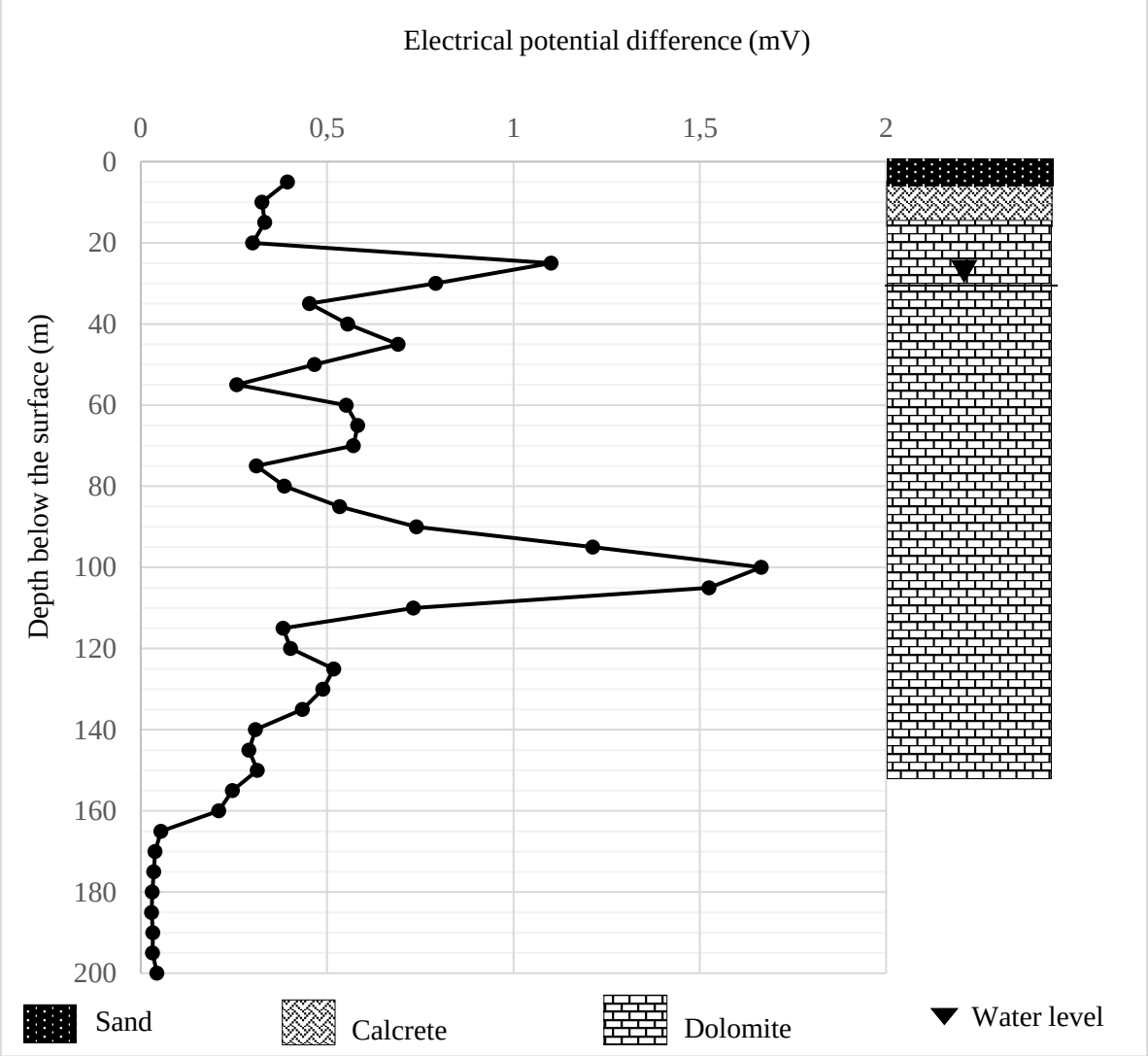

Figure 4.9 Electric potential difference profile for ADMT station S50 and 2524CC00236 borehole data

The electric potential difference profile shows an electric potential difference of 0.393 mV at 5 m, which is at the contact between the sand, and calcrete. The electric potential difference appears to decrease towards the contact between calcrete and dolomite. The high electric potential difference at the contact between sand and calcrete suggests that the sand might have been dry and the calcrete occurring as a hard pan hence the higher the electric potential difference.

The profile shows an enormous jump in electric potential difference from 0.303 mV to 1.10 mV at 20 m and 25 m, respectively, in the dolomite. This change in electric potential difference can be interpreted as a contact between two different formations. It is most likely that the

contact between calcrete and dolomite was recorded at 15 m; according to the borehole information, it is actually at 20 m.

The electric potential difference of the dolomite appears to be varying from 0.25 mV and 1.66 mV. The range in electric potential difference may be attributed to variation in dolomite formations and their electric properties. A gradual increase of electric potential difference occurring from 80 m (0.385 mV) to 100 m (1.66 mV) is observed, then the electric potential difference gradually decreases again after 100 m. No changes in lithology were recorded at this particular zone.

The borehole information of 2524CC00236 does not have any records of water strikes and water levels after drilling, suggesting that the borehole might have been dry during drilling. The water level information about this borehole on NGA shows that the first water level was recorded at 52.5 m after 4 months the borehole was drilled. This implies that there might have been water seepages, particularly from the contact zones between the lithology at 55 m and 75 m, where the electric potential difference profile shows that there may be a reasonable possibility for water at these depths.

4.4.8 Summary

The correlation between the electric potential difference and the available borehole data serves as the critical step toward the calibration of the electric potential difference measurement. It is evident from the correlation analysis that some of the borehole information did not coincide well with the electric potential difference profiles. The discrepancy between these two data sets can be attributed to numerous factors, such as 1) human error, which may have happened during the logging of the drilling samples or when the data was entered into NGA. 2) The ADMT tool measures at 5 m depth intervals, which may miss some information such as the precise depth of the geological contacts, resulting in an inaccuracy of 5 m in the electric potential difference data. 3) Drillers often collect drilling data in the field voluntarily; thus, it is conceivable that some critical information, such as depth of geological contacts or the proper lithology identification, may be overlooked. Since the geophysical data was gathered and inspected in the field by hydrogeology professionals, it can be used to correct the drilling data in this regard. Because the disparity between the electric potential difference data and the borehole information in this study was not greater than 10 m, the drilling data was not adjusted. This discrepancy complements geophysical equipment's 5 m sampling interval.

Table 4.3 shows that the boreholes 2524CC00093, 2524CC00091, and 2523DD00095 had water levels measured the next day after drilling. This suggests that these boreholes had enough water for the water levels to be measured the next day after drilling compared to the other boreholes (2523DD00099, 2523DD00097, 2523DD00096, and 2524CC00236) that had water levels measurements days or months after drilling. Boreholes 2524CC00093, 2524CC00091, and 2523DD00095 had water strikes recorded during drilling. The electric potential difference for water strike zones for these boreholes ranges from 0.02 mV to 0.26 mV.

Table 4.3 A summary of the electric potential difference properties and the boreholes information

NGA BH ID	**Electric potential difference range of the (mV)**	**Electric potential difference at water strike (mV)**	**Borehole depth (m)**	**Water level (m)**		**Air blow yield (L/s)**
2523DD00099	0.274 - 7.958	No water strike	118	16	Measured after 2 months	Not Available
2523DD00097	0.307 – 4.321	0.364 (at 11 m) and 0.409 (at 34 m)	116	4.8	Measured 16 days after drilling	0.0002
2524CC00093	0.022 – 0.140	0.037 (at 31 m) and 0.0325 (at 81 m)	130	13.21	Measured the next day after drilling (affected by pumping)	0.5
2524CC00091	0.037 – 0.25	0.065 (at 21.57 m) and 0.11 (at 147 m)	166	21.57	Measured the next day after drilling (affected by pumping)	5
2523DD00095	0.023 – 0.71	0.023 (at 55 m), 0.226 (at 111 m) and 0.328 (at 120 m)	166	45.65	Measured the next day after drilling	0.25
2523DD00096	0.096 – 0.822	0.680 (81 m), 0.48 (104 m) and 0.164 (at 116 m)	150	25.86	Measured 16 days after drilling	2
2524CC00236	0.258 – 1.665	No water strike	150	52.50	Measured 4 months after drilling	Not Available

In principle, groundwater lowers the resistivity nature of the host rock. In electric geophysical methods, the relatively low resistivity is generally linked to softer zones within the rock that may occur as weathered or fractured zones, which are capable of being aquifers. Generally, the rock is disintegrated when a zone is weathered or fractured (Figure 4.10). Therefore, the water in this zone will drain until it reaches a less disintegrated rock that can hold the water. Applying this principle and the general understanding of groundwater occurrence in weathered-fractured rocks, the electric potential difference range characterizing the weathered-fractured zone in the subsurface can be derived from the electric properties of the dolomite.

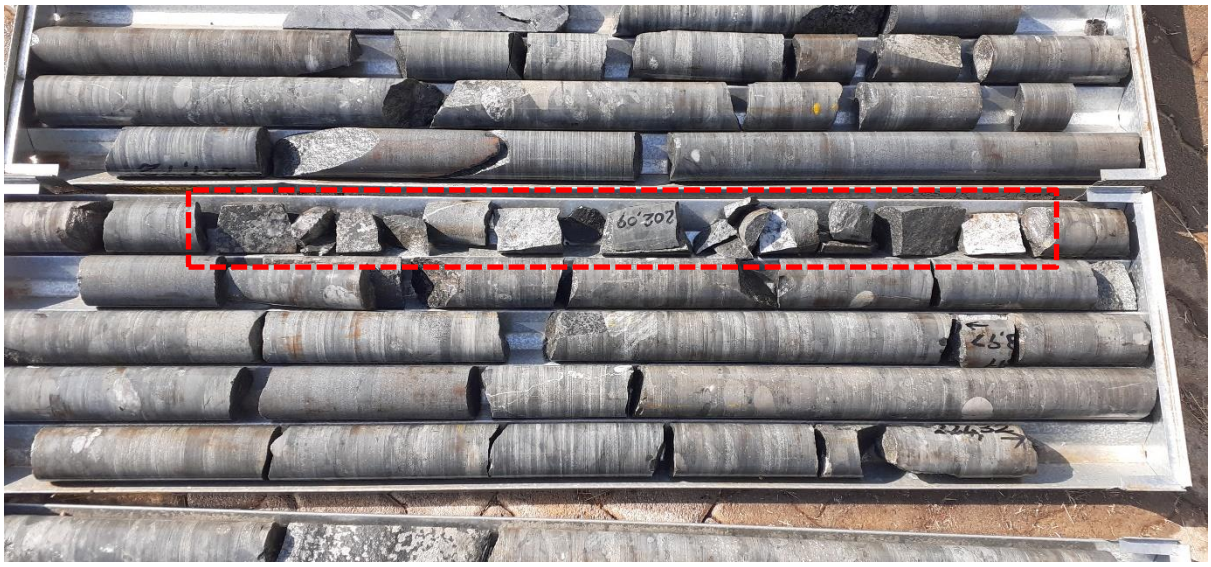

Figure 4.10 A typical example of a weathered-fractured zone in dolomite (marked in red). This picture was taken from borehole BHW 289 during core logging

The first water strike at 31 m for borehole 2524CC00093 occurs where the rock shows an electric potential difference value of 0.037 mV. The electric potential difference profile for this borehole in Figure 4.10 shows that the zone above the water strike has relatively lower electric potential difference values of 0.02 mV at 20 and 25 m below the surface. The fact that the water was intercepted at a zone with a higher electric potential difference than the zone above suggests that the water at the highly weathered zone (20 and 25 m) might have drained and collected at 31 m. This implies that the water strike is linked to a fractured-weathered aquifer zone. The second water strike at 81 m occurs where the electric potential difference is relatively low (0.0325 mV) compared to the electric potential difference at 75 m (0.054 mV) and 85 m (0.084 mV). This suggests that at 81 m, the rock might be weathered and saturated with water hence the lower the electric potential difference.

The boreholes information summary in Table 4.3 shows that the first water strike for borehole 2524CC00091 occurs where the electric potential difference is 0.065 mV at 21.57 m. According to the electric potential difference profile for this borehole Figure 4.7, the zone above the water strike at 15 m shows a relatively lower electric potential difference at 15 m (0.053 mV). Therefore, this suggests that the water strike at 21.57 m is linked to the highly weathered zone at 15 m, where the water might have drained and collected at 21.57 m. Therefore, this water strike is linked to a weathered-fractured zone in the dolomite. The second water strike at 147 m occurs at a zone showing an electric potential difference of 0.11 mV. The zones above show similar electric potential difference values suggesting the same dolomite formation. However, just below the water strikes, there is a recorded contact between the dolomite and granite, suggesting that this water strike might be linked to the geological contact.

The first water strike for borehole 2523DD00095 occurs where the electric potential difference is 0.023 mV. According to the electric potential difference profile for this borehole in Figure 4.7 the water strike is at the lowest electric potential difference in the borehole column. This suggests that the water strike at the weathered or fractured zone is saturated with water. The second and third water strike electric properties suggest that this water strikes are associated with contact between different dolomite formations.

From this discussion about the water strikes of the boreholes that intercepted water during drilling, it can be observed that the electric potential difference range that shows a weathered-fractured aquifer zone within the dolomite is between 0.020 mV and 0.065 mV. The fact that the boreholes drilled on this weathered-fractured zone aquifer had water strikes suggests that the weathered-fractured zones in dolomite are a factor influencing the groundwater occurrence in the study area.

Boreholes 2523DD00099, 2523DD00097, 2523DD00096, and 2524CC00236 electric properties does not show the electric potential difference range between 0.020 mV and 0.065 mV characterizing fractured-weathered aquifer. The electric property of the water strikes for boreholes 2523DD00097 and 2523DD00096 suggest that the geological contacts were targeted when drilling these boreholes. This makes the geological contacts another possible factor for groundwater occurrence in the dolomite rock. Geological contacts are generally preferential flow paths for groundwater, as shown in Figure 4.11. Boreholes 2523DD00099 and 2524CC00236 did not have water strikes, while the geophysical data suggests that there are geological contacts. This implies that the geological contacts do not always yield water. The

water levels for the boreholes drilled on the contact zone were measured days and months after drilling, indicating that the contacts were not giving much water. This is supported by the poor blow yield of 0.0002 L/s measured in borehole 2523DD00097. The yields were not measured for the other boreholes without water strikes, implying that there might not have been enough water. The poor yields in geological contacts may be linked to the poor storage in the contacts.

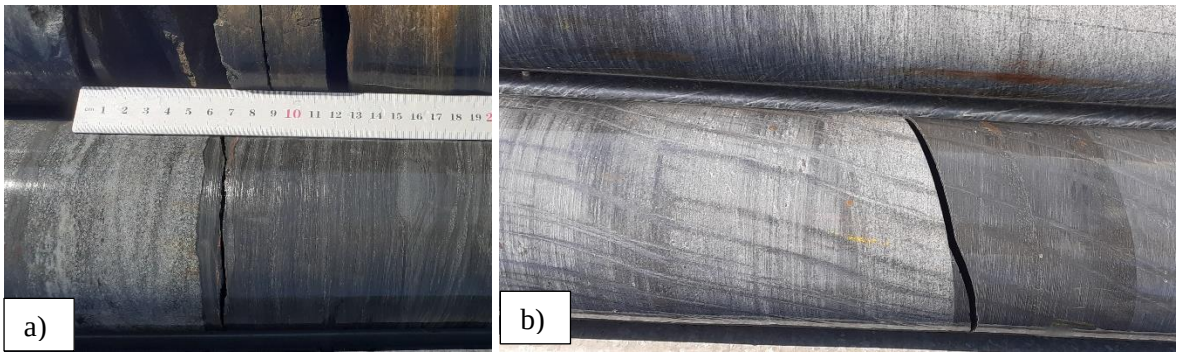

Figure 4.11 A picture showing preferential flow paths in geological contacts a) contact between cherty dolomite and chert poor dolomite b) contact between cherty dolomite and a lense of shale (core logs of borehole BH289)

The boreholes drilled on the weathered fractured zones show better yields, particularly borehole 2524CC00091, which has a yield of 5 L/s. This could be explained by the thicker (45 m) aquifer zone, which translates to better aquifer storage. The weathered-fractured zones within the dolomite appear to be the dominating influencing factor for groundwater occurrence in the dolomite of the TBA. Therefore, during groundwater exploration, it would be advisable to target the weathered-fractured zones than just the contacts zones alone.

4.5 ELECTRIC POTENTIAL DIFFERENCE MODELLING

This section of chapter 4 presents the processed MT data into electric potential difference cross sections models using Rock Works 2021. The evaluation process of the interpolation algorithms available on Rockworks was carried out to identify the optimum interpolation method for the MT geophysical methods.

4.5.1.1 Evaluation of modelling algorithms

To identify the optimum interpolation method on Rockworks (2021), Figure 4.12 to Figure 4.20 present the models generated from nine interpolation methods under the model-based P data section in Rockworks (2021). The potential difference data from sounding stations (S12, S13, S14, S15, S16, S17, and S62) along cross-section A-A' were used to generate these

models. Table 4.4 gives a summary of the interpolation algorithms from the Rockworks software.

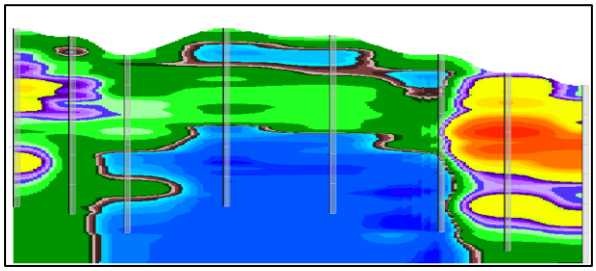

Figure 4.12 IDW Anisotropic

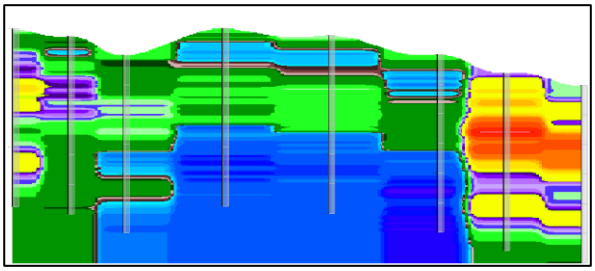

Figure 4.13 Closest Point

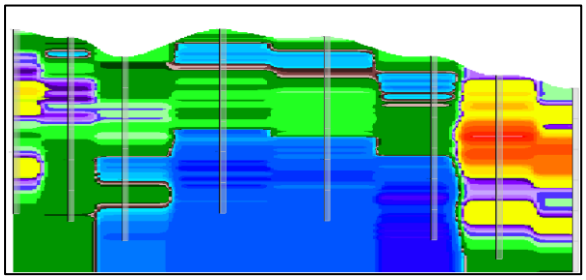

Figure 4.14 Highest Probability

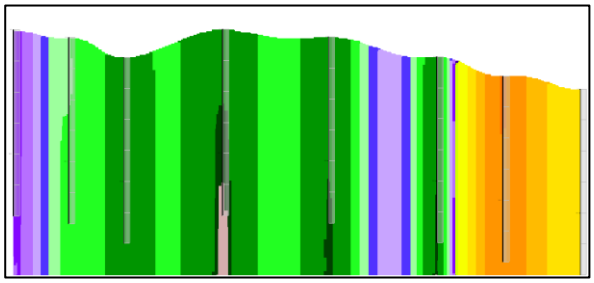

Figure 4.15 IDW Advanced

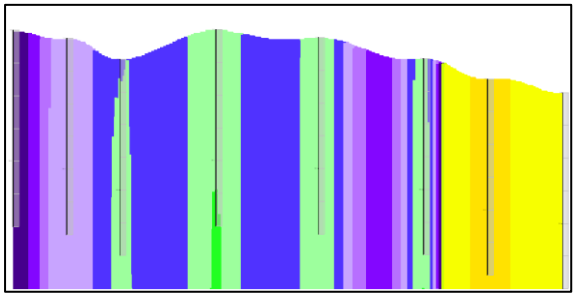

Figure 4.16 Trend Polynomial

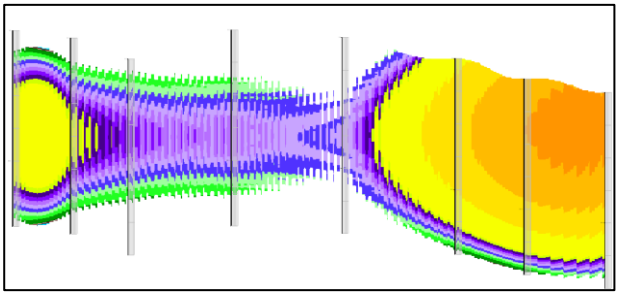

Figure 4.17 IDW Isotropic

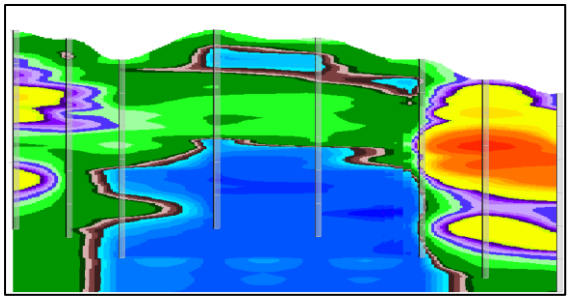

Figure 4.18 Kriging

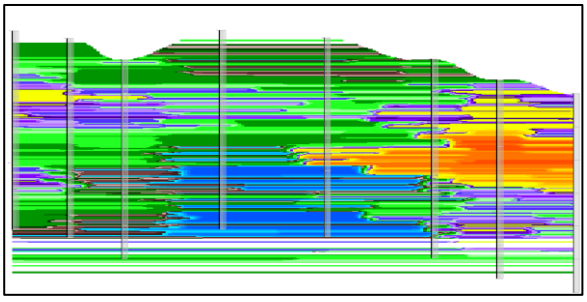

Figure 4.19 Lateral Blending

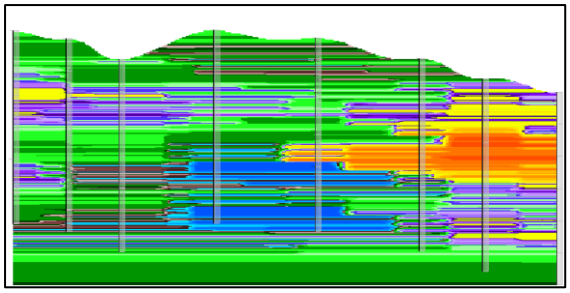

Figure 4.20 Lateral Extension

Table 4.4 summary of observations from the interpolation algorithms

Interpolation method	**Observations**
Closest point	The EPD values do not correlate well with the field data as some stations appears not show the true field values.
IDW anisotropic	The EPD values correlated with the field data.
Highest probability	The EPD values correlated with the field data.
IDW advanced	Shows similar EPD values for each station from the surface to 300m. No changes of EPD with depth.
Trend polynomial	Shows similar EPD values for each station from the surface to 300m. No changes of EPD with depth can be observed.
IDW Isotropic	The data appears to be incomplete as some stations data appears to have been omitted.
Kriging	The EPD values do not correlate well with the field data as some stations appears not show the true field values.
Lateral blending	Shows exaggerated lateral changes of the EPD
Lateral extension	Shows exaggerated lateral changes of the EPD

The optimum interpolation algorithm for the models of electric potential difference was identified after cross validation of the various models produced from the nine interpolation methods. It was observed that the Inverse Distance Weighting (IDW) anisotropic method shows a better representation of the original data. The IDW anisotropic plot shows smooth contours, which represent the subsurface better than the other interpolation algorithms.

Figure 4.21 present the IDW anisotropic interpolated model cross-validated the electric potential difference profile plots for three stations (S12, S15, and S62). This was done to compare the measured electric potential difference values and the modelled electric potential difference values at the same locations. The results show that the electric potential difference values in the model are coherent with the original field data. Therefore, the IDW anisotropic algorithm was applied to generate the electric potential difference models for all the cross-sections in this study.

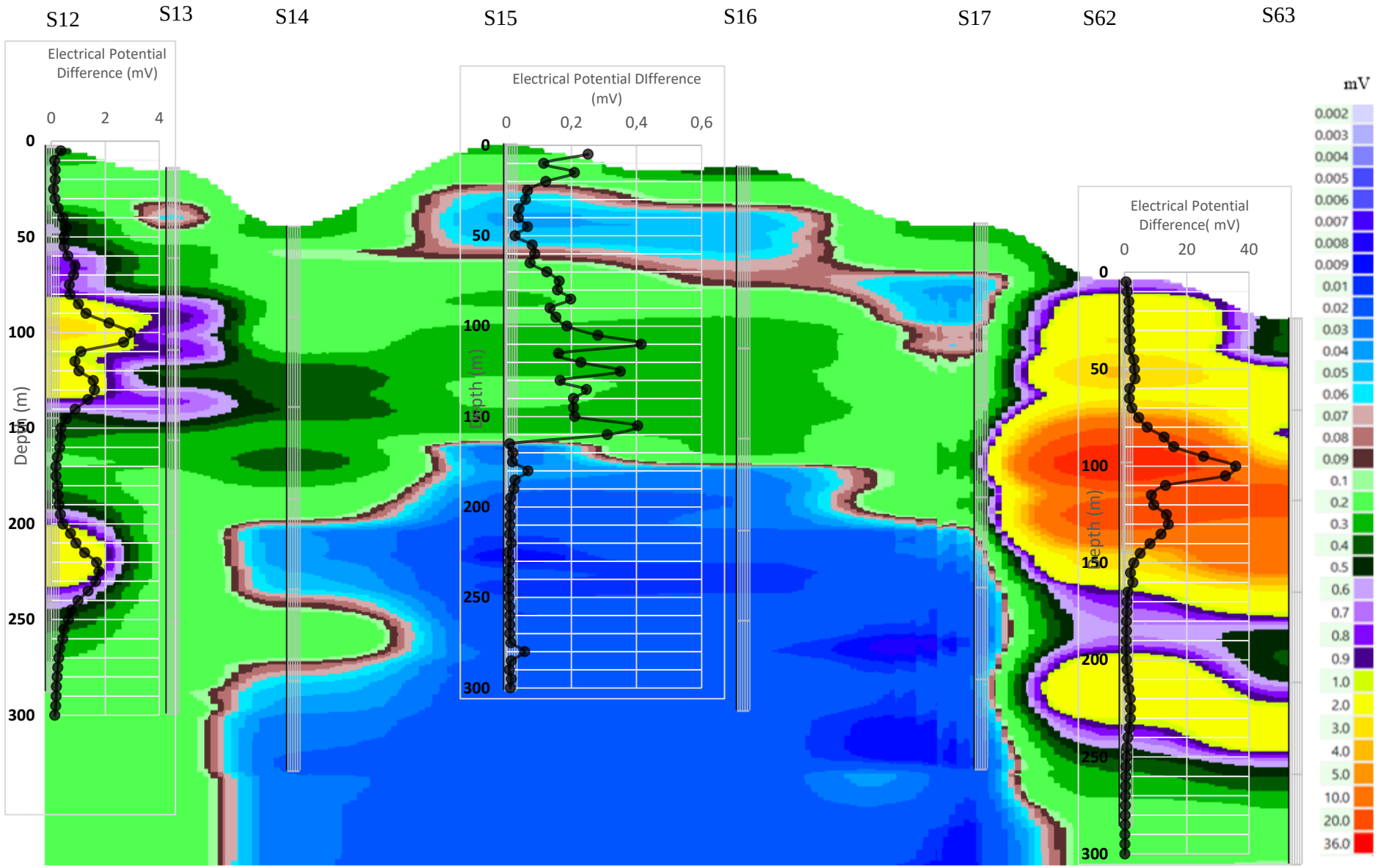

Figure 4.21 Electric potential difference model of cross-section A-A' plotted with the electric potential difference profiles from stations S12, S15 and S16

4.6 CROSS-SECTIONS MODELS

This section presents the electric potential difference models generated on Rockworks (2021) using the IDW–anisotropic interpolation method. The electric potential difference data for each sounding station along transverse lines were interpolated to generate cross-section models showing the electric potential difference properties of the subsurface. A hydrogeological conceptual model is presented for each cross section. Figure 4.22 present a Google Earth image showing the location of the ADMT sounding stations on each cross-section.

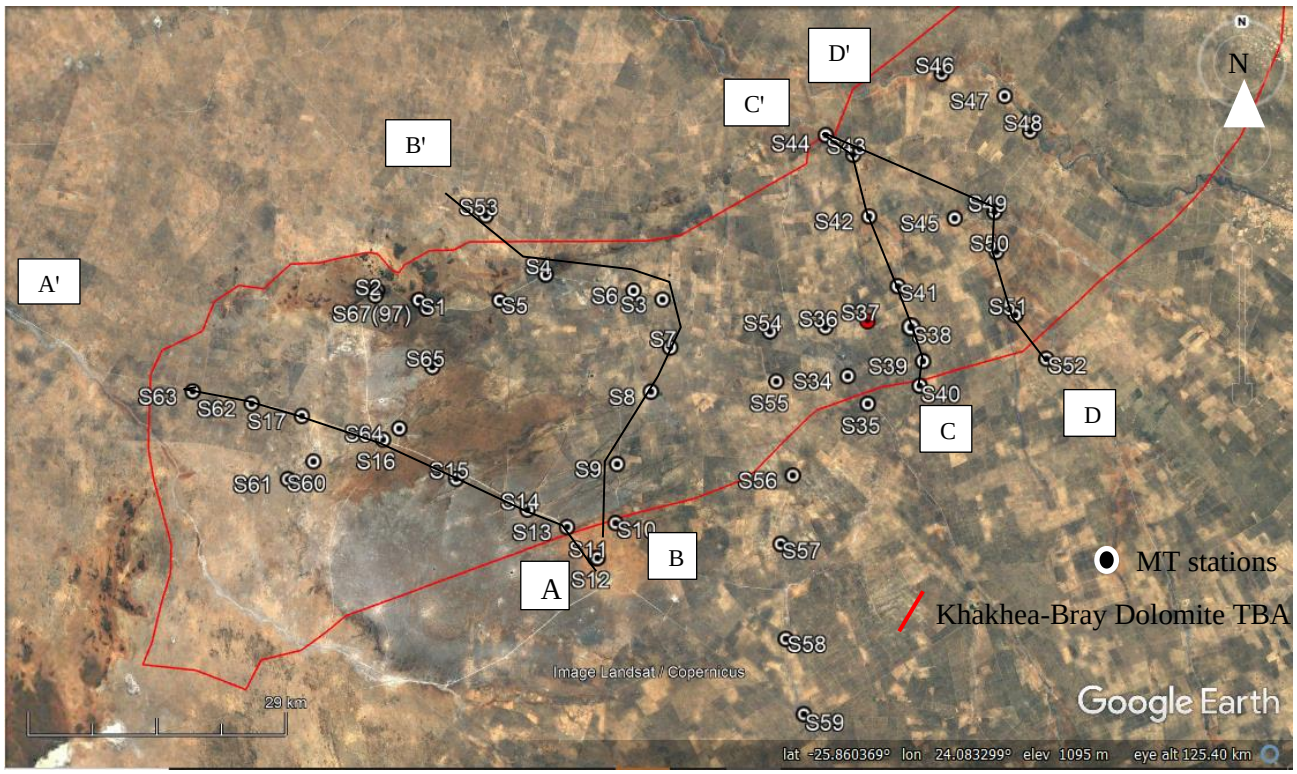

Figure 4.22 Google Earth image showing the location of the cross-sections in relation to the inferred dolomite boundary.

4.6.1.1 Cross-section A-A'

Figure 4.23 presents the sub-surface's 2D electric potential difference model of the 51 Km long cross-section A-A'. The cross-section consists of eight ADMT sounding stations spaced five to ten kilometres apart. S12 is the only sounding station that is located outside the TBA boundary.

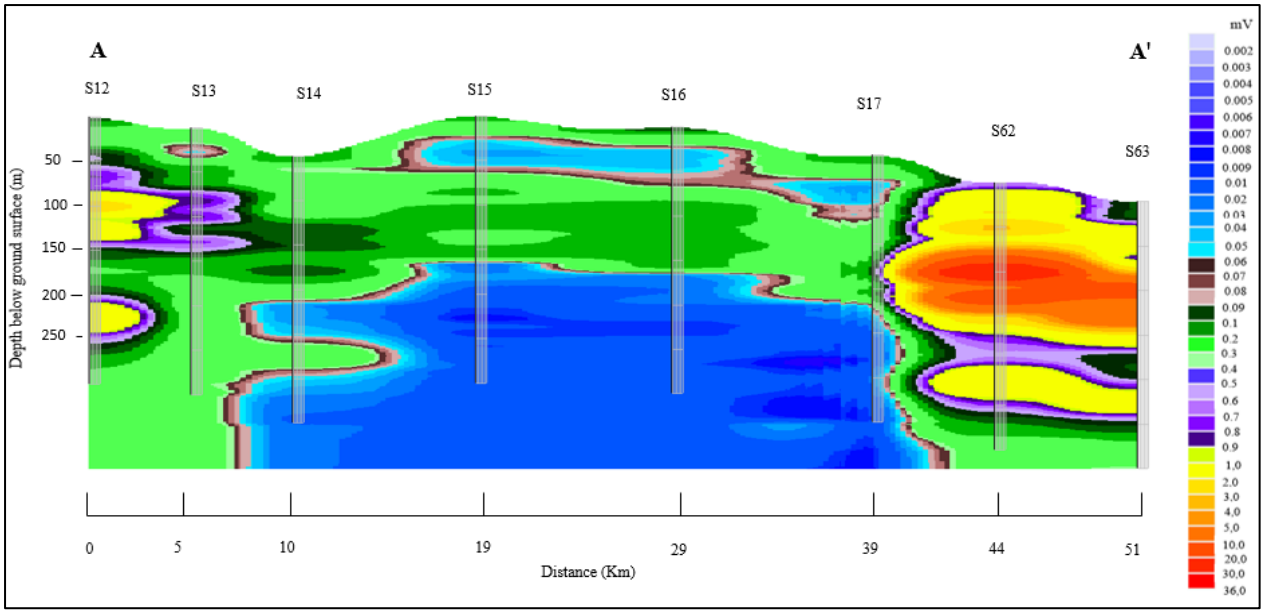

Figure 4.23 Electric potential difference model for cross section A-A'

The model shows that the study area along cross-section A-A' is both conductive and resistive, with electric potential values ranging from 0.002 mV to 36 mV. The stratigraphic layers of the different geological formations with varying electric properties could be identified by the contrast in electric potential difference reflected by the different colours. The electric potential contrast is more pronounced at stations 12, 13, and between stations S17 and S62. This may indicate different geological formations at these stations.

The highest potential difference values are observed in stations S12, S62, and S63. According to the TBA's regional geological map, the Transvaal dolomite unit is bounded by granite rock. The elevated potential difference values in stations S12, S62, and S63 may be pointing to granite because granite is generally harder than dolomite or another dolomite formation of different electrical properties.

Station S15 to stations S17 show consistent variation in electric properties of the subsurface. Because stations S15, S16, and S17 are situated in the inner part of the Khakhea-Bray TBA, their subsurface electrical properties may be reflecting the optimal electric properties of a typical dolomite with minimal effect from the contact with the granite. On the other hand, it appears that at stations S13, which is situated at the boundary of the TBA shows almost similar electric properties to S12 (occurring outside the TBA boundary), S62 and S63. Therefore, this suggests that these stations might be situated at the contact between the dolomite and the granite outside the boundary or the dolomite at these stations is relatively different in terms of the electric properties.

The model shows two zones of the lowest electric potential difference values. The shallow zones is observed in stations S13 to S17at varying depths between 7.5 m and 85 m. The electric potential difference in this zone ranges from 0.02 mV to 0.065 mV. The deeper zone of the lowest electric potential difference is observed in stations S14 to S17 at depths ranging between 165 and 300 m.

The electric potential difference model of the subsurface in cross section A-A' in Figure 4.24, can be simplified to Figure 4.24 showing the aquifers characterized by the electric potential difference range between 0.02 mV and 0.065 mV.

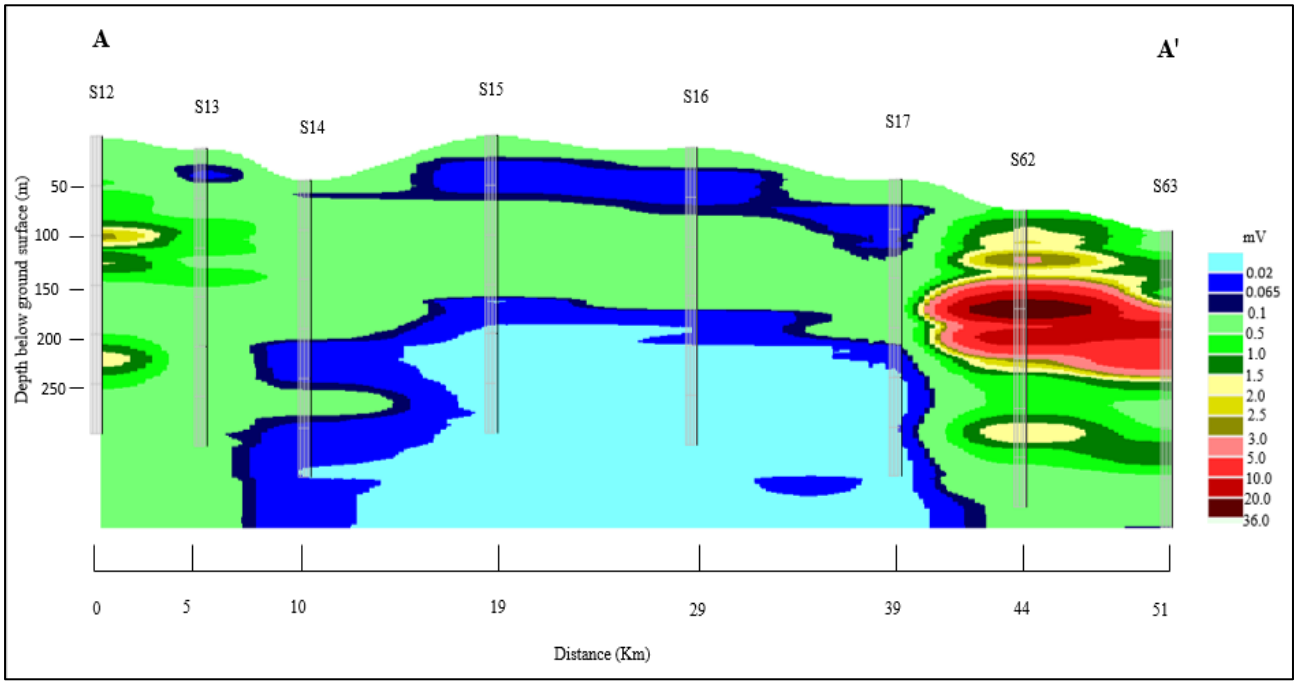

Figure 4.24 Electric potential difference model for section A-A' showing the potential groundwater aquifers characterized by the fractured-weathered zone

In Figure 4.24, a shallow weathered-fractured aquifer zone is observed in depths varying between 7.5 m and 85 m in stations S13, S15, S16, and S17. At S13, the aquifer appears to be 10 m thick and about 50 m thick for stations S15 to S17. At station 14, the aquifer occurs from 7.5 m to 20 m below the surface.

This shallow weathered-fractured aquifer zone in this cross section is confirmed by the municipal borehole 12-83443 in Station 13. The information board for this borehole (Figure 7.6) reveals that the borehole depth of the municipal borehole is 65.7 m, indicating that the drilling stopped where the formation was changing, as shown in Figure 4.25. The borehole

yield was recorded to be 5 l/s. This implies that the potential aquifer zone at 22.5 m -32.5 m might have a good yielding capacity.

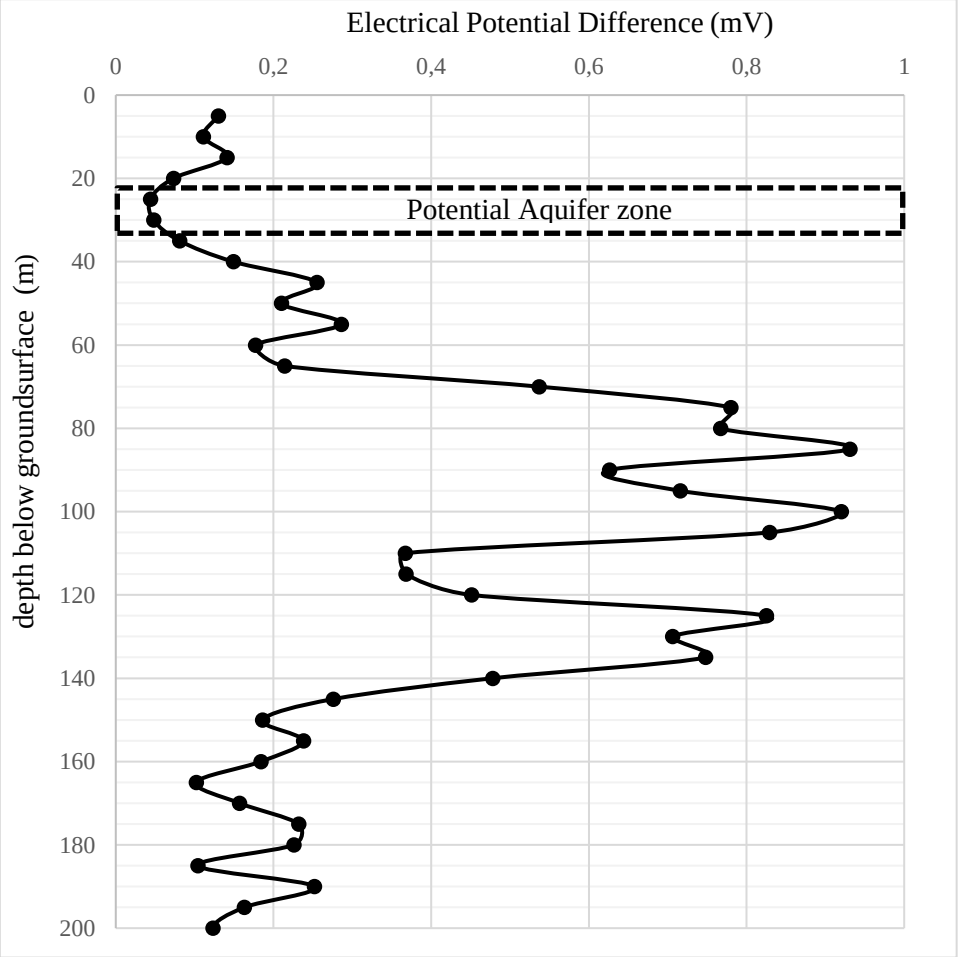

Figure 4.25 Electric potential difference profile of S13

Another borehole (borehole ID T0757) along this cross-section was identified closer to survey station S14. This borehole was not equipped with a pump when the data was collected. The borehole information was not available during the data collection. The groundwater level was measured to be 2.65 m below the surface during the geophysical survey. The borehole might be getting water from the weathered-fractured aquifer zone occurring between 7.5 m and 22.5 m. The shallow measured groundwater level suggests that the formation above the potential aquifer is a confining layer; hence the groundwater rises to a shallow level.

The survey at station S16 was conducted closer to a community windmill. The borehole information was not available during the data collection. The community windmill is most likely getting water from the weathered-fractured aquifer zone at 22.5 m–75.5 m.

In all the stations, the aquifer zone appears to be bounded by higher electric potential difference formation, suggesting that the aquifer may be confined. In reference to the geological data of the boreholes in section 4.4 the high resistive layer corresponds to calcrete layer.

A deeper zone showing electric potential difference values at the range of a weathered fractured zone in dolomite is observed. This zone is observed in stations S14 to S17. At stations S15 to S17, this zone occurs between 165 and 195 m below the ground surface. At stations 14 and 15, the zones are located between 165 and 200 m and 245 to 290 m, respectively. With the absence of the borehole drilling data for the boreholes within this cross section and the area at large limits the quantification of these zones to be aquifers. However, since they exhibit the electric properties of a weathered-fractured dolomite aquifer zone they can be referred to as potential aquifers that are pending confirmation.

The potential aquifer zone pending confirmation is overlain by a formation with a higher electric potential difference (0.07 to 0.1 mV) and underlain by a formation with an electric potential difference of less than 0.02 mV. The formation showing electric potential difference of less than 0.02 mV appears to only occur at deeper depths in the stations within the dolomite boundary. There were no borehole logs in this cross-section to establish the geology at this zone. It might be an entirely distinct formation from the dolomite or a different dolomite formation at greater depths.

There was no borehole with drilling data located in this cross section to confirm the subsurface geological formation. However, this cross section is located where the dolomite rock is outcropping therefore the subsurface geology is unconfirmed. Based on the lithology data of the boreholes within the study area, the dolomite in the subsurface is confirmed by the boreholes until 166 m and after this depth the geology pends confirmation. Therefore, the groundwater occurrence model in Figure 4.26 shows the dolomite from surface until 166 m. The elevated electric potential difference on stations S12, S62 and S63 were generalized to dolomite rock since there are borehole logs for any of the boreholes in this cross station to confirm the subsurface geology.

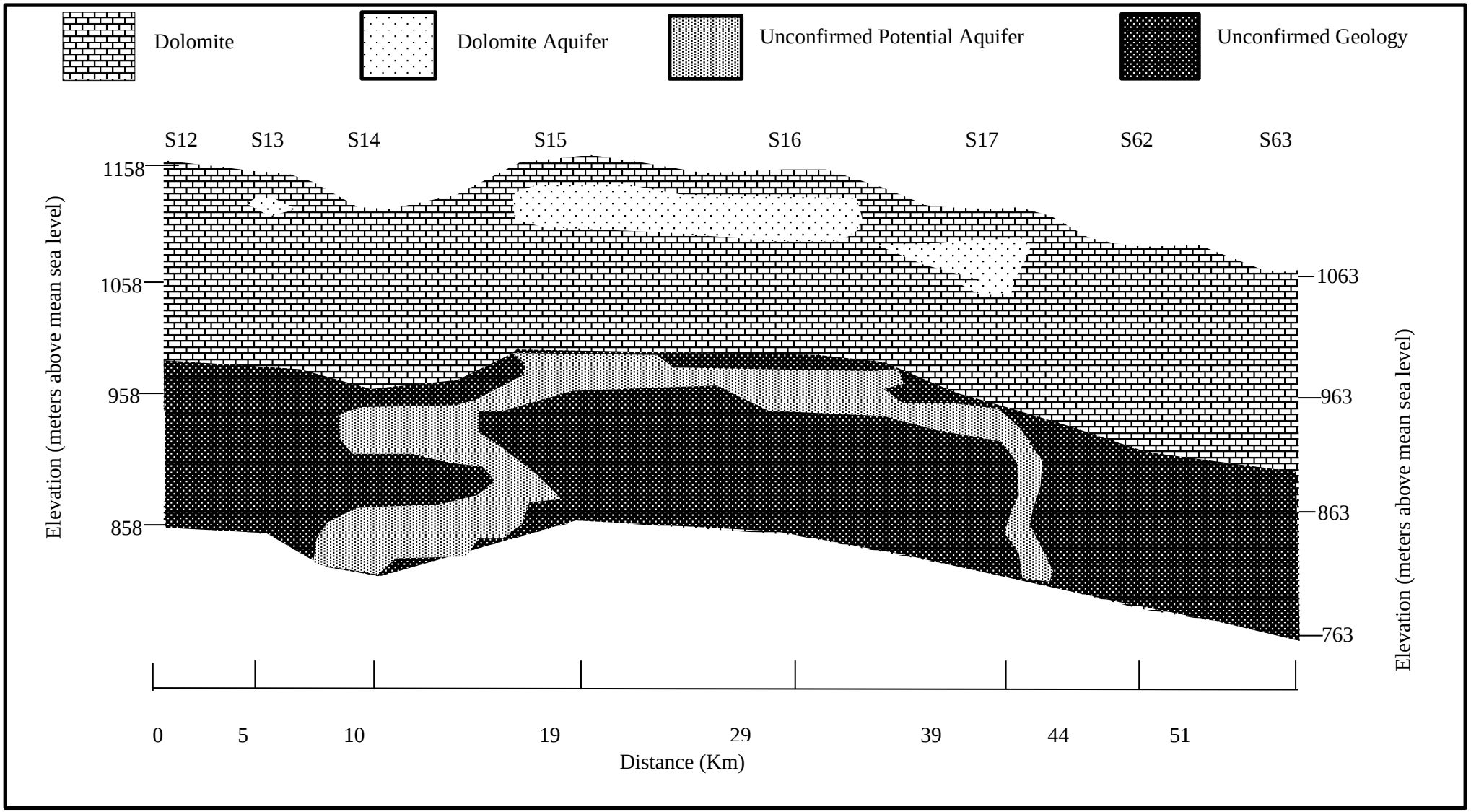

Figure 4.27 A groundwater occurrence model for cross section A-A'

4.6.1.2 Cross-section B-B'

Figure 4.28 presents the electric potential difference model for cross-section B-B '. This cross-section is 51 Km long and comprises of eight sounding stations. Two of the stations (S10 and S53) are located outside the boundary of the Khakhea Bray TBA.

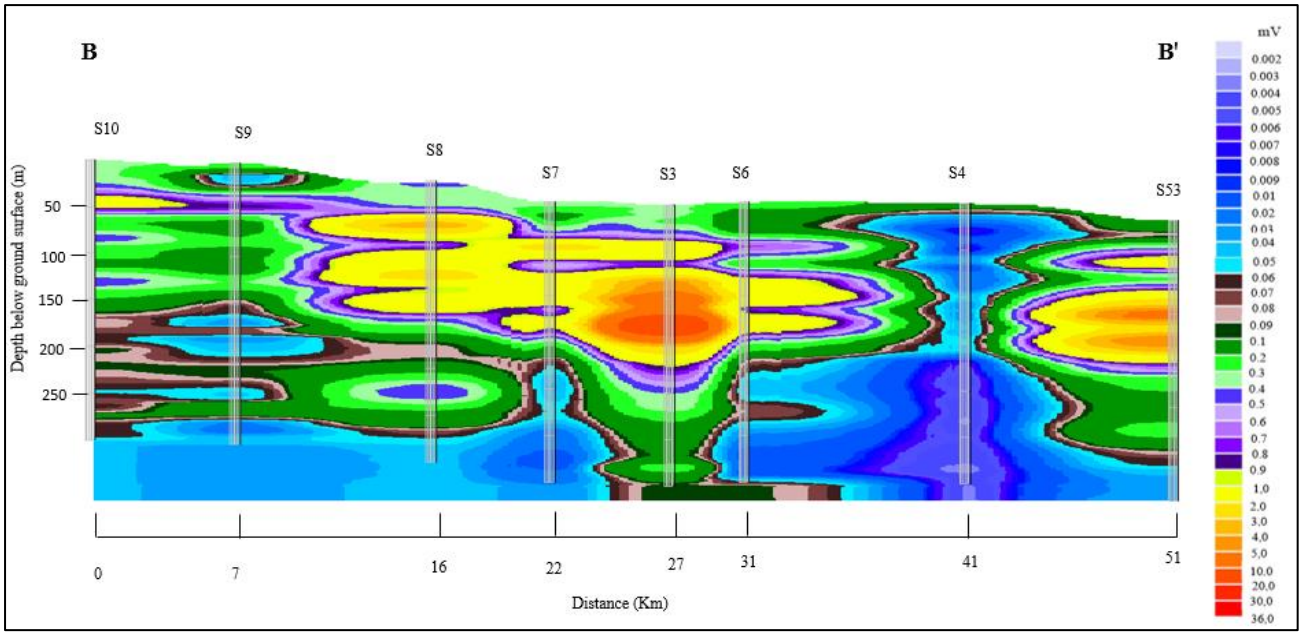

Figure 4.28 Electric potential difference model for cross-section B-B'

The electric potential difference cross-section model shows the varying nature of the subsurface with electric potential difference values ranging from less than 0.002 mV to 36 mV. The variation in electric potential difference of the subsurface implies that the geology in this cross-section comprises rocks with varying electric properties hence the contrast in electric potential difference.

The highest potential difference in this cross-section is observed between 125 m and 145 m in station S3. Potential difference values between 2 mV and 36 mV are observed as thick continuous zones in stations S10, S8 to S6, and S53. At S10, this zone occurs between 45 m and 50 m, between 45 m and 150 m at S8, and from 50 m to 165 m for S7. In S3, this zone occurs from 50 m to 185 m and in S53 occurs from 45 m to 50 m, and 85 m to 175 m. According to the borehole data of borehole 2523DD00099, which is closer to S3, the lithology from 45 m below the surface was logged as a dolomite rock and the attributes to varying electric properties of the dolomite has been discussed in section 4.4.1. The lithology from 15 m to 60 m below the ground surface in S8 has been logged as dolomite for borehole 2523DD00097.

Since S53 is situated outside the dolomite boundary, the elevated electric potential difference observed between 45 m and 50 m, and at 85 m to 175 m might be linked to granite rock outside the dolomite unit. S3 shows relatively lower electric potential difference values compared to the other stations. Figure 4.29 presents S3's electric potential difference profile showing an electric potential difference range between 0.003 mV and 0.127 mV and some isolated anomalies at 60 m, 100 m, and 145 m. The electric properties of the subsurface at this station suggest a completely different formation from dolomite, more so because the station is situated outside the dolomite boundary or the contact between the dolomite and granite rock.

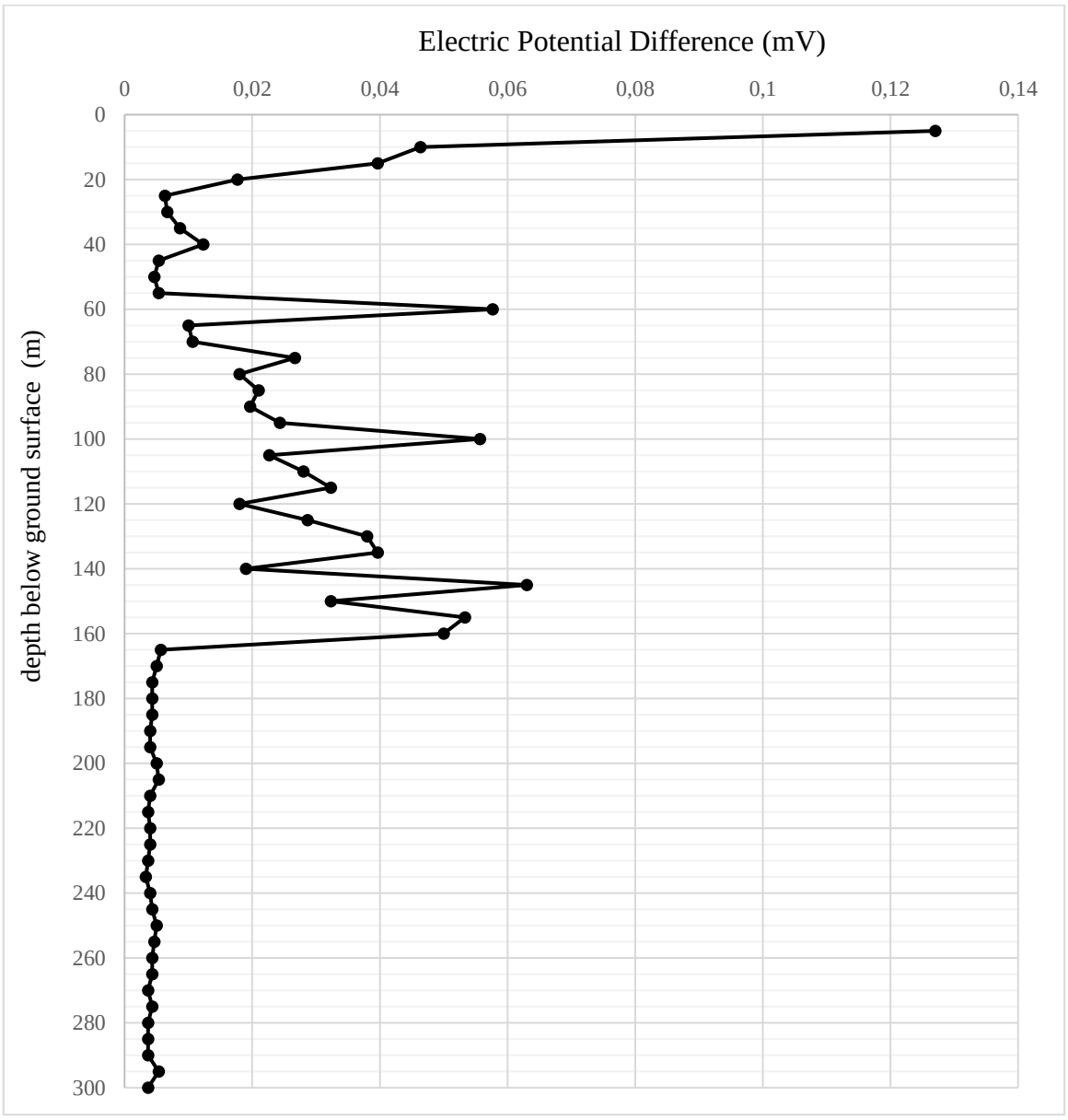

Figure 4.29 Electric potential difference profile for S4

The overall electric potential difference model for this cross-section suggests that geological contacts are the main influencing factor for groundwater occurrence. There is significant variation in geological formation compared to weathered or fractured zones characterized by potential difference values between 0.02 mV and 0.065 mV.

Figure 4.29 presents the electric potential difference model showing the aquifer zones characterized by electric properties between 0.02 mV and 0.065 mV (blue colour).

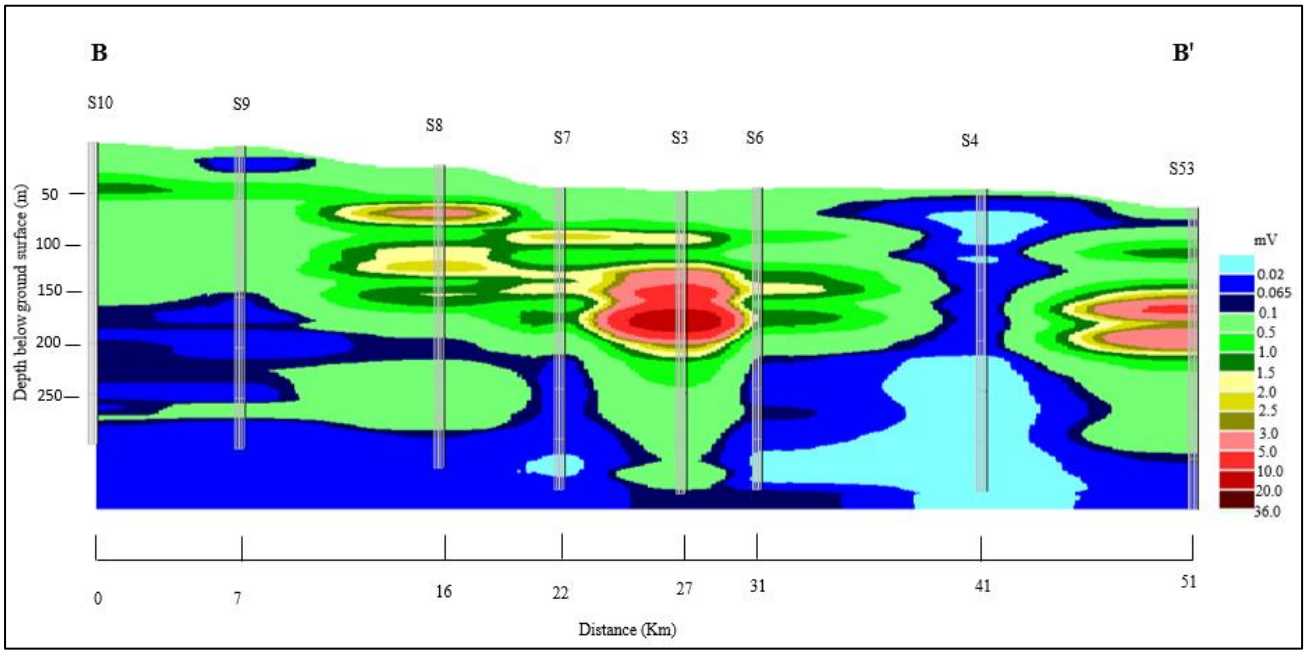

Figure 4.29 Electric potential difference for cross-section B-B' to show the groundwater potential in terms of the fractured-weathered zone

The electric potential difference model in Figure 4.29 generally shows shallow groundwater potential between 10 m to 25 m at station 9. The shallow groundwater potential zone at station S9 is bounded by higher electric potential difference formation, suggesting that the aquifer might be confined. At station S9, the groundwater potential zones also occur as isolated zones at deeper depths: from 155 m to 175 m, 185 m to 210 m, 240 m to 260 m, and 275 m to 300 m. Station 10, which is located outside the dolomite boundary also shows potential zones at deeper depths: 185 m to 195m, 245 m to 250 m, and 280 m to 300 m. S8, on the other hand, shows a potential zone between 270 m and 300 m. Station S7 shows a potential zone at 175 m to 300 m with a relatively lower electric potential at 265 m to 280 m. S3 does not show any potential groundwater zones, even at deeper depths. This may be attributed to the formation causing elevated electric potential difference zone extending to 200 m below the ground surface. S6

shows a groundwater potential zone from 165 m to 260 m, and lower electric potential difference formation occurs below the aquifer.

Station S53 does not show groundwater potential zones at shallow depths but occurs at depths between 265 m and 300 m. This station occurs outside the dolomite boundary but shows similar electric subsurface properties as the other in the cross-section. This might suggest that the station is within the dolomite boundary.

It appears that station 9 is the only station in the cross-section that shows groundwater potential at shallow depth exception of station S4 which has been discussed above. Therefore, the groundwater occurrence in all the other stations within this cross-section are dependent on the geological contact zones.

Figure 4.30 presents the groundwater occurrence model derived from the simplified electric potential difference model of cross section B-B'. The Stations S3 and S8 in this cross section were closer to boreholes with lithological logs. The borehole at S3 had calcrete from 2 m to 43 m then dolomite rock from 43 m to 118 m. The borehole at station S8 on the other hand, showed calcrete from 2 to 11 m then dolomite rock until 56 m. On the geophysical model it is not easy to differentiate between the calcrete and dolomite zones because they appear to show almost similar electric potential properties. It is for this reason that on the hydrogeological conceptual model the subsurface is generalized to dolomite expect for station S4 which show unique electric properties. Just like the other cross sections, the geology occurring below 166 m is characterized as unconfirmed geology and the associated zone showing weathered-fractured properties labelled unconfirmed potential aquifer zone.

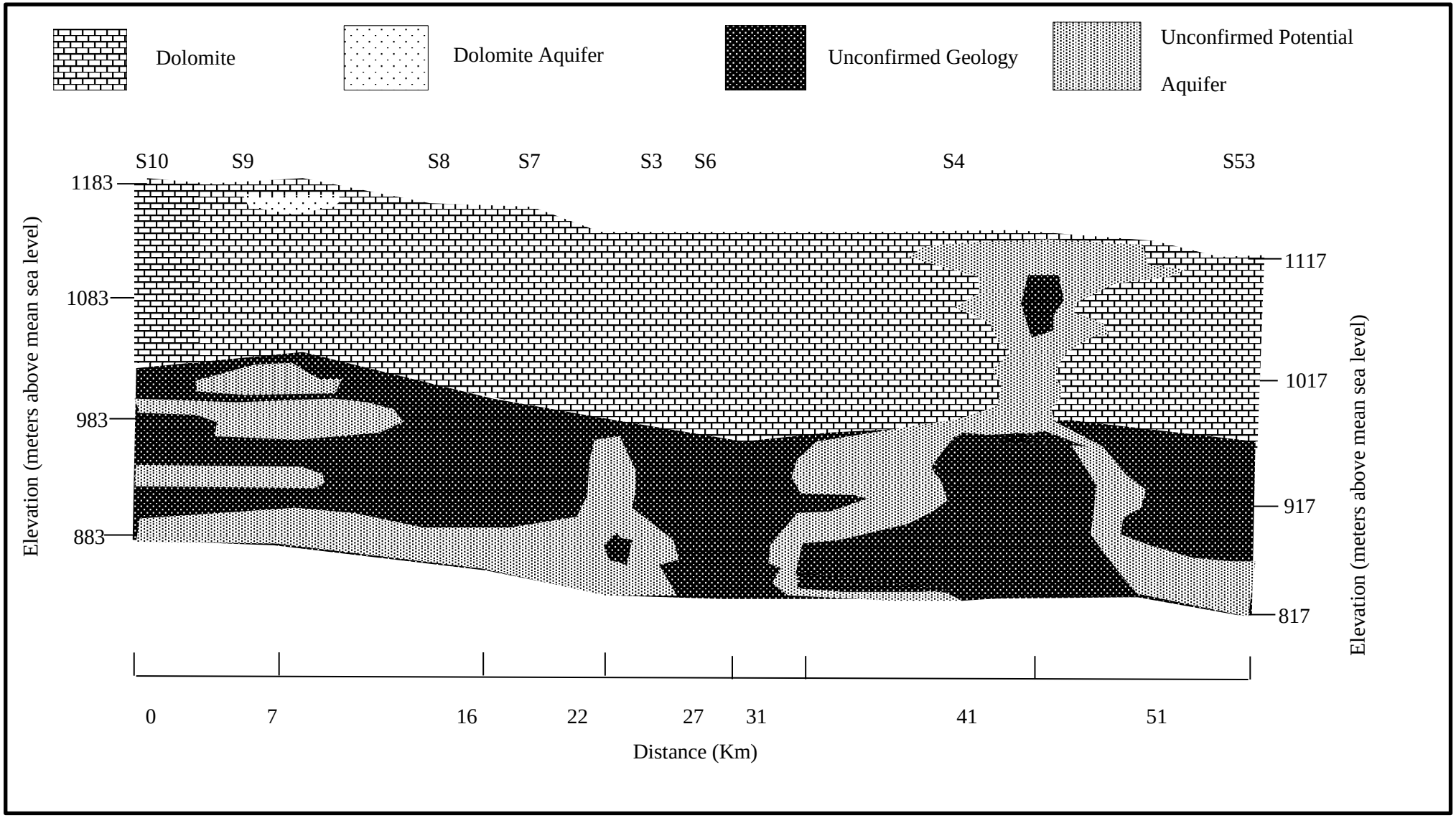

Figure 4.30 A groundwater occurrence model for cross section B-B'

4.6.1.3 Cross-section C-C'

Figure 4.31 presents the electric potential difference model along the cross-section C-C'. This cross-section is 31 Km across the inferred dolomite boundary and comprises of seven sounding stations. Stations S40 and S44 occur outside the inferred dolomite boundary.

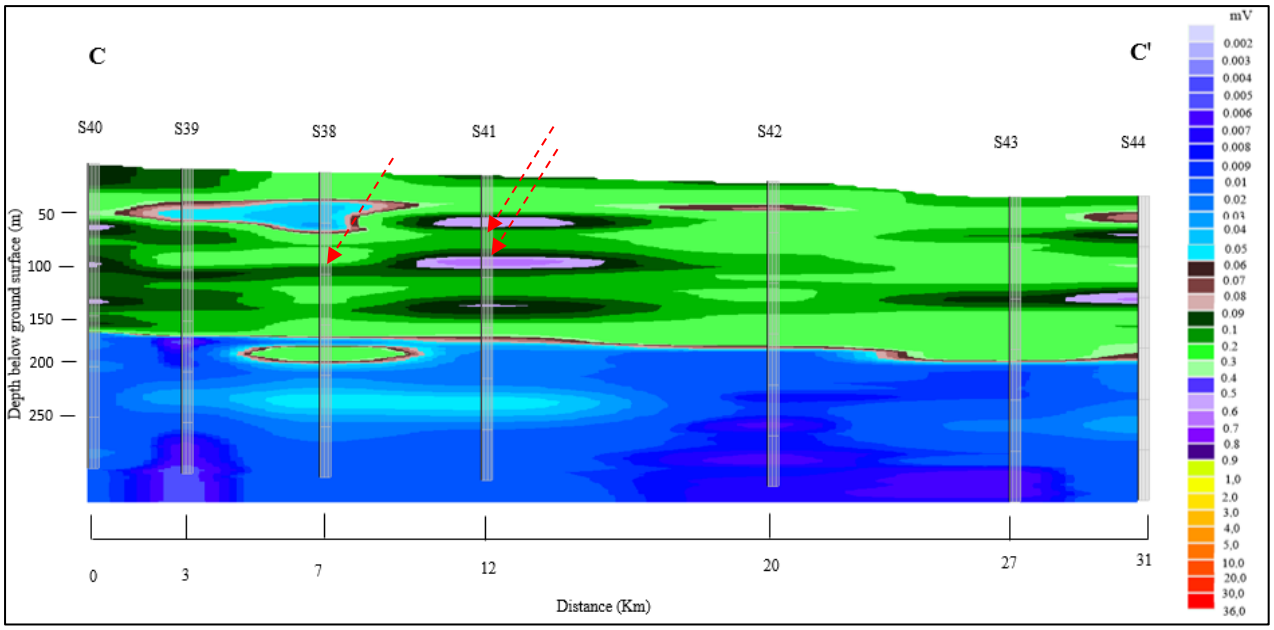

Figure 4.31 Electric potential difference model along cross-section C-C' (the red dotted arrows show the water strike zones for the boreholes closer to S38 and S41)

This cross section's electric potential difference varies from values less than 0.002 mV to 0.8 mV. The highest electric potential difference zones are observed as isolated zones in Station S41 at depths 40 m to 45 m and 80 m to 85 m as well at the station outside the boundary. The lowest electric potential difference zones occur at depths ranging between 45 m and 65 m in S39 and S38. The lowest electric potential difference zone is again observed at 165 m to 300 m below ground surface and is consistently in all the stations. The zone at the depth between 165 m and 300 m shows some variations in electric properties, suggesting varying geological formations.

The borehole data for borehole 2523DD00096, located closer to S41, shows water strikes recorded at 81 m, 90 m, and 110 m. The electric potential difference values at these depths are 0.680 mV, 0.48 m V, and 0.164 mV, respectively. According to the borehole lithology data, dolomite is the formation that is exhibiting elevated electric potential difference values. The electric potential model shows that the water strikes are associated with the contact zones between the dolomite formation of the elevated electric potential difference (0.6 mV- 0.7 mV)

and the dolomite formation with electric potential difference ranging from 0.2 mV - 0.3 mV (shown by the red arrows on the model). Therefore, the dolomite formation of elevated potential difference appears to influence the occurrence of groundwater at this station.

Stations 42 and 43 show less variation in electric properties of the rocks between the surface and 165 m compared to the other stations. This suggests that it might be the same formation from the surface to 165 m. The stations outside the dolomite boundary show almost similar electric properties with some elevated electric potential zones above 165 m. The elevated electric potential difference zones at these stations might be attributed to the granite occurring outside the dolomite boundary.

Figure 4.32 presents the electric potential difference model showing the zones of potential aquifers characterized by electric properties between 0.02 mV and 0.065 mV (blue colour).

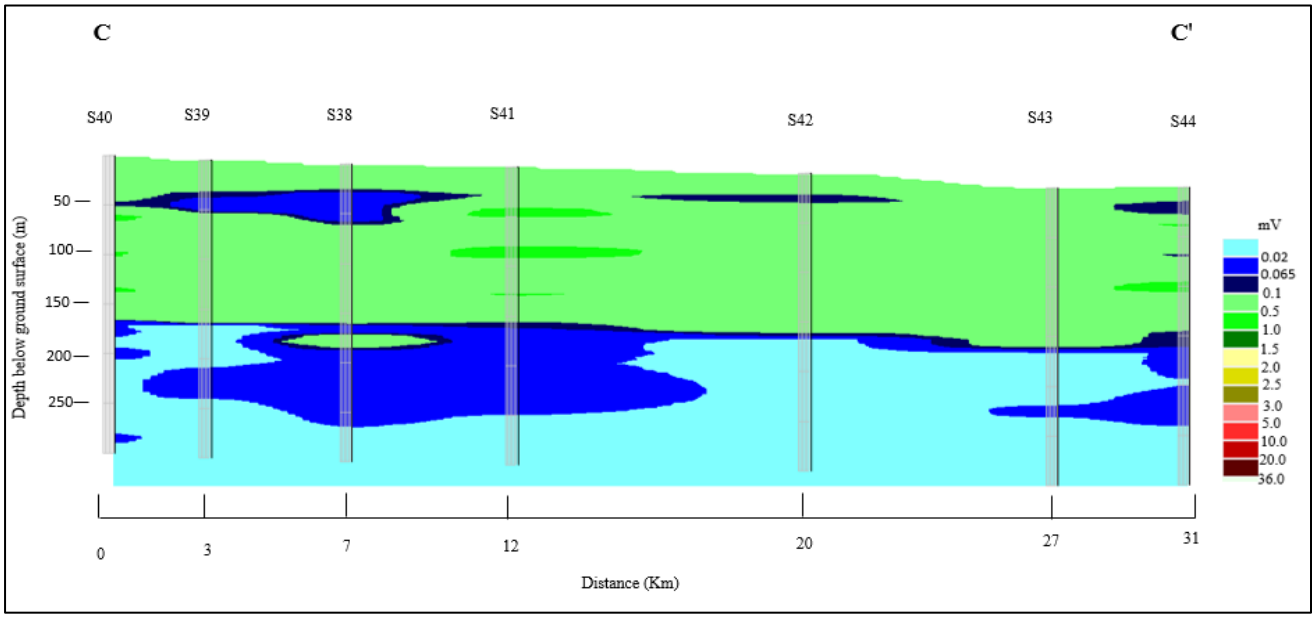

Figure 4.32 Electric potential difference cross-section through C-C' to show the groundwater potential in terms of the fractured-weathered zone

The model in Figure 4.32 shows two zones that has electric potential difference at the range between 0.02 mV and 0.065 mV. The first zone is observed at a shallow depth in station S39 between 35 m and 57.5 m below surface, and in S38 between 27.5 m and 57.5 m. The shallow aquifer zone in station S38 is confirmed by the first water strike at 55 m for borehole 2523DD00095. The stations S41 and S44 shows some potential zones even though the electric potential difference at these zones are between 0.065 mV and 0.1 mV but they can be targeted for water during drilling.

Station S41 and S43 do not show potential aquifer zones at the shallow depths. On Google Earth, the stations S41 and S43 appear to be plotting a couple of meters away from a sand-filled stream, whereas all the other stations plot on the stream. Therefore, this suggests that the stream influences the shallow potential aquifer zone along this cross-section. The aquifer zones are overlain by formations showing electric potential difference values above 0.065 mV. This implies that the aquifer might be confined.

The second zone showing potential aquifer is observed after 165 m below the ground surface. At S40, the groundwater potential occurs at isolated zones not exceeding 10 m thickness (165 -175 m; 195 -205 m and 275 -280 m). At S39, the potential zone occurs at 165 m to 170 m and 220 m to 245 m. At S38, the potential zone occurs at 165 m to 175 m and 180 m to 265 m. At station 41, the aquifer appears to be thickest, attaining the thickness of about 80 m. In stations S42 and 43, the aquifer occurs between 165m and 170 m, and at 235 m to 245 m in S43. In station 45, outside the boundary, the aquifer occurs between 170 m to 190 m and from 200 to 240 m. However, with the available boreholes' information data, this zone cannot be confirmed that it is an aquifer.

In all the stations, the potential aquifer occurring after 165 m below the ground surface is underlain by formation showing an electric potential difference of less than 0.02 mV. As discussed in section 4.6, this formation might be a different formation of dolomite or a completely different rock type.

Figure 4.33 presents the hydrogeological conceptual model for cross section C-C'. This conceptual model is derived from the simplified electric potential difference model Figure 4.32 Stations S38 and S41 have boreholes with lithology data. Both the boreholes show a calcrete layer above the dolomite rock. However, it is not easy to assign a single electric potential difference value to the dolomite and calcrete because their electric properties appear to be similar on the electric potential difference model. It is for this reason that the subsurface of this cross section is generalized to dolomite from surface to 166 m. The geology from 166 m to 300 m is categorised as unconfirmed geology and the zone showing electric potential difference values between 0.02 mV and 0.065 mV is categorized as the unconfirmed potential aquifer zone because none of the boreholes was drilled beyond 166 m.

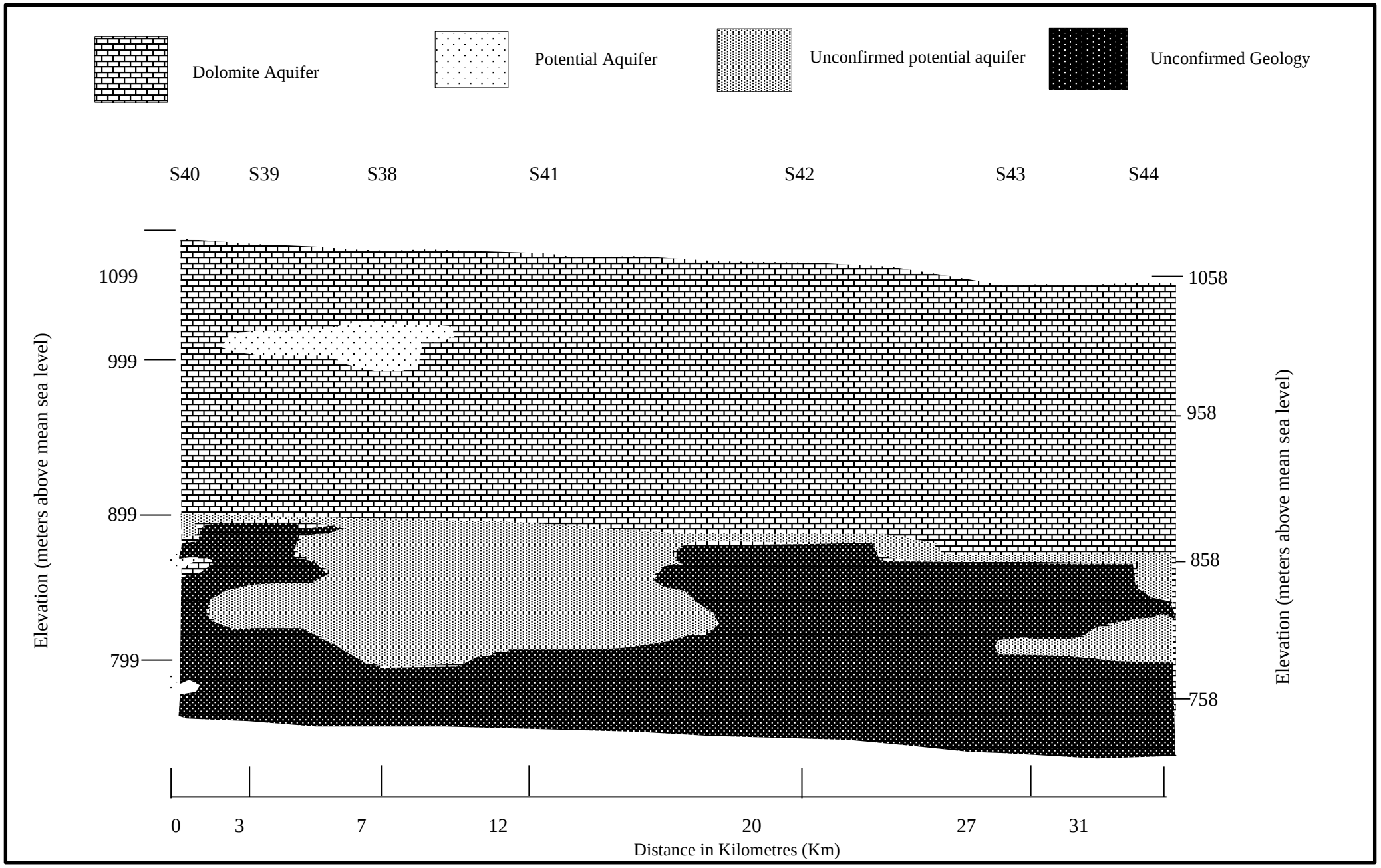

Figure 4.33 A Groundwater occurrence model for cross section C-C'

4.6.1.4 Cross-section D-D'

Figure 4.34 presents the electric potential difference cross-section through survey stations S52, S51, S50, S49, S45, S43, and S44, respectively. This cross-section is situated on the west of the study area. Station 44 occurs outside the inferred dolomite boundary. The spacing between the stations varies from 5 km to 14 km.

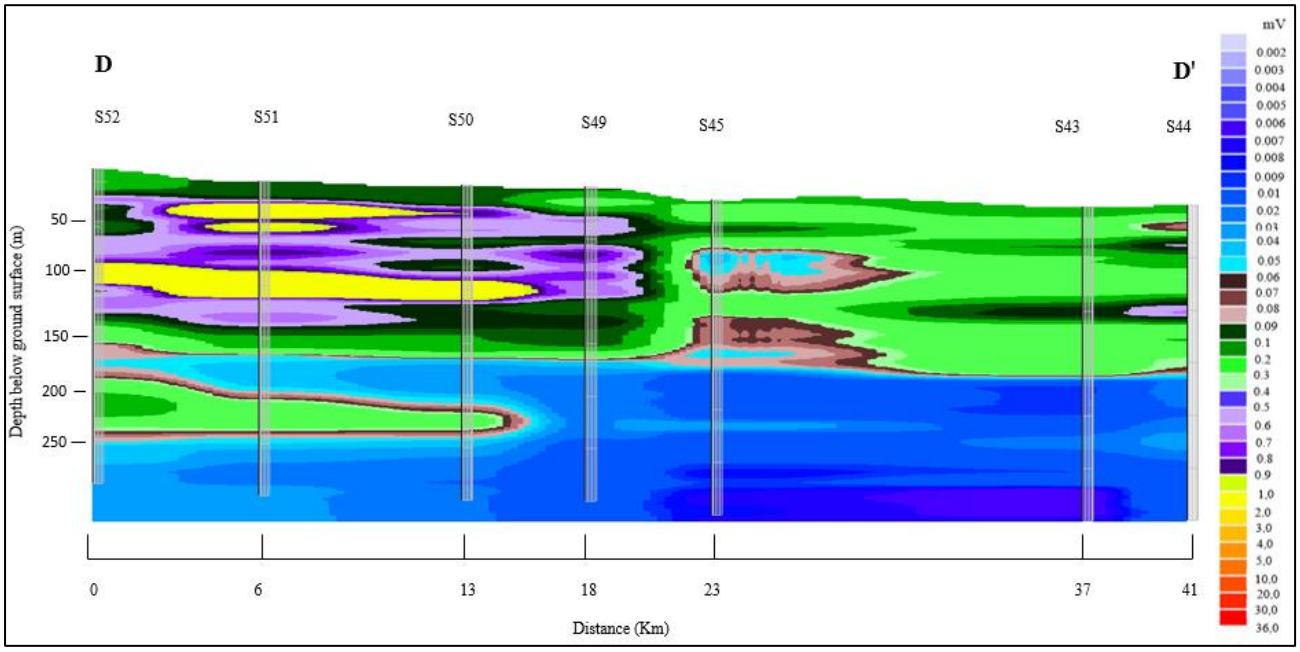

Figure 4.34 Electric potential difference model cross-section along D-D'

The model shows varying electric properties of the subsurface along the cross-section. The electric potential difference recorded on the survey stations along the cross-section shows values varying from less than 0.002 mV to 2 mV. The highest electric potential difference values were recorded on stations S52 to S50. The lowest electric potential difference occurs from 165 m below the ground surface on all the stations.

Stations S52 to S49 exhibit significant variations in the electric properties of the subsurface compared to the electric properties at stations S45 to S44. According to the borehole information of borehole 2524CC00236, located closer to station S50, the rock showing variation in electric properties was identified as dolomite, occurring from the 20 m to end of borehole at 150 m below surface. The attributes to variations in electric properties of the dolomite rock has already been as discussed in section 4.4.7.

Figure 4.35 present the electric potential difference cross-section D-D' model showing the groundwater potential zones catergorized by the electric potential difference range of 0.02mV to 0.065 mV.

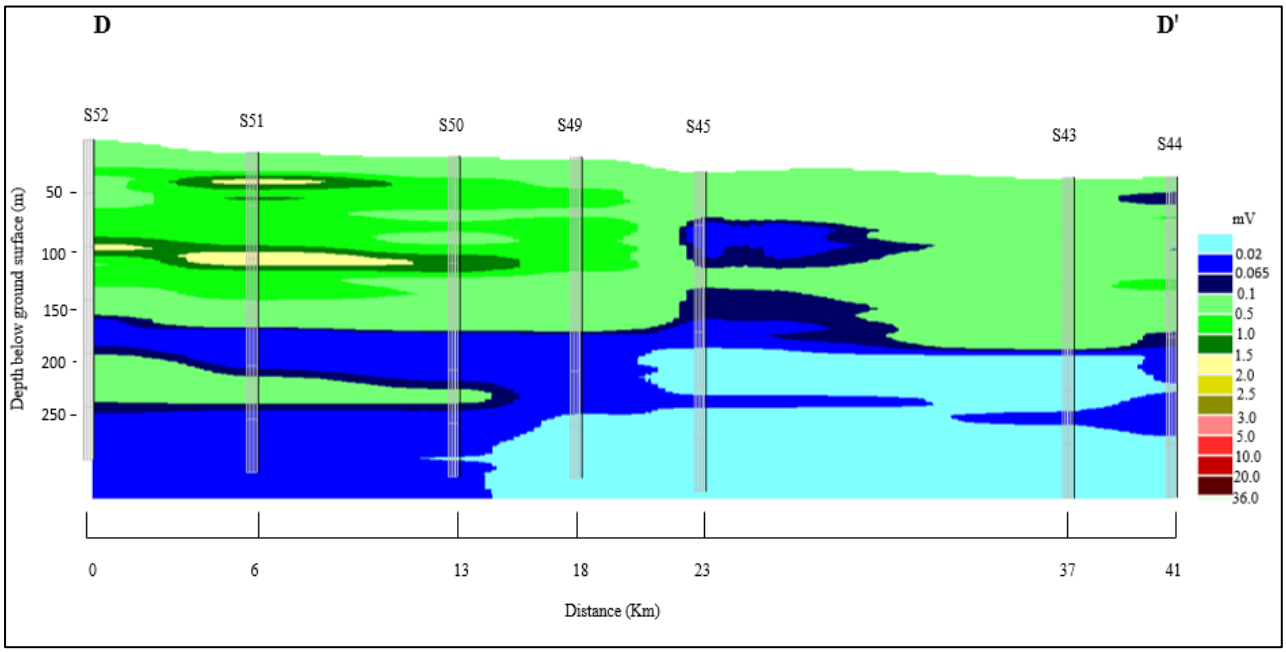

Figure 4.35 Electric potential difference model cross-section along D-D' to show the groundwater potential in terms of the fractured-weathered zones

The cross-section shows that the shallow groundwater aquifer zone is only present at S45 from 47.5 m to 87.5 m. This potential groundwater zone appears to be bounded by the formation of electric potential difference ranging from 0.065 to 0.5 mV, suggesting that the aquifer system is confined. The shallow potential aquifer at S45 may be attributed to the fact that this station occurs in a depression zone; this is more visible on Google Earth. It is suggesting that the high-lying areas might be draining towards the area of depression where S45 is situated.

The electric potential model also shows a potential aquifer zone from 165 m below the surface on all the stations except for S45, where the deeper potential starts at 140 m to 160m and from 245 m to 255 m. In stations S52, S51, and S50, the deeper aquifer occurs in two zones that are subdivided by formation with an electric potential difference between 0.1 mV and 0.5 mV. In S49, the aquifer extends to 250 m and is underlain by formation showing electric properties of less than 0.02 mV. In S4, the aquifer occurs as a 15 m thick zone in between the formation with electric potential difference values of less than 0.02 mV. In S44, the aquifer occurs from 165 m to 200 m and from 215 m to 245 m.

Figure 4.36 presents the groundwater occurrence model for cross D-D. The model shows that the only chance of getting water shallow weathered-fractured aquifer zone is in station 945. The rest of the stations it would be to target geological contact zones which does not guarantee a successful borehole. The shallow aquifer at station 9 is confined by the calcrete layer and hard dolomite zone shown in borehole at station 50. Just like the other cross sections, the geology occurring below 166 m is characterized as unconfirmed geology and the associated zone showing weathered-fractured properties is labelled unconfirmed potential aquifer zone.

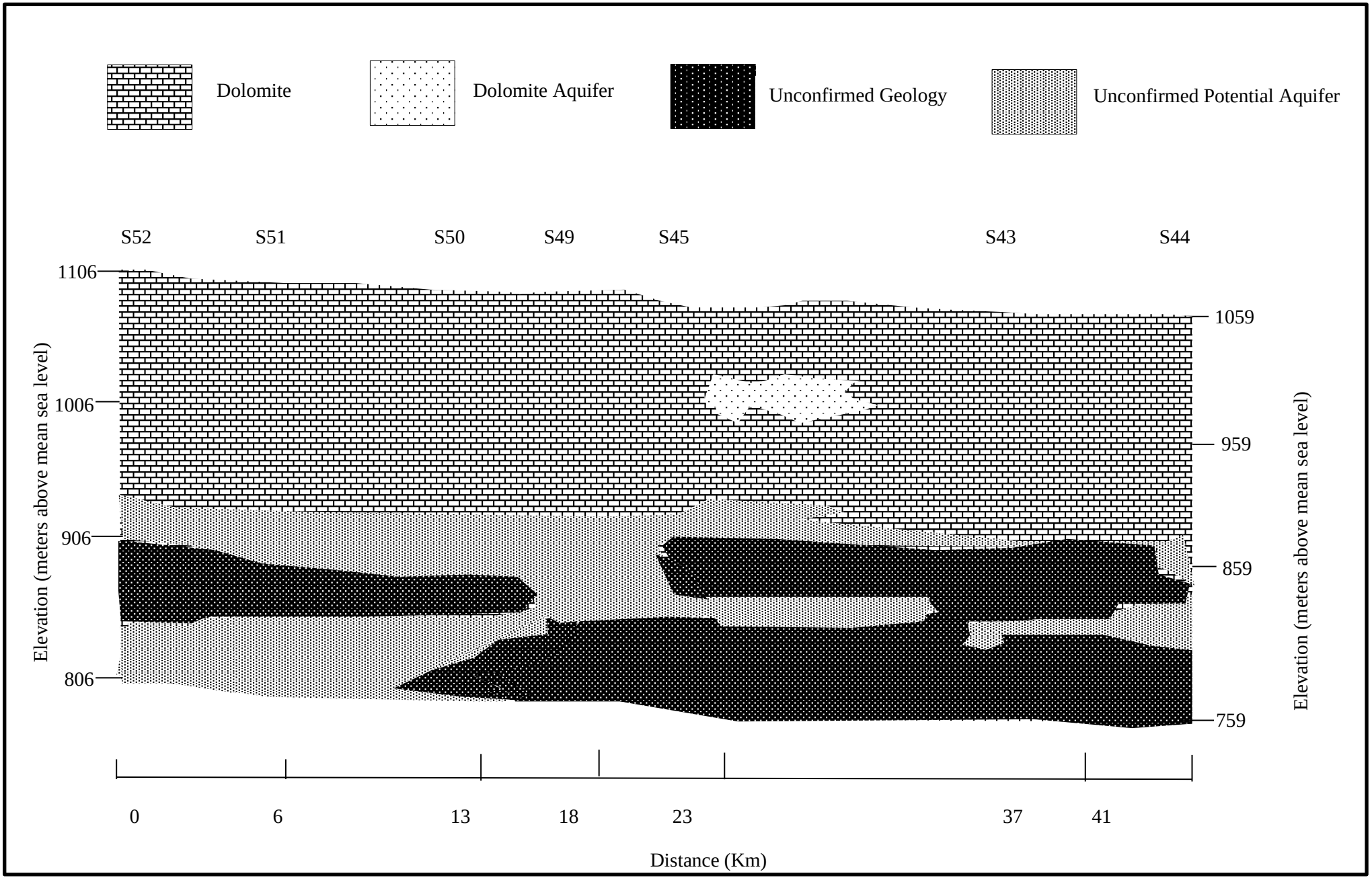

Figure 4.36 A groundwater occurrence model for cross section D-D'

4.7 OVERALL DISCUSSION

The processed MT data into electric potential difference models cross sections of the study area presents the electric properties of the subsurface geology. The model indicates that the subsurface geology has variable electric properties, with electric potential difference values ranging from 0.004 to 36 mV. These variations can be attributed to the different geological characteristics of dolomite formations and the other attributes listed in section 4.4.1. It may be inferred from the core logs of boreholes closer to the study area that there are different types of dolomite formations, which may be the reason for the dolomite's varying electric properties.

The core logs of the boreholes typically display disintegrated zones in the dolomite interchanging with fresh dolomites, light grey cherty dolomite interchanging with lamination of chert beds, and dark grey chert poor dolomite. Figure 4.37 shows a typical dolomite core from borehole LB1, where the grey dolomite interchanges with shale and brecciated dolomite. In borehole BHW 289, dark grey dolomite with quartz veins and brecciated dolomites were found. The various dolomite deposits that were found during the core logging are depicted in Figure 4.38. The appendices contain a detailed description of the core logs.

Figure 4.37 Picture showing dolomite core logs with some weathered shale lenses (marked in red)

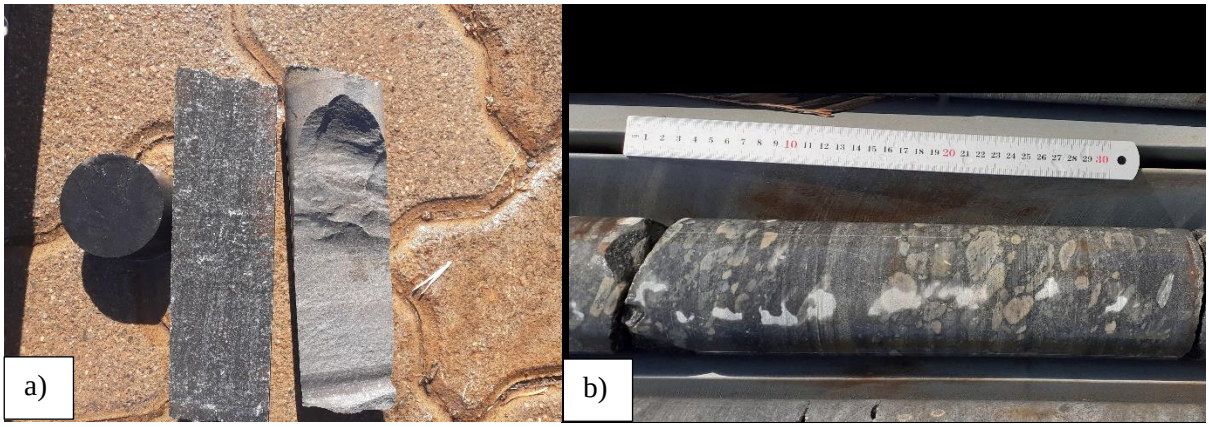

Figure 4.38 Pictures showing the different dolomite formations (a) chert poor to chert rich dolomite (samples from borehole LB1) b) brecciated dolomite (from borehole BHW 289)

The correlated borehole data with the geophysical data clearly showed that all boreholes that targeted the weathered-fractured zones had water strikes compared to those that targeted geological contacts. This implies that there are more chances of intercepting groundwater in areas where MT data indicates weathered-fractured zone properties, as 4.4.8. In order to maximize the success rates of boreholes in this study area, it is preferable to target mainly the weathered-fractured zones than the geological contact zones. Therefore, knowledge on the location of the weathered-fractured zones in the dolomite is essential for groundwater investigation. This information given by the established hydrogeological models. It is observed that the shallow (less than 100 m below surface) weathered-fractured aquifer zone are common in areas around cross section A-A' where the dolomite rock is an outcrop and in areas around cross section C-C' where there is a sand filled channel.

The shallow weathered-fractured aquifer zones are observed to be confined by the dolomite rock layer showing higher electric potential difference values. The confining layer can prevent direct rainfall from replenishing the shallow aquifers. The preferential flow recharge mechanism may be the tentative recharge process of the aquifer from preferential flow paths on the rock on surface. The confining layer above the groundwater aquifer also plays a role in reducing the vulnerability of the aquifer to surface pollution sources.

The geophysical investigation results illustrate the MT method’s viability in characterizing and delineating the groundwater aquifer zones in dolomite rock. This study characterized the weathered-fractured aquifer zones by an electric potential difference values between 0.02 mV and 0.065 mV. The MT method additionally mapped the stratification layers of the subsurface from their electric responses. As a result, the geological contact zones can be precisely defined using the MT approach.

CHAPTER 5 CONCLUSION AND RECOMMENDATIONS

5.1 CONCLUSION

The key objectives of the geophysical investigation in the Khakhea-Bray dolomite transboundary aquifer were in three folds. Understanding the groundwater occurrence in the dolomite, establishing geophysical models of the groundwater occurrence in the study area, and understanding the application of the magnetotelluric method in groundwater investigation.

Results showed that the weathered-fractured zones within the dolomite are the primary influencing factor for groundwater occurrence. These zones had electric potential difference values between 0.02 mV and 0.065 mV. The weathered-fractured zones within dolomites are developed by the rock's dissolution nature, improving its porosity and permeability, resulting in groundwater potential aquifers with improved storage. The geophysical data shows two zones that had electric potential difference ranging between 0.02 mV and 0.065 mV: at shallow depths between 7.5 m and 90 m and at deeper depths between 165 m and 300 m below the ground surface. The shallow zone was classified as a weathered-fractured dolomite aquifer, supported by the water strikes of the existing boreholes. These boreholes data did not enable the deeper zone to be classified as a weathered-fractured dolomite aquifer zone despite having similar electric properties to the shallow zone. The deeper zone was therefore considered to be an unconfirmed potential weathered-fractured zone.

Additionally, results showed that some existing boreholes were drilled to target the geological contacts between various formations. These geological contacts were characterized by contrasts in the electric properties of the subsurface. Geological contacts generally form a preferential flow path for groundwater. The data revealed that some of these boreholes that targeted the geological contacts for water had no water strikes during drilling, and those that did had poor yields. This was linked to the poor storage associated with the contacts. As a result, the geological contacts are not considered as another factor that influences groundwater occurrence in the TBA's dolomite.

The created groundwater occurrence models provided a systematic overview of potential zones of groundwater in the dolomites within the study area. The models display the confirmed confined shallow weathered-fractured dolomite aquifer zones and the unconfirmed potential weathered-fractured zones underlain by unconfirmed geology. The confining layer of the aquifer zones suggests that the aquifer does not recharge directly from the top. However, it can be recharged through a preferential flow mechanism where water percolates through the open cracks on the dolomite to replenish the aquifer. The confining layer also contributes to reducing the aquifer's susceptibility to pollution from surface sources.

In this study, the MT geophysical approach has demonstrated the ability to image the stratigraphic layers of the subsurface. The study has also shown the capabilities of the MT method to rapidly locate and delineate the groundwater potential zones in dolomite settings. As a result, this method can be utilized for rapid groundwater exploration.

5.2 RECOMMENDATIONS

The following recommendations are made based on the findings of this study:

- The cross-sectional electric potential difference models can be utilized to offer the baseline data, such as the depth and thickness of the aquifer, which could be used for numerical modelling of the Khakhea-Bray dolomite transboundary aquifer.
- With detailed lithology and water strike data from boreholes drilled up to 300 m, the calibration of the geophysical data can be revised to improve groundwater occurrence models of the study area.
- The developed models can be refined through a detailed geophysical investigation, which will include conducting surveys at all the boreholes with available drilling data, including the boreholes within privately owned farms. This will improve the calibration of the electric potential difference data.
- Practitioners can further use the developed models as a starting point for groundwater exploration within the TBA. The findings of this study provided insight into areas that can be targeted for weathered-fractured aquifer zones.
- This study has shown how the magnetotelluric geophysical technique coupled with general geology can effectively delineate the potential aquifers in TBA. Therefore, the magnetotelluric geophysical method can be applied for groundwater exploration at the regional level.
- Research investigations using the MT geophysical technique in other aquifer systems should be conducted and published. This will increase understanding of the method and provide additional literature

CHAPTER 6 REFERENCES

Abderahman, A. & Kotb, A., 2019. Magnetetolluric deep into ground water exploration.. *Research Essay at the facality of science geology department (unpublished 4th year Bsc research essay),*

Abound, E., Saudi, R., Asch, T., Aldamegh, K., & & Mogran, S., 2014. Water exploration using Magnetotelluric and gravity data analysis; Wadi Nisah, Riyadh, Saudi Arabia. *NRIAG Journal of Astronomy and Geophysics*, pp. 184-191.

Agerberg, F., 2020. *Data interpolation for groundwater modelling. Masters Thesis,* s.l.: Luleå University of Technology.

Agyemang, V., 2020. Application of magnetotelluric geophysical technique in delineation of zones of high groundwater potential for borehole drilling in five communities in the Agona East District, Ghana. *Applied water science ,* pp. 1-6.

Aidu Energy Technology, 2020. ADMT Series Products. Shanghai, China.

Ailes, C. & Rodriguez, B., 2015. *Magnetotelluric data collected to charectirize aquifers in the San Luis, New Mexico,* Virginia: U.S. Geological Survey Open-File Report.

Al-Amri, A., 2018. *Applied Geophysics ,* Riyadh: Depart,ent of Geology and Geophysics .

Altchenko, Y., Genco, A., Pierce, K. & Woolf, R. &. N. G., 2017. *Resilience in the Limpopo Basin : The potential role of the transboundary Raotswa aquifer - Final draft. [Research Report],* s.l.: USAID Southern Africa.

Amatyakul, P., Wood, S., Rung-arunwan, T., Vachiratienchai, C., Prommakorn, N., & Chanapiwat, P., 2021. An assessment of a shallow geothermal reservoir of Mae Chan hot spring, northern Thailand via magnetotelluric surveys. *Geothermics*, pp. 1-12.

Babak, O. & Deutsch, C., 2008. Statistical Approach to Inverse Distance Interpolation. pp. 131-1 to 131-12.

Babarinde, B. & Nwankwo, L., 2020. A review of the application of telluric and magnetotelluric methods in geophysical exploration. *Tropical Journal of Science and Technology,* 1(1), pp. 35-47.

Bai, D., Meju, M. & Liao, Z., 2001. Magnetotelluric images of deep crustal structure of the Rehai geothermal field near Tengchong, southern China. *Geophysical Journal International,* 147(3), pp. 677-687.

Betancur, T., Alberto, C. & Escobar, F., 2012. Conceptual Models in Hydrogeology,Methodology and Results. *Hydrogeology – A Global Perspective,* pp. 203-221.

Bootsman, C., 1998. *The Evelotion of the Molopo Drainage ,* University of the Witwatersrand: A published PhD thesis.

Botha, J., Verwey, J., Van der Voort, I., Colliston, W. &. L. J., 1998. *Karoo aquifers: their geology, geometry and physical behaviour.*, Pretoria: Water Research Commission.

Carlsson, L., Masalila-Dodo, C., Sola, L., Alemaw, B. & Madec, G. M., 2009. *Groundwater Review of the Molopo-Nossob Basin for Rural Communities including Assessment of National Databases atthe Sub-basin Level for Possible Future Integration (Final Report-ORASECOM/005/2009),* Gaborone: ORASECOM through Geotechnical Consulting Services (Pty) Ltd.

Castells, A., 2006. *A Magnetotelluric Investigation of Geoelectrical Dimensionality and Study of the Central Betic Crustal Structure ,* s.l.: Universitat de Barcelona (Unpublished Ph.D. Thesis).

Christopherson, K., 1991. Application of magnetotellurics to petroleum exploration in Papua New Guinea: A model for frontier areas. *Geophysics,* pp. 21-27.

Delhaye, R., Rath, V., Jones, A., Muller, M., & Reay, D., 2016. Correcting for static shift of magnetotelluric data with airborne electromagnetic measurements: a case study from Rathlin Basin, Northern Ireland. *Solid Earth ,* pp. 637-660.

Dippenaar, M., Swart, D., Van Rooy, J. & Diamond, R., 2019. *The Karst vadose zone: Influence on recharge, vulnerability and surface stability ,* Pretoria: Water Research Commission .

DWAF, 2004. *International strategic Perspective, Lower Vaal Water Management Area (Report: P WMA 10/000/00/0304)*: Department of Water Affairs and Forestry.

Enemark, T., Peeters, L., Batelaan, O. & Mallants, D., 2018. Hydrogeological conceptual model building and testing: A review. *Journal of Hydrology,* pp. 1-66.

Eren, M., Kadir, S., Hatipoglu, Z. & Gul, M., 2008. Quaternary Calcrete Development in the Mersin Area, Southern Turkey. *Turkish Journal of Earth Sciences,* pp. 763-784.

Fuentes-Arreazola, M., Núñez, D., Núñez-Cornú, F., Calderón-Moctezuma, A., Ruiz-Aguilar, D., & Romo-Jones, J., 2021. Magnetotelluric imaging of the Ceboruco Volcano, Nayarit, Mexico. *Journal of Volcanology and Geothermal Research,* pp. 1-12.

Ganat, T., 2020. *Technical guidance for petroleum exploration and production plans.* Switzerland : Springer .

Georgson, L., 2013. Geophysical methods used in geothermal exploration. Short Course VIII on Exploration for Geothermal Resources. Volume 22 October-November , pp. 1-16.

Giroux, B., Chouteau, M., Descloitres, M. & Ritz, M., 1997. Use of magnetotelluric method in the study of deep Maestrichtian aquifer in Senegal. *Applied Geophysics ,* pp. 77-96.

Godfrey, L. & van Dyk, G., 2002. *Reserve determination for the Pomfret-Vergelegen dolomitic aquifer, North West Province part of catchments D41C, D, E and F (Report No ENV-P-C 2002 -031),* s.l.: Department of Water Affairs and Forestry and CSIR .

Gomaa, M., Kassab, M. & El-Sayed, N., 2014. Study of prtrographical and electrical properties of some Jurassic carbonate rocks, North Sinai, Egypt.. *Egyptian Journal of Petroleum ,* pp. 343-352.

Gomo, M., 2021. *Magnetotelluric technique: Examples of geophysical surveys for production boreholes: Some local Examples.*. Bloemfontein, Geoscience: the fulcrum of humam development Council for Geoscience Annual Conference, 4th-5th March 2021.

Gomo, M., 2023. Use of electric potential difference in audio magnetotelluric (AMT) geophysics for groundwater exploration. *Groundwater for sustainable development,* 20(100864), pp. 1-6.

Gomo, M. & Vermeulen, D., 2017. A Transboundary Aquifer of a potential concern in South Africa. *Water Policy,* pp. 1160-1171.

Gomo, M., Vermeulen, D. & Lourens, P., 2017. Groundwater Sampling: Flow-Through Bailer Passive Method versus conventional Purge Method.. *Natural Resources Research ,* Volume 27, pp. 51-65.

Goubau, W., Gamble, T. & Clarke, J., 1978. Magnetotelluric data analysis: removal of bias. *Geophysics,* 43(6), pp. 1157-1166.

Handush, W., 2018. *Magnetotelluric in Geothermal exploration at Aluto-Langano, Ethopia.* Ethopia , Ethiopia Electric Power: Geothermal Sector Development Program.

Han, Q., Kelbert, A. & Hu, X., 2019. An electrical conductivity model of a coastal geothermal field in Southeastern China based on 3D magnetotelluric imaging. *Geophysics ,* 86(4), pp. 1-8.

Heinson, G., Dirren, N. & Grill, R., 2006. Magnetotelluric evidence for a deep crustal mineralizing system beneath the Olympic Dam oxide copper-gold deposit, southern Australia. *Geology,* pp. 573-576.

Hersir, G., 2015. Resistivity Surveying And Electromagnetic Methods. *LaGeo S.A. de C.V.*, pp. 1-14.

Hubert, J., 2016. Three diemnsional imaging of a Ag-Au-rich epithermal system in British Columbia, Canada using airborne Z-axis tipper electromagnetic and ground based magnetotelluric data. *Geophysics,* 81(1), pp. B1-B12.

Jinbiao, Y., Bo, W. & Qinghua, H., 2021. An anisotropic IDW interpolation method with multiple parameters cooperative optimization. *Cartography and Geoinformation,* 20(5), pp. 675-684.

Kalscheuer, T., Juhojuntti, N. & Vaittinen, K., 2017. Two DImensional Magnetotelluric Modelling of the Ore Deposits: Improvements min model contsraints by Inclusion of borehole measurements. *Suvery Geophysics* , pp. 1-41.

Kashouty, M., Aziz, A., Soliman, M. & Mesbah, H., 2010. Hydrogeophysical investigation of groundwater potential in the El Bawiti, Northern Bahariya Oasis, Western Desert,Egypt. *Arab J Geosci,* pp. 1-18.

Kumar, P., Rao, P., Singh, A., Kumar, A. & Rao, P., 2021. Dimensionality and directionality analysis of magnetotelluric data by using different techniques:A case study from northern part of Saurashtra region, India. *Indian Academy of Science,* pp. 1-16.

Loke, M., 1999. *Electrical imaging surveys for Environmental and Engineering studies (A practical guide to 2-D and 3-D surveys),* s.l.: s.n.

Mansoori, I., Oskooi, B. & Pedersen, L., 2015. Magnetotelluric signature of anticlines in Iran's Sehqanat oil field. *Tectonophysics* , pp. 101-112.

Mitsuhata, Y., Matsuo, K. & Minegishi, M., 1999. Magnetotelluric survey for exploration of volcanic-rock reservoir in the Yurihara oil and gas field, Japan.. *Geophysical proscpecting* , 47(2), pp. 195-218.

Moore, D. S., Notz, W. I. & Flinger, M. A., 2013. One-Way Analysis of Variance: Comparing Several Means. In: *The basic practice of statisticss (6th ed.).* New York, NY: W: . Freeman and Company.

Nijsten, G., Christelis, G., Villhoth, K., Braune, E., & Gaye, C., 2018. Transboundary aquifers of Africa: Review of the current state of knowledge and progress towards sustainable development and management. *Journal of Hydrology: Regional Studies,* pp. 21-34.

Orange, A., 1989. *Magnetic exploration for hydrocarbons.* Geology;Proc, IEEE.

ORASECOM, 2018. *Khakhea-Bray Transboundary Dolomitic Aquifer*. [Online] Available at: http://gis.orasecom.org/maps/137 [Accessed 06 August 2022].

Patro, P., 2017. Magnetotelluric studies for Hydrocarbon and Geothermal Resources. *Survey Geophysics,* pp. 1005-1041.

Pham, V., Boyer, D., Yuan, X. & Liu, S., 1995. Application of telluric profiling combined with magnetotelluric and self-potential methods to geothermal exploration in the Fujian Province. *Journal of Volcanology and Geothermal Research* , 62(3-4), pp. 227-236.

Reynolds, J., 1997. Electromagnetic method. In: *An introduction to applied and environmental geophysics.* England: John Wiley & Sons Ltd, pp. 553-681.

Rix, G., Wainaina, N., Ebrahimi, A., Buchus, R., Sancio, R., Limas, M. & Mayne, P., 2019. *The Manual on Subsurface Investigations* , s.l.: National Academy of Sciences (NCHRP Project 21-10).

Rockwares, 2022. *Rockware,Earth Science Software, Consulting and Training.* [Online] Available at: https://www.rockware.com/product/rockworks/#links

Sakindi, G., 2012. *Analysing The Subsurface Resistivity Structure On Two Profiles Across The Námafjall Hightemperature Geothermal Field, Ne-Iceland, Temperature Geothermal Field, Ne-Iceland,Through 1d Joint Inversion Of Tem And Mt Data* , Rwanda: United Nations University.

Sawyer, S., 2017. Analysis of Variance: The Fundamental Concepts. *The Journal of Manual & Manipulative Therapy,* 17(2), p. E27 to E38.

services, S. A. w., n.d. *North West Province Climate and weather.* [Online] Available at: https://www.sa-venues.com/weather/northwest.php#:~:text=Summer%20temperatures%20range%20between%2022,20%C2%BAC%20in%20a%20single%20day.
[Accessed 25 08 2022].

Simpson, F., 2005. *Practical Magnetotellurics.* UK: University Press, Cambridge.

Singarimbun, A., Gaffar, E. & Tofani, P., 2017. Modelling of reservoir structure by using magnetotelluric method in the area of Mt. Argopuro, East Java, Indonesia. *gineering Technology Science* , 49(6), pp. 833-847.

Sternberg, B. & Washburne, J., 1988. Correction for static shift in magnetetolluric using transient electromagnetic soundings. *Society of exploration Geophysics* , 53(11), pp. 1379-1492.

Sumanovac, F., 2012. *Magnetotelluric Method in the Exploration of Deeper Aquifers.* s.l., s.n.

Telford, W., Geldart, L. & Sheriff, R., 1990. Methods employing natural electric sources . In: *Applied Geophysics.* Second edition ed. New York: Cambridge University Press, pp. 302-317.

Tikhonov, A., 1973. On determining the electric characteristics of the deep layers of the Earth's crust. *Geophysical Institute academyof science, USSR Institute of scientific Investigations of the Earth magnetism*, pp. 295-297.

Tuncer, V., Unsworth, M., Craven, J. & Siripunvaraporn, W., 2006. Exploration for unconformity typeuranium deposits with audiomagnetetolluric data; A case study from the McArthur River mine, Sasktchewan, Canada.. *Geophyics* , 71(6), pp. B201-B206.

UNESCO-IHP, 2016. *Stampriet transboundary aquifer system assessment (technical report)*, France: UNESCO.

Unsworth, M., Soyer, W. & Tuncer, V., 2005. *Magnetotelluric measurements for determining the subsurface salinity and porosity structure of Amchitka Island, Alaska* , Canada: Department of Physics and Institute for Geophysical Research, University of Alberta .

Vozoff, K., 1990. Magnetolluric principles and practice. *Earth Science* , pp. 441-471.

Wu, C., 2018. Magnetotelluric Imaging of the Zhangzhou Basin Geothermal Zone, Southeastern China. *Energies*, pp. 1-15.

Zaher, M., Younis, A., Shaaban, H. & Mohamaden, M., 2021. Integration of geophysical methods for groundwater exploration: A case study of El Sheikh Marzouq area, Farafra Oasis, Egypt. *The Egyptian Journal of Aquatic Research* , 47(2), pp. 239-244.

Zeng, Q., Di, Q., Liu, T., Li, G., Yu, C. S., Liu, H., & Ye, J., 2020. Explorations of gold and lead-zinc deposits using a magnetotelluric method: Case studies in the Tianshan-Xingmeng Orogenic Belt of Northern China. *Ore Geology reviews,* Volume 117.

Zhang, K., Wei, W., Lu, Q., Dong, H., & & Li, Y., 2014. Theoretical assessment of 3-D magnetotelluric method for oil and gas exploration: Synthetic examples. *Journal of applied geophysics*, Volume 106, pp. 23-36.

Zhang, P. & Chouteau, M., 1991. The use of magnetotelluric for mineral exploration: an experiment in the Chibougamau region of Quebec. *Department of mineral Engineering*, Volume 29, pp. 621-634.

Zhdanov, M., 2010. Electromagnetic geophysics; Notes from past and the road ahead. *Geophysics* , 75(5), pp. 5A49-75A66.

CHAPTER 7 APPENDICES

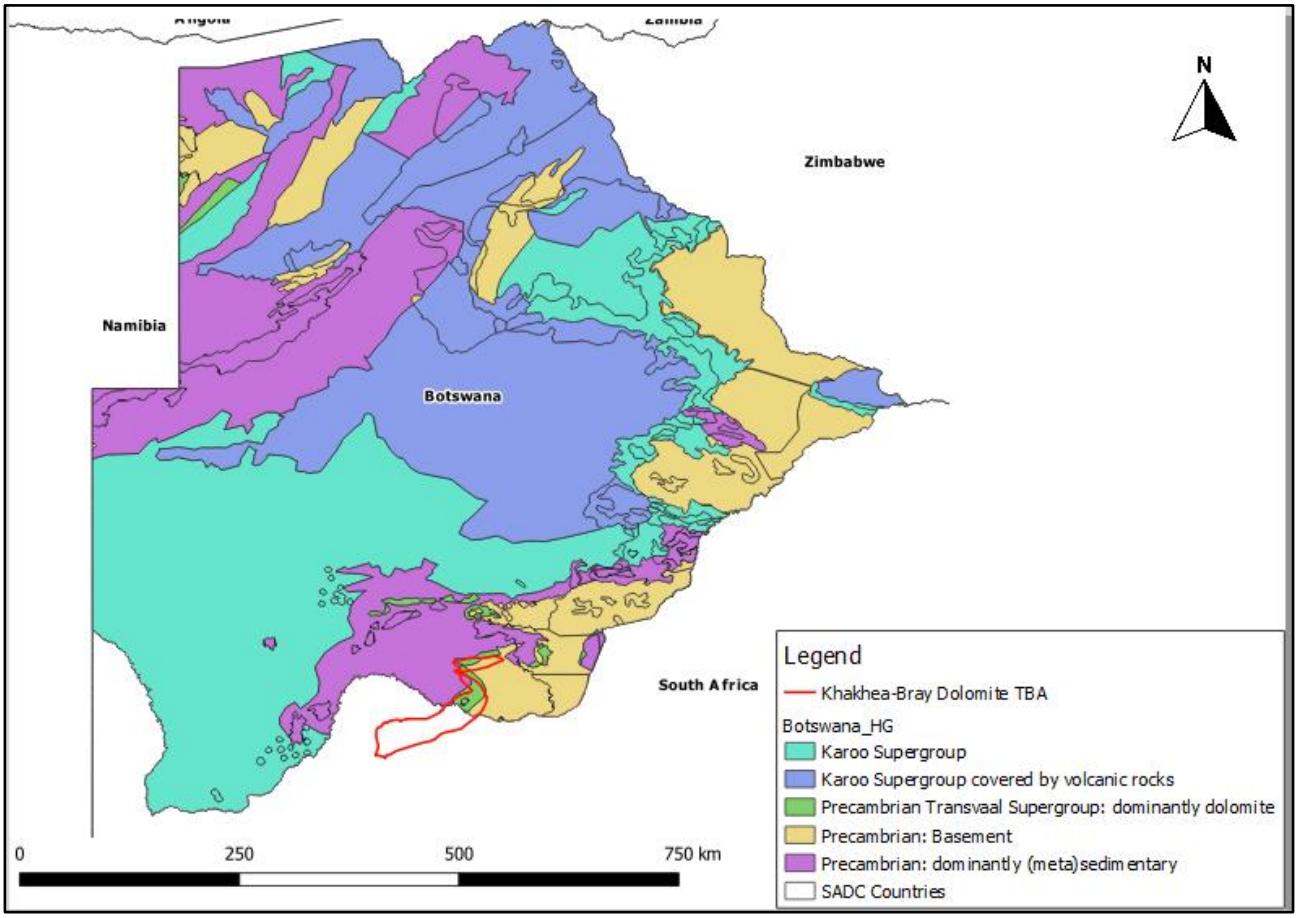

Figure 7.1 Geological map of Botswana

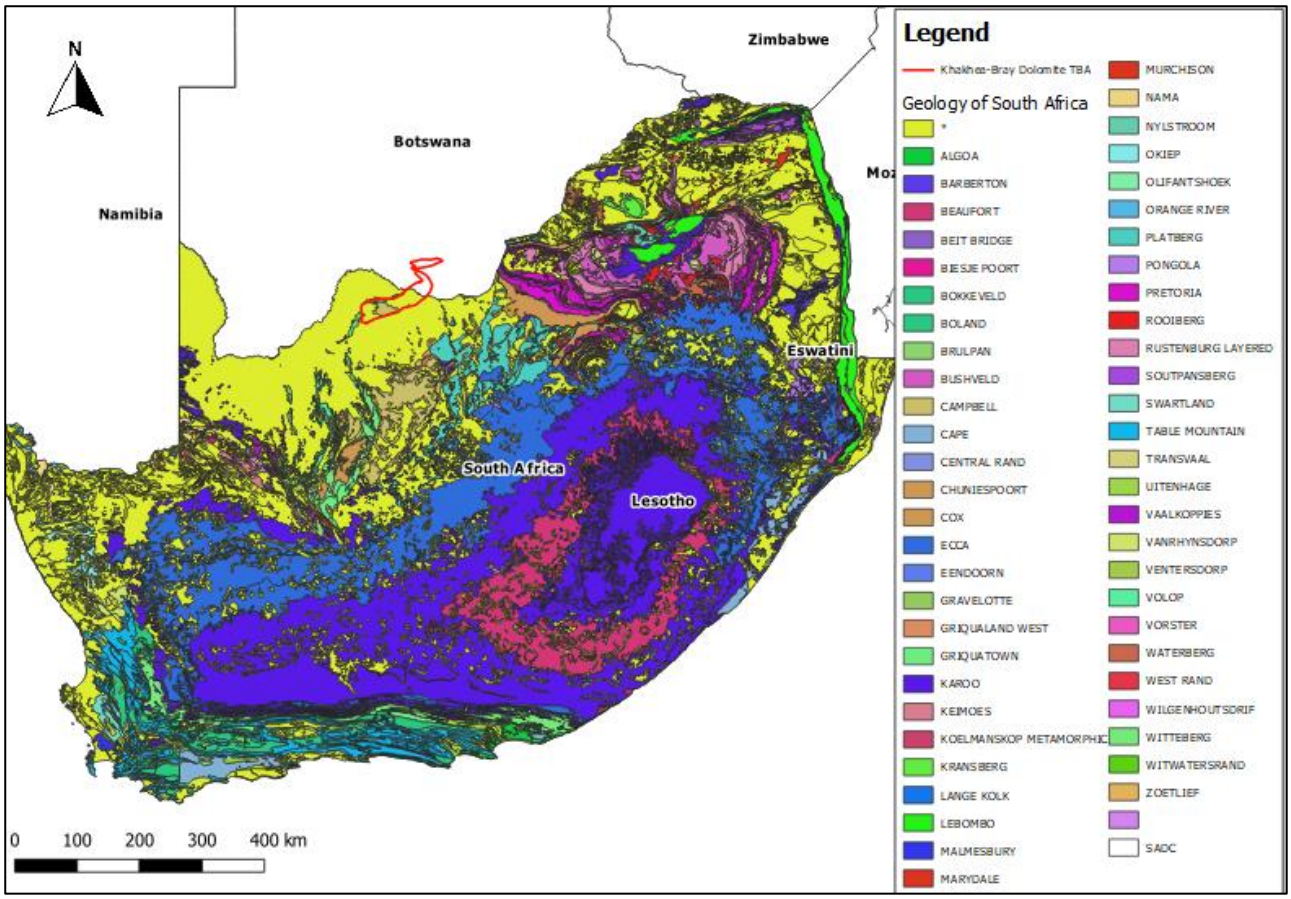

Figure 7.2 Geology Map of South Africa

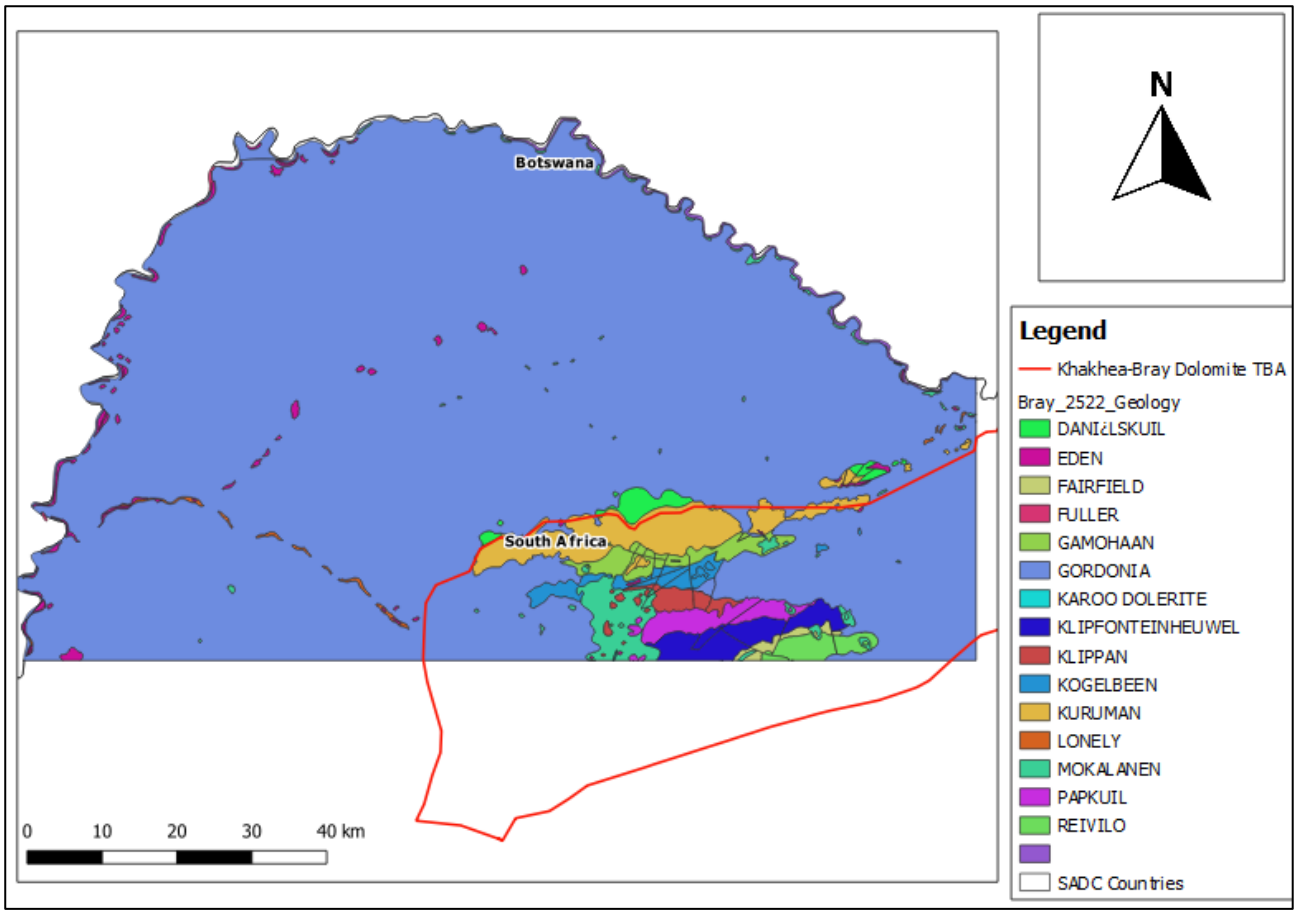

Figure 7.3 Bray Geology Map (1:25 000)

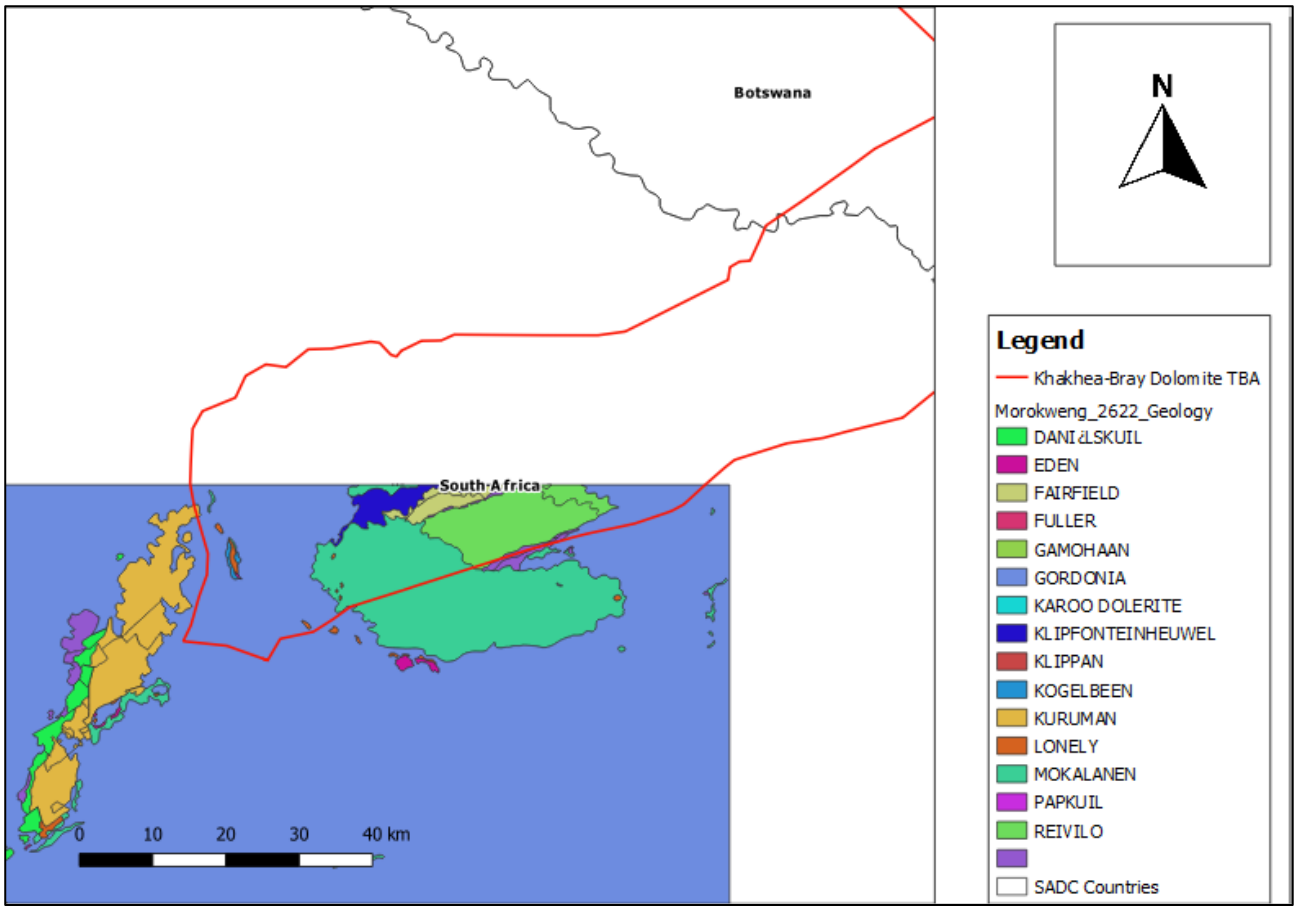

Figure 7.4 Morokweng Geology Map (1:25 000)

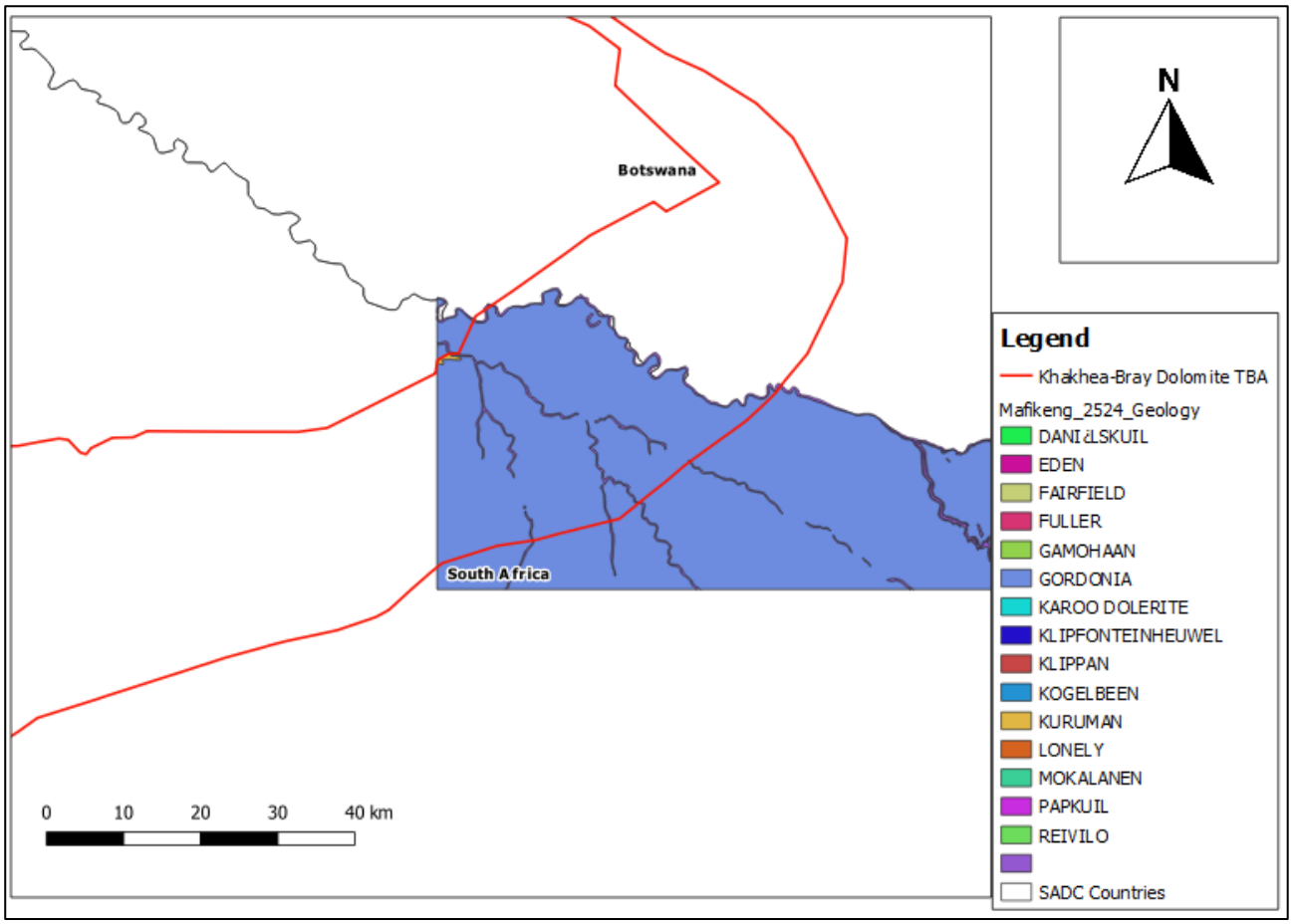

Figure 7.5 Mafikeng Geology Map (1: 25 000)

Figure 7.6 Borehole 12-83443 information board

Table 7.1 Core logs for CGS borehole LB1

Borehole- LB1		
Depths (m)	**Rock type**	**Description**
0- 0,26	Cherty dolomite	weathered
0,26 – 7,40	dolomite	Fresh dark grey
7,40 – 7,54	shale	fresh
7,54-7,87	dolomite	Fresh dark grey
7,87-7,97	chert	fresh
7,97-8,04	dolomite	Fresh dark grey
8,04-8,36	dolomite	Fresh chert rich
8,36-8,66	Shale	Fresh
8,66-14,28	dolomite	Fresh dark grey dolomite
14,28-25,00	dolomite	Fresh chert rich
25,00-25,10	Shale	weathered
25,10-36,7	dolomite	weathered
36,70-87,25	dolomite	Fresh Dark grey with cherts lamination
87,25-94,10	Shale	Fresh, slicken sides lineation at the contact with dolomite
94,10-124,37	dolomite	Fresh, dark grey
124,37-130,89	Shale	Weathered, with rusty particles
130,89-146,57	dolomite	Fresh, fresh dark grey
146,57-154,25	dolomite	Weathered
154,25-154,87	Shale	Fresh
154,87-182,88	dolomite	Chert rich with dissolution features

Table 7.2 Core logs for CGS borehole ST1

Borehole- ST1		
Depths (m)	**Rock type**	**Description**
0,00-6,00	Log not available	
6,00-22,68	Quartzite	Fresh un-weathered, with carbonate minerals zones
22,68-23,77	Shale	Fresh
23,77-53,79	dolomite	Un-weathered, dark grey
53,79-63,98	dolomite	weathered
63,98-65,79	dolerite	Reddish, fresh
65,79-85,00	dolomite	Chert rich, fresh
85,00-94,56	dolomite	Dark grey, fractured zones at 86,00 m, 93,7 m and 94,5 m
94,56-135,00	dolomite	Fresh, chert rich
135,00-172,63	dolomite	Interchanging chert rich dolomite with dark grey dolomite
172,63-179,88	shale	Weathered, rusty colours
179,88-187,39	dolomite	Dark grey, fresh, quartz vain
187,39-199,99	shale	Chert rich, fresh
199,99-209,90	dolomite	Fresh, dark grey with chert bedding
209,90-240,03	dolomite	Dark grey with signs of disintegrations
240,03-242,70	shale	Fresh
242,70-250,22	dolomite	Chert rich, fresh
250,22-253,80	shale	Weathered
253,80-260,26	dolomite	Fresh, dark grey
260,26-270,94	mudrock	Reddish un-weathered
270,94-273,87	shale	Weathered
273,87-280,64	dolomite	Chert, fresh
280,64-290,23	dolomite	Fresh, dark grey
290,23-299,11	dolomite	Chert rich, fresh

Table 7.3 Core logs for CGS borehole- BHW 289

Borehole- BHW 289		
Depths (m)	**Rock type**	**Description**
0-10,95	Cores mixed up	Cores mixed up
10,95-14,98	dolomite	Chert rich
14,98-19,18	dolomite	Fresh, un-weathered, light grey
19,18-23,44	dolomite	Fractured, dark grey
23,44-29,58	shale	Weathered
29,58-33,37	dolomite	Un-weathered
33,37-33,89	Shale	Fresh
33,89-54,94	dolomite	Dark grey, fresh
54,94-70,70	dolomite	light grey,
70,70-71,09	shale	Fresh
71,09-84,00	dolomite	Dark grey, fresh
84,00-102,00	dolomite	Grey brecciated, fresh dolomite
102,00-103,8	shale	Fresh
103,8-108,72	dolomite	Dark grey, fresh
108,72-112,00	shale	Fresh un-weathered
112,00-113,16	dolomite	Chert rich, fresh

113,16-117,27	Shale	Fresh
117,27-134,27	dolomite	Light grey, brecciated
134,27-151,13	Dolomite	Dark grey, discontinuities along joints
151,3-168,58	shale	Fresh, interchanging with weathered zones
168,58-189,55	dolomite	Fresh, brecciated (white angular crystals)
189,55-228,19	dolomite	Dark grey, fresh
228,19-258,78	dolomite	Light grey, fresh, brecciated
258,78-264,89	Shale	Weathered
264,89-279,46	dolomite	Dark grey, un-weathered
279,56-298,57	dolomite	Light grey, chert rich
298,57-311,65	shale	fresh
311,65-334,89	dolomite	Fresh brecciated, discontinuities along joints
334,89-398,88	dolomite	Dark grey, fresh
398,88-405,64	dolomite	Chert rich, fresh
405,64-449,97	dolomite	Dark grey,fresh
449,97-467,34	dolomite	Brecciated, un-weathered
467,34-471,67	shale	Un-weathered
471,67-507,81	dolomite	Dark grey unweathered with thin 0,02m thick quartz veins
507,81-534,87	Dolomite	Un-weathered chert rich

Table 7.4 Electrical Potential Difference data S1 to S13

DEPTH (m)	STATION NUMBERS												
	S1	S2	S3	S4	S5	S6	S7	S8	S9	S10	S11	S12	S13
5	0,421	0,363	0,317	0,127	0,398	0,276	0,342	0,439	0,315	0,302	0,397	0,364	0,113
10	0,262	0,363	0,338	0,046	0,039	0,122	0,157	0,364	0,045	0,315	0,335	0,135	0,097
15	0,164	0,388	0,275	0,040	0,018	0,120	0,150	0,344	0,038	0,304	0,316	0,152	0,108
20	0,294	0,370	0,278	0,018	0,046	0,118	0,148	0,347	0,045	0,296	0,250	0,148	0,097
25	0,084	0,379	0,332	0,006	0,020	0,097	0,267	0,308	0,046	0,472	0,231	0,086	0,042
30	0,052	0,450	0,483	0,007	0,014	0,110	0,314	0,409	0,102	0,335	0,343	0,147	0,050
35	0,042	0,649	0,519	0,009	0,025	0,213	0,525	0,736	0,507	0,811	0,609	0,253	0,082
40	0,023	1,188	0,881	0,012	0,015	0,293	0,723	1,320	0,498	0,771	0,976	0,439	0,165
45	0,048	1,803	2,073	0,005	0,034	0,852	2,599	4,321	1,019	1,590	1,347	0,573	0,266
50	0,066	1,611	1,824	0,005	0,018	0,584	2,064	3,327	0,724	1,113	0,592	0,479	0,237
55	0,075	2,190	1,350	0,005	0,014	0,584	1,862	2,568	0,400	0,596	0,402	0,478	0,289
60	0,102	2,557	0,815	0,058	0,070	0,267	0,866	1,286	0,193	0,290	0,450	0,619	0,176
65	0,065	3,028	0,602	0,010	0,018	0,172	0,540	0,741	0,110	0,188	0,553	0,879	0,216
70	0,098	5,310	1,070	0,011	0,037	0,259	0,423	0,557	0,097	0,194	0,703	0,833	0,550
75	0,111	6,395	2,070	0,027	0,069	0,496	0,757	1,041	0,163	0,300	0,900	0,673	0,775
80	0,124	5,627	3,400	0,018	0,126	0,815	1,228	1,457	0,205	0,394	0,993	0,697	0,786
85	0,169	8,985	5,136	0,021	0,175	1,270	1,809	2,257	0,284	0,508	1,490	1,014	0,972
90	0,205	14,166	4,189	0,020	0,174	1,054	1,256	1,640	0,168	0,329	1,703	1,291	0,644
95	0,252	24,795	5,673	0,024	0,229	1,449	1,433	1,981	0,140	0,233	2,752	2,141	0,687
100	0,178	35,251	7,958	0,056	0,295	1,971	1,864	2,592	0,165	0,224	3,734	2,933	0,919
105	0,253	32,341	7,128	0,023	0,290	1,762	1,633	2,409	0,157	0,223	3,400	2,683	0,802
110	0,193	13,453	4,790	0,028	0,169	0,741	0,679	1,009	0,134	0,148	1,432	1,103	0,359
115	0,255	11,832	8,973	0,032	0,275	0,682	0,591	0,789	0,131	0,190	1,420	0,880	0,378
120	0,234	13,822	11,287	0,018	0,346	0,791	0,675	0,970	0,173	0,275	1,741	1,031	0,435
125	0,331	21,996	18,781	0,029	0,565	1,264	1,050	1,513	0,337	0,425	2,710	1,560	0,759
130	0,307	23,115	19,375	0,038	0,599	1,329	1,089	1,563	0,264	0,464	2,819	1,602	0,716
135	0,355	19,499	16,342	0,040	0,477	1,113	0,905	1,356	0,232	0,416	3,516	1,363	0,645
140	0,325	13,144	10,682	0,019	0,325	0,743	0,602	0,897	0,152	0,268	2,355	0,894	0,459
145	0,238	8,062	6,535	0,063	0,240	0,461	0,382	0,569	0,099	0,199	1,449	0,557	0,286
150	0,239	4,755	3,803	0,032	0,119	0,273	0,232	0,368	0,071	0,213	0,865	0,364	0,241
155	0,183	3,219	2,375	0,053	0,126	0,199	0,167	0,254	0,060	0,125	0,587	0,353	0,270
160	0,212	3,160	2,379	0,050	0,136	0,199	0,175	0,270	0,068	0,137	0,584	0,317	0,208
165	0,048	13,281	1,328	0,006	0,043	0,093	0,079	0,119	0,055	0,059	0,377	0,233	0,209
170	0,035	7,278	0,938	0,005	0,036	0,066	0,057	0,097	0,022	0,092	0,377	0,173	0,181
175	0,053	7,334	0,939	0,004	0,034	0,066	0,056	0,089	0,021	0,082	0,375	0,179	0,167
180	0,050	4,846	0,721	0,004	0,039	0,053	0,054	0,081	0,135	0,086	0,466	0,238	0,159
185	0,047	4,845	0,722	0,004	0,030	0,052	0,043	0,083	0,028	0,065	0,550	0,259	0,201
190	0,063	3,927	0,581	0,004	0,028	0,043	0,036	0,093	0,036	0,063	0,657	0,293	0,160
195	0,047	3,959	0,506	0,004	0,030	0,041	0,034	0,103	0,043	0,058	0,757	0,344	0,165
200	0,050	4,495	0,444	0,005	0,027	0,039	0,033	0,128	0,043	0,094	0,979	0,437	0,121
205	0,054	6,880	0,359	0,005	0,039	0,044	0,040	0,205	0,054	0,101	1,621	0,721	0,141
210	0,063	8,825	0,374	0,004	0,038	0,050	0,041	0,257	0,062	0,074	2,080	0,921	0,157
215	0,078	11,978	0,346	0,004	0,052	0,061	0,047	0,346	0,082	0,097	2,751	1,237	0,138
220	0,102	16,192	0,344	0,004	0,068	0,077	0,058	0,471	0,101	0,093	3,669	1,679	0,159
225	0,106	17,035	0,236	0,004	0,067	0,079	0,057	0,493	0,099	0,089	3,787	1,770	0,174
230	0,099	15,726	0,216	0,004	0,066	0,071	0,054	0,459	0,089	0,088	3,529	1,648	0,156
235	0,084	12,660	0,192	0,003	0,051	0,058	0,045	0,376	0,075	0,070	2,891	1,373	0,137
240	0,059	8,800	0,168	0,004	0,035	0,041	0,032	0,260	0,054	0,077	1,989	0,995	0,181

245	0,044	6,511	0,148	0,004	0,027	0,031	0,024	0,194	0,050	0,052	1,458	0,740	0,115
250	0,043	5,567	0,140	0,005	0,024	0,028	0,023	0,163	0,043	0,054	1,249	0,640	0,132
255	0,042	4,226	0,127	0,005	0,027	0,022	0,018	0,196	0,034	0,082	0,917	0,475	0,163
260	0,037	3,709	0,123	0,004	0,018	0,021	0,022	0,116	0,218	0,075	0,797	0,429	0,129
265	0,025	2,647	0,104	0,004	0,017	0,016	0,020	0,084	0,106	0,051	0,573	0,326	0,124
270	0,028	2,295	0,100	0,004	0,023	0,015	0,014	0,068	0,135	0,094	0,484	0,282	0,131
275	0,028	2,002	0,145	0,004	0,013	0,015	0,013	0,059	0,032	0,124	0,418	0,246	0,108
280	0,025	1,808	0,330	0,004	0,011	0,013	0,012	0,052	0,026	0,066	0,396	0,220	0,150
285	0,026	1,543	0,161	0,004	0,016	0,010	0,012	0,043	0,025	0,064	0,328	0,191	0,118
290	0,024	1,524	0,167	0,004	0,013	0,010	0,026	0,044	0,022	0,064	0,302	0,186	0,090
295	0,020	1,157	0,080	0,005	0,014	0,011	0,014	0,040	0,070	0,076	0,253	0,169	0,129
300	0,021	1,042	0,099	0,004	0,030	0,092	0,031	0,045	0,032	0,042	0,225	0,134	0,126

Table 7.5 Electric Potential Difference data from S14 to S41

DEPTH (m)	**STATION NUMBERS**												
	S14	**S15**	**S16**	**S17**	**S33**	**S34**	**S35**	**S36**	**S37**	**S38**	**S39**	**S40**	**S41**
5	0,296	0,274	0,352	0,280	0,093	0,251	0,122	0,378	0,234	0,137	0,323	0,469	0,326
10	0,093	0,103	0,113	0,154	0,032	0,063	0,075	0,316	0,144	0,135	0,309	0,479	0,202
15	0,091	0,218	0,130	0,193	0,046	0,053	0,018	0,322	0,161	0,087	0,342	0,472	0,191
20	0,098	0,116	0,109	0,152	0,045	0,066	0,027	0,320	0,209	0,150	0,337	0,513	0,194
25	0,120	0,049	0,065	0,089	0,020	0,058	0,005	0,267	0,171	0,089	0,214	0,327	0,120
30	0,120	0,051	0,031	0,034	0,039	0,061	0,007	0,214	0,129	0,041	0,109	0,157	0,082
35	0,092	0,046	0,046	0,049	0,037	0,068	0,029	0,382	0,194	0,054	0,070	0,147	0,129
40	0,145	0,030	0,047	0,018	0,063	0,062	0,006	0,474	0,310	0,036	0,060	0,105	0,252
45	0,195	0,047	0,039	0,049	0,043	0,043	0,014	1,418	1,144	0,054	0,050	0,129	0,809
50	0,127	0,033	0,056	0,021	0,036	0,037	0,009	0,791	0,582	0,024	0,051	0,068	0,434
55	0,122	0,055	0,066	0,035	0,038	0,042	0,006	0,457	0,329	0,031	0,026	0,084	0,219
60	0,111	0,086	0,072	0,079	0,091	0,082	0,047	0,502	0,443	0,098	0,373	0,650	0,220
65	0,114	0,072	0,082	0,047	0,020	0,050	0,016	0,580	0,547	0,105	0,316	0,492	0,265
70	0,215	0,133	0,102	0,052	0,046	0,092	0,015	0,478	0,413	0,247	0,444	0,481	0,234
75	0,303	0,187	0,160	0,102	0,081	0,106	0,029	0,724	0,625	0,189	0,326	0,195	0,337
80	0,341	0,202	0,187	0,070	0,049	0,080	0,016	1,118	1,017	0,144	0,199	0,173	0,549
85	0,450	0,204	0,195	0,111	0,077	0,100	0,022	1,636	1,522	0,120	0,211	0,534	0,820
90	0,329	0,211	0,327	0,119	0,096	0,109	0,035	1,116	0,930	0,130	0,082	0,215	0,488
95	0,356	0,162	0,267	0,149	0,093	0,094	0,031	1,232	0,755	0,472	0,179	0,602	0,331
100	0,411	0,202	0,292	0,135	0,108	0,111	0,049	1,569	0,852	0,253	0,312	0,439	0,314
105	0,405	0,266	0,294	0,098	0,065	0,100	0,059	1,430	0,755	0,355	0,609	0,610	0,275
110	0,213	0,302	0,240	0,138	0,084	0,096	0,036	0,585	0,356	0,190	0,284	0,196	0,165
115	0,224	0,194	0,214	0,126	0,063	0,057	0,022	0,406	0,345	0,151	0,252	0,456	0,257
120	0,265	0,201	0,244	0,113	0,065	0,073	0,026	0,419	0,414	0,194	0,297	0,346	0,312
125	0,323	0,251	0,210	0,130	0,070	0,073	0,038	0,593	0,603	0,189	0,456	0,347	0,502
130	0,392	0,140	0,245	0,154	0,118	0,125	0,036	0,627	0,639	0,142	0,235	0,289	0,538
135	0,297	0,196	0,301	0,115	0,081	0,111	0,026	0,518	0,531	0,394	0,485	0,712	0,451
140	0,215	0,177	0,233	0,114	0,103	0,116	0,050	0,351	0,359	0,197	0,236	0,428	0,302
145	0,203	0,189	0,203	0,113	0,106	0,120	0,039	0,256	0,226	0,205	0,233	0,261	0,200
150	0,147	0,215	0,227	0,184	0,092	0,113	0,066	0,168	0,143	0,174	0,244	0,294	0,125
155	0,118	0,246	0,197	0,140	0,161	0,159	0,080	0,174	0,122	0,133	0,306	0,412	0,090
160	0,122	0,226	0,259	0,136	0,122	0,121	0,058	0,169	0,129	0,143	0,369	0,486	0,112
165	0,032	0,019	0,032	0,018	0,015	0,075	0,019	0,053	0,045	0,015	0,006	0,018	0,038
170	0,027	0,016	0,028	0,020	0,019	0,065	0,027	0,038	0,032	0,016	0,005	0,016	0,031
175	0,035	0,027	0,023	0,015	0,013	0,092	0,021	0,050	0,033	0,214	0,005	0,025	0,029
180	0,029	0,041	0,018	0,027	0,045	0,069	0,015	0,030	0,026	0,195	0,006	0,022	0,022

185	0,031	0,024	0,022	0,015	0,072	0,095	0,035	0,030	0,028	0,044	0,007	0,019	0,030
190	0,043	0,019	0,018	0,013	0,092	0,082	0,067	0,024	0,023	0,069	0,007	0,016	0,027
195	0,038	0,020	0,024	0,013	0,112	0,091	0,016	0,024	0,023	0,023	0,008	0,020	0,021
200	0,050	0,014	0,020	0,014	0,044	0,079	0,025	0,024	0,022	0,029	0,010	0,030	0,022
205	0,073	0,012	0,013	0,010	0,024	0,070	0,017	0,027	0,026	0,032	0,017	0,018	0,028
210	0,091	0,014	0,019	0,010	0,053	0,072	0,018	0,029	0,032	0,036	0,020	0,019	0,033
215	0,120	0,009	0,011	0,008	0,013	0,061	0,015	0,035	0,040	0,044	0,027	0,012	0,043
220	0,159	0,010	0,009	0,011	0,012	0,038	0,012	0,044	0,052	0,056	0,036	0,015	0,055
225	0,165	0,008	0,009	0,008	0,028	0,056	0,012	0,047	0,053	0,059	0,038	0,014	0,058
230	0,153	0,008	0,010	0,006	0,013	0,089	0,013	0,042	0,050	0,054	0,035	0,015	0,054
235	0,127	0,011	0,009	0,007	0,011	0,061	0,016	0,036	0,042	0,046	0,029	0,014	0,044
240	0,089	0,010	0,010	0,007	0,018	0,058	0,012	0,026	0,030	0,035	0,019	0,018	0,032
245	0,066	0,008	0,028	0,009	0,030	0,060	0,018	0,023	0,024	0,030	0,015	0,016	0,024
250	0,057	0,012	0,009	0,010	0,063	0,092	0,017	0,021	0,021	0,026	0,013	0,013	0,021
255	0,043	0,009	0,013	0,009	0,065	0,074	0,012	0,016	0,017	0,025	0,010	0,012	0,017
260	0,039	0,010	0,011	0,008	0,075	0,110	0,028	0,015	0,017	0,022	0,009	0,021	0,015
265	0,038	0,010	0,010	0,009	0,025	0,053	0,019	0,016	0,012	0,020	0,007	0,017	0,013
270	0,026	0,012	0,010	0,009	0,019	0,107	0,022	0,016	0,011	0,016	0,007	0,021	0,013
275	0,025	0,010	0,013	0,007	0,032	0,076	0,017	0,011	0,011	0,018	0,006	0,018	0,011
280	0,023	0,025	0,010	0,008	0,020	0,094	0,014	0,011	0,009	0,014	0,006	0,019	0,012
285	0,021	0,013	0,014	0,007	0,012	0,088	0,016	0,010	0,010	0,018	0,007	0,028	0,012
290	0,020	0,013	0,016	0,008	0,013	0,094	0,014	0,011	0,009	0,014	0,006	0,017	0,011
295	0,016	0,019	0,012	0,007	0,036	0,106	0,014	0,012	0,010	0,013	0,006	0,023	0,009
300	0,021	0,012	0,011	0,008	0,032	0,096	0,023	0,019	0,015	0,017	0,005	0,011	0,012

Table 7.6 Electric Potential Difference data from S42 to S54

DEPTH (m)	**STATION NUMBERS**												
	S42	**S43**	**S44**	**S45**	**S46**	**S47**	**S48**	**S49**	**S50**	**S51**	**S52**	**S53**	**S54**
5	0,335	0,288	0,300	0,220	0,121	0,110	0,112	0,334	0,393	0,392	0,296	0,167	0,385
10	0,122	0,216	0,147	0,120	0,117	0,091	0,108	0,148	0,325	0,359	0,191	0,085	0,087
15	0,130	0,105	0,073	0,095	0,108	0,076	0,111	0,156	0,333	0,373	0,198	0,087	0,033
20	0,111	0,121	0,088	0,095	0,122	0,058	0,112	0,166	0,300	0,395	0,203	0,084	0,040
25	0,061	0,111	0,058	0,375	0,375	0,017	0,161	0,263	1,101	1,656	0,541	0,224	0,019
30	0,071	0,147	0,090	0,317	0,548	0,018	0,157	0,585	0,791	1,868	0,819	0,445	0,010
35	0,157	0,334	0,566	0,249	0,733	0,013	0,161	0,664	0,453	0,743	0,396	0,684	0,015
40	0,217	0,334	0,517	0,112	0,389	0,013	0,145	0,467	0,555	0,915	0,305	1,008	0,078
45	0,104	0,174	0,283	0,079	0,388	0,022	0,503	0,691	0,691	1,235	0,557	1,653	0,031
50	0,107	0,180	0,275	0,036	0,159	0,019	0,528	0,329	0,467	0,773	0,378	0,821	0,217
55	0,142	0,223	0,333	0,029	0,147	0,026	0,361	0,295	0,258	0,442	0,234	0,440	0,063
60	0,170	0,119	0,159	0,043	0,205	0,032	0,183	0,996	0,551	0,633	0,313	0,246	0,058
65	0,147	0,114	0,100	0,044	0,333	0,033	0,174	0,780	0,582	0,893	0,544	0,250	0,052
70	0,184	0,128	0,094	0,048	0,355	0,064	0,271	0,906	0,571	0,946	0,600	0,478	0,075
75	0,217	0,156	0,112	0,057	0,217	0,052	0,249	0,539	0,310	0,526	0,438	0,906	0,134
80	0,204	0,147	0,108	0,057	0,191	0,065	0,314	0,677	0,385	0,636	0,482	1,335	0,068
85	0,384	0,175	0,203	0,061	0,242	0,080	0,524	0,957	0,534	0,957	0,744	2,286	0,161
90	0,189	0,228	0,290	0,079	0,173	0,101	0,597	0,662	0,740	1,037	0,812	2,719	0,111
95	0,195	0,352	0,494	0,118	0,161	0,079	0,996	0,577	1,213	1,607	1,286	4,465	0,070
100	0,201	0,490	0,692	0,146	0,181	0,087	1,331	0,702	1,665	2,245	1,781	6,336	0,120
105	0,213	0,436	0,628	0,144	0,178	0,097	1,183	0,680	1,525	2,090	1,679	5,855	0,079
110	0,172	0,237	0,267	0,069	0,127	0,081	0,490	0,299	0,731	0,846	0,687	2,486	0,091
115	0,196	0,153	0,162	0,065	0,114	0,078	0,309	0,348	0,382	0,497	0,454	2,467	0,114
120	0,178	0,135	0,152	0,081	0,103	0,070	0,307	0,325	0,402	0,510	0,479	2,935	0,131

125	0,273	0,143	0,187	0,062	0,184	0,085	0,250	0,488	0,518	0,644	0,674	4,779	0,157
130	0,200	0,175	0,226	0,074	0,135	0,108	0,268	0,503	0,489	0,693	0,674	5,098	0,165
135	0,178	0,149	0,161	0,073	0,119	0,062	0,229	0,420	0,434	0,605	0,577	4,274	0,323
140	0,184	0,135	0,124	0,061	0,083	0,095	0,278	0,343	0,308	0,435	0,415	2,862	0,124
145	0,176	0,135	0,091	0,053	0,119	0,065	0,218	0,356	0,291	0,331	0,282	1,749	0,093
150	0,152	0,135	0,093	0,049	0,101	0,089	0,162	0,383	0,313	0,201	0,169	1,013	0,137
155	0,169	0,124	0,090	0,084	0,128	0,083	0,156	0,239	0,246	0,248	0,155	0,677	0,165
160	0,175	0,151	0,088	0,054	0,088	0,076	0,150	0,183	0,209	0,226	0,141	0,640	0,167
165	0,013	0,014	0,024	0,017	0,031	0,022	0,028	0,046	0,054	0,059	0,075	0,356	0,051
170	0,013	0,009	0,019	0,012	0,019	0,031	0,025	0,040	0,038	0,055	0,053	0,253	0,028
175	0,010	0,009	0,026	0,011	0,022	0,017	0,028	0,041	0,035	0,046	0,065	0,256	0,030
180	0,010	0,009	0,022	0,016	0,029	0,036	0,026	0,029	0,031	0,044	0,067	0,200	0,022
185	0,012	0,010	0,022	0,019	0,053	0,019	0,025	0,027	0,029	0,041	0,052	0,198	0,022
190	0,015	0,010	0,020	0,015	0,023	0,023	0,032	0,023	0,032	0,045	0,063	0,156	0,086
195	0,010	0,009	0,020	0,012	0,021	0,024	0,029	0,020	0,032	0,048	0,069	0,146	0,019
200	0,010	0,010	0,018	0,011	0,027	0,023	0,036	0,023	0,043	0,054	0,081	0,140	0,018
205	0,012	0,012	0,022	0,012	0,038	0,019	0,056	0,017	0,054	0,080	0,127	0,144	0,029
210	0,007	0,014	0,025	0,010	0,020	0,015	0,070	0,023	0,065	0,094	0,163	0,159	0,040
215	0,009	0,017	0,028	0,059	0,015	0,013	0,093	0,020	0,090	0,122	0,220	0,190	0,065
220	0,009	0,021	0,035	0,014	0,013	0,016	0,124	0,024	0,112	0,154	0,291	0,239	0,031
225	0,010	0,023	0,036	0,012	0,013	0,012	0,131	0,025	0,118	0,156	0,300	0,241	0,037
230	0,009	0,021	0,035	0,012	0,020	0,013	0,125	0,025	0,110	0,140	0,269	0,218	0,042
235	0,007	0,018	0,029	0,010	0,017	0,011	0,103	0,024	0,089	0,112	0,213	0,174	0,044
240	0,006	0,013	0,021	0,012	0,012	0,016	0,073	0,022	0,062	0,080	0,147	0,123	0,029
245	0,007	0,010	0,017	0,013	0,017	0,016	0,055	0,015	0,046	0,058	0,108	0,092	0,017
250	0,010	0,011	0,021	0,010	0,022	0,013	0,048	0,015	0,041	0,050	0,090	0,081	0,017
255	0,007	0,008	0,016	0,009	0,020	0,013	0,037	0,016	0,032	0,041	0,081	0,063	0,020
260	0,010	0,017	0,023	0,008	0,014	0,020	0,033	0,012	0,031	0,037	0,061	0,072	0,025
265	0,007	0,008	0,015	0,009	0,014	0,014	0,025	0,011	0,024	0,032	0,047	0,049	0,023
270	0,007	0,006	0,015	0,011	0,024	0,018	0,031	0,010	0,022	0,029	0,040	0,043	0,018
275	0,006	0,006	0,015	0,009	0,013	0,014	0,020	0,012	0,022	0,028	0,054	0,037	0,012
280	0,007	0,006	0,012	0,007	0,018	0,017	0,018	0,014	0,021	0,025	0,048	0,035	0,017
285	0,010	0,007	0,017	0,008	0,019	0,022	0,016	0,012	0,018	0,026	0,029	0,031	0,015
290	0,007	0,006	0,012	0,008	0,013	0,012	0,016	0,009	0,026	0,030	0,033	0,034	0,036
295	0,008	0,006	0,011	0,009	0,013	0,016	0,013	0,011	0,020	0,035	0,038	0,033	0,017
300	0,007	0,008	0,015	0,008	0,016	0,015	0,014	0,011	0,022	0,034	0,031	0,044	0,010

Table 7.7 Electric potential difference data from S55 to S67

DEPTH(m)	**STATION NUMBERS**												
	S55	**S56**	**S57**	**S58**	**S59**	**S60**	**S61**	**S62**	**S63**	**S64**	**S65**	**S66**	**S67**
5	0,411	0,199	0,424	0,387	0,126	0,404	0,141	0,636	0,371	0,429	0,446	0,563	0,452
10	0,135	0,083	0,110	0,110	0,054	0,532	0,294	1,061	0,415	0,442	0,510	0,565	0,318
15	0,119	0,113	0,097	0,035	0,067	0,292	0,160	1,459	0,314	0,406	0,936	0,736	0,295
20	0,097	0,058	0,098	0,285	0,030	0,795	0,191	1,575	0,364	0,533	0,668	0,622	0,270
25	0,107	0,252	0,301	0,038	0,068	0,130	0,154	1,394	0,574	0,132	0,206	0,970	0,089
30	0,075	0,170	0,190	0,077	0,054	0,120	0,138	2,460	1,124	0,119	0,191	1,571	0,068
35	0,157	0,116	0,183	0,053	0,049	0,111	0,163	1,828	1,302	0,089	0,245	2,621	0,080

40	0,181	0,061	0,137	0,076	0,020	0,120	0,154	1,651	0,938	0,110	0,349	2,551	0,087
45	0,184	0,111	0,161	0,055	0,101	0,081	0,166	3,039	1,498	0,162	0,319	3,005	0,104
50	0,093	0,118	0,190	0,051	0,028	0,160	0,113	3,059	1,443	0,194	0,362	4,066	0,102
55	0,196	0,113	0,123	0,115	0,096	0,138	0,115	3,401	1,271	0,156	0,267	5,312	0,091
60	0,210	0,040	0,128	0,089	0,043	0,253	0,149	1,718	0,705	0,216	0,415	9,032	0,149
65	0,121	0,130	0,125	0,213	0,086	0,266	0,125	1,489	0,656	0,227	0,569	11,313	0,178
70	0,204	0,147	0,126	0,108	0,066	0,263	0,120	2,378	1,112	0,246	0,424	10,969	0,350
75	0,205	0,077	0,341	0,288	0,085	0,234	0,166	4,579	2,022	0,253	0,515	11,511	0,231
80	0,164	0,189	0,352	0,168	0,101	0,178	0,233	7,229	3,158	0,336	0,553	12,605	0,254
85	0,167	0,241	0,529	0,124	0,074	0,275	0,358	12,737	5,817	0,301	0,588	18,962	0,362
90	0,198	0,208	0,410	0,177	0,103	0,168	0,372	16,089	7,616	0,286	0,559	22,901	0,338
95	0,237	0,144	0,448	0,073	0,111	0,315	0,457	26,296	12,745	0,351	0,619	37,009	0,493
100	0,224	0,264	0,524	0,161	0,101	0,291	0,572	37,048	18,168	0,299	0,607	51,072	0,509
105	0,250	0,256	0,499	0,232	0,171	0,161	0,547	33,904	16,833	0,362	0,427	46,212	0,399
110	0,137	0,102	0,209	0,147	0,083	0,178	0,272	13,801	6,804	0,332	0,495	31,361	0,450
115	0,165	0,128	0,138	0,114	0,073	0,253	0,211	9,023	4,957	0,320	0,757	60,001	0,293
120	0,197	0,070	0,155	0,203	0,076	0,194	0,163	9,614	5,559	0,394	0,776	75,209	0,528
125	0,308	0,144	0,141	0,144	0,105	0,370	0,175	13,881	8,455	0,431	0,621	124,663	0,444
130	0,256	0,143	0,176	0,117	0,086	0,355	0,155	14,561	8,952	0,504	0,357	129,663	0,335
135	0,203	0,095	0,110	0,191	0,100	0,249	0,222	12,278	7,624	0,360	0,583	106,629	0,410
140	0,377	0,083	0,180	0,078	0,080	0,252	0,125	8,524	5,173	0,476	0,534	70,809	0,404
145	0,132	0,058	0,102	0,150	0,090	0,302	0,158	5,230	3,118	0,402	0,573	43,113	0,394
150	0,148	0,184	0,162	0,176	0,085	0,156	0,173	3,081	1,864	0,435	0,622	25,114	0,350
155	0,233	0,131	0,070	0,219	0,086	0,181	0,148	2,220	1,202	0,338	0,642	15,697	0,314
160	0,117	0,238	0,102	0,161	0,089	0,188	0,155	2,351	1,291	0,320	0,461	15,700	0,284
165	0,028	0,105	0,046	0,188	0,051	0,019	0,023	1,104	0,651	0,029	0,286	14,769	0,071
170	0,032	0,035	0,078	0,097	0,052	0,022	0,027	0,810	0,476	0,021	0,109	8,774	0,105
175	0,018	0,174	0,121	0,089	0,045	0,017	0,029	0,803	0,474	0,025	0,079	8,771	0,072
180	0,034	0,031	0,080	0,072	0,025	0,021	0,038	0,644	0,395	0,024	0,065	6,108	0,067
185	0,013	0,053	0,084	0,074	0,038	0,016	0,037	0,641	0,394	0,023	0,083	6,086	0,080
190	0,023	0,127	0,086	0,105	0,042	0,018	0,054	0,576	0,382	0,039	0,058	4,428	0,038
195	0,014	0,094	0,087	0,055	0,019	0,029	0,062	0,587	0,402	0,015	0,039	4,098	0,053

200	0,012	0,188	0,103	0,099	0,023	0,014	0,079	0,643	0,451	0,015	0,066	3,640	0,079
205	0,013	0,037	0,057	0,112	0,033	0,013	0,130	0,925	0,676	0,014	0,040	3,448	0,054
210	0,010	0,064	0,027	0,032	0,047	0,011	0,164	1,116	0,816	0,020	0,028	3,705	0,044
215	0,012	0,045	0,036	0,038	0,026	0,014	0,222	1,454	1,076	0,012	0,034	4,258	0,040
220	0,020	0,053	0,068	0,056	0,029	0,016	0,299	1,926	1,439	0,010	0,034	5,019	0,047
225	0,019	0,025	0,047	0,040	0,013	0,013	0,310	2,007	1,483	0,009	0,037	4,877	0,051
230	0,016	0,043	0,052	0,062	0,061	0,012	0,292	1,892	1,383	0,010	0,044	4,446	0,050
235	0,016	0,041	0,037	0,065	0,024	0,016	0,243	1,574	1,107	0,016	0,052	3,717	0,037
240	0,013	0,059	0,033	0,048	0,024	0,014	0,168	1,119	0,761	0,016	0,053	2,673	0,039
245	0,011	0,064	0,051	0,068	0,026	0,012	0,123	0,819	0,546	0,010	0,023	2,131	0,031
250	0,009	0,058	0,049	0,049	0,036	0,012	0,106	0,700	0,463	0,013	0,031	1,838	0,031
255	0,008	0,104	0,046	0,048	0,027	0,025	0,079	0,527	0,353	0,011	0,201	1,610	0,036
260	0,008	0,093	0,034	0,044	0,037	0,008	0,070	0,468	0,314	0,012	0,080	1,376	0,024
265	0,010	0,035	0,066	0,066	0,024	0,012	0,050	0,337	0,227	0,022	0,057	1,156	0,066
270	0,009	0,062	0,034	0,055	0,032	0,011	0,043	0,291	0,195	0,035	0,087	1,012	0,032
275	0,010	0,045	0,079	0,147	0,026	0,015	0,038	0,257	0,171	0,013	0,034	0,940	0,026
280	0,008	0,183	0,097	0,082	0,026	0,010	0,034	0,244	0,152	0,014	0,026	0,905	0,022
285	0,011	0,087	0,072	0,034	0,024	0,012	0,029	0,203	0,133	0,013	0,017	0,931	0,034
290	0,013	0,021	0,091	0,077	0,041	0,009	0,027	0,141	0,125	0,014	0,024	0,908	0,032
295	0,011	0,089	0,070	0,083	0,032	0,016	0,028	0,112	0,104	0,012	0,208	0,712	0,052
300	0,009	0,053	0,085	0,067	0,022	0,010	0,021	0,117	0,094	0,013	0,036	0,707	0,037